**Title**
Vault Nanoparticles-Based Enzyme Immobilization Platform for Environmental Applications



**Author**
Wang, Meng

**Publication Date**
2018

Peer reviewed|Thesis/dissertation

UNIVERSITY OF CALIFORNIA

Los Angeles

# Vault Nanoparticles-Based Enzyme Immobilization Platform for Environmental Applications

A dissertation submitted in partial satisfaction of the requirements for the degree Doctor of Philosophy in Civil Engineering

by

Meng Wang

2018

ABSTRACT OF THE DISSERTATION

Vault Nanoparticles-Based Enzyme Immobilization Platform

for Environmental Applications

by

Meng Wang

Doctor of Philosophy in Civil Engineering

University of California, Los Angeles, 2018

Professor Shaily Mahendra, Chair

Free enzymes are promising catalytic agents because their activities can be achieved in the absence of growth substrates and conditions required for live microorganisms. Immobilizing enzymes on solid supports have been shown to improve their stability and longevity. To date, numerous enzyme immobilization supports and techniques have been developed, however, several associated issues, such as reduced enzymatic activity, low immobilization efficiency, and involvement of toxic substances, still limit the application of enzymes, particularly in environmental remediation.

In this research, a novel enzyme immobilization approach was developed and evaluated for removing environmental contaminants. The vault particles, members of protein nanocages, are entirely biocompatible and biodegradable, and have large empty cores for anchoring enzyme molecules, thus serving as eco-friendly enzyme carriers in environmental applications.

Manganese peroxidase (MnP), which has been demonstrated to be efficient in biodegrading various environmental contaminants, was employed as a model enzyme in the present study.

MnP was encapsulated into vault nanoparticles through the previously developed INT strategy, and the resultant vault-encapsulated MnP showed improved thermal stability and wider pH adaptability than free enzymes. The encapsulated MnP exhibited significantly better biodegradation of phenol than that catalyzed by native MnP. The performance of vault-encapsulated MnP was subsequently evaluated for removing and detoxifying three bisphenolic compounds, BPA, BPF, BPAP, which are trace contaminants of concern in water supplies. Compared with free MnP enzymes, encapsulated MnP showed longer durability in reactions, high removal rates and efficiency, and different product profiles. Further reproductive toxicity studies in *Caenorhabditis elegans* demonstrated that products resulted from catalysis by vault-encapsulated MnP induced less germline apoptosis and led to lower fertility damage.

Synthesis and proper assembly of vault particles in yeast *Pichia pastoris* cells were demonstrated for the first time in this study. The yeast production system showed comparable vault yield to the currently used insect cell system, but at more than ten times lower cost, which makes production of large quantities of vault particles for industrial, commercial, and environmental applications possible.

A vault-templating route to porous silica nanoparticles was developed. Combining it with vault encapsulation, a new enzyme immobilization approach with high immobilization efficiency and enzyme activity yield, and low leakage was demonstrated. MnP immobilized in vault/silica was more stable than free MnP as well as vault-encapsulated MnP, and accomplished high activity and excellent reusability.

Taken together, this research demonstrates the feasibility of using vault particles as enzyme carriers for water treatment and environmental applications. This work serves as a foundation for using customized vaults packaged with biodegradative enzymes to target specific contaminant groups in various industrial and environmental applications.

This dissertation of Meng Wang is approved.

Michael K. Stenstrom

Jennifer Ayla Jay

Yi Tang

Shaily Mahendra, Committee Chair

University of California, Los Angeles

2018

## Table of Contents

## List of Figures

## List of Tables

**Acknowledgements**

First and foremost, I would like to express my sincere gratitude and appreciation to my advisor Professor Shaily Mahendra. She has always been supportive to my doctoral study and research. Her guidance, instruction, encouragement and immense knowledge helped me throughout my life at UCLA. She sets me a model example of an advisor and a research group leader, as well as a university professor. I am also truly grateful for her continuous support when she was suffering from the disease. I wish and pray that she can win this battle and return to good health.

I would also like to thank my committee members, Professor Michael Stenstrom, Professor Jennifer Jay, and Professor Yi Tang for their time and help with my research and dissertation.

Very special thanks to Professor Leonard Rome and Dr. Valerie Kickhoefer from the Department of Biological Chemistry at UCLA. I truly appreciate their guidance and advice throughout my PhD studies. This work would not have been possible without their help. I would also like to thank Hedi Roseboro and Danny Abad, who were in Professor Leonard Rome's lab, for teaching me cell biology skills.

Thank you to Professor Patrick Allard and Yichang Chen from the Department of Molecular Toxicity at UCLA, who are co-authors for Chapter Three. I am very thankful for their help in designing the toxicity examination experiments, running the assays, and interpreting the data. This chapter would not have existed without their contribution.

I would like to express my gratitude to Dr. Bruce Dunn and Dr. Esther Lan for advising me on sol-gel experiments. I would also like to thank Dr. Sim-lin Lau for her help with analytical

issues. I greatly appreciate Oliver Foellmer's invitation to intern at Vault Nano, Inc. to learn more about vault synthesis and production.

I am also grateful to Dr. Phillip Gedalanga, Dr. Linda Tseng and Dr. Nancy Merino, who taught me a lot of lab techniques and helped me with experimental designs and setup when I first joined Professor Mahendra's group. Thank you to my former high-school and undergraduate assistants, An Gao, Brianna Plancarte, Sidney Poon, and Christina Najm for their help in my research projects. Thank you to Dr. Yun Liu, Dr. Peerapong Pornwongthong, Dr. Vincent Reyes, Dr. Shu Zhang, Robert Cudd, Stephen Opot, Ellen O' Connor, Michelle Myers, Siwen Wang, Tina Phan, Nicholas Johnson, Yu Miao, Alexandra Polasko, Shashank Kalra, Anjali Lothe, Catherine Clark, Thomas Folker, Fiona Guo, Ly Tan, Sylvia Liang, Jamie Liu, Rocio Ambrocio. Victor Xue, Dominic Robolino, Jerry Ngo, Alessandro Zulli, and all other Mahendra lab past and present members.

I would like to thank many people in the Department of Civil and Environmental Engineering, who have helped me a lot in ordering and other graduate school matters: Reba Glover, Jesse Dieker, Dr. Vanessa Thulsiraj, Dr. Ben Rossi, Helen Weary, Dylan Giron, Paula Columbia, Paula Green, and Maida Bassili.

This research was supported by Strategic Environmental Research and Development Program (SERDP) Contract ER-2422, National Science Foundation (NSF) Small Business Innovation Research Program (SBIR) Grant No: 1647632, NSF Faculty Early Career Development (CAREER) award to Professor Mahendra, DuPont Young Professor Award to Professor Mahendra, Paul L. Busch Award to Professor Mahendra, Vault Nano Inc., and UCLA Civil and Environmental Engineering Department. Studies in this research were performed in a renovated collaboratory funded by the NSF Grant Number 0963183, which was awarded under

the American Recovery and Reinvestment Act of 2009 (ARRA). The TEM images were taken using the instruments at the Electron Imaging Center for NanoMachines supported by NIH (1S10RR23057 to ZHZ) and CNSI at UCLA. The UPLC/MS analysis was conducted at the UCLA Molecular Instrumentation Center (MIC). I would also like to thank UCLA graduate division, Sustainable Nanotechnology Organization (SNO) for supporting my travel to professional conferences and meetings.

At last, I would like to express my deepest gratitude to my parents, who always stand behind me and give me support. I would not be where I am today without them.

# Vita

## EDUCATION

M.S., Civil and Environmental Engineering, University of California, Los Angeles 2012-2015

B.S., Environmental Science, Nanjing University, China 2008-2012

## PUBLICATION

1. Wang, M.; Abad, D.; Kickhoefer, V. A.; Rome, L. H.; Mahendra, S. Vault nanoparticles packaged with enzymes as an efficient pollutant biodegradation technology. *ACS Nano* **2015,** *9* (11), 10931-10940.
2. Wang, M.; Kickhoefer, V. A.; Rome, L. H.; Foellmer, O. K.; Mahendra, S. Synthesis and Assembly of Human Vault Particles in Yeast. *Biotechnology and Bioengineering* **2018**.
3. Merino, N.; Wang, M.; Ambrocio, R.; Mak, K.; O'Connor, E.; Gao, A.; Hawley, E. L.; Deeb, R. A.; Tseng, L. Y.; Mahendra, S. Fungal biotransformation of 6: 2 fluorotelomer alcohol. *Remediation Journal* **2018,** *28* (2), 59-70.

## BOOK CHAPTER

1. Wang, M.; Abad, D.; Kickhoefer, V. A.; Rome, L. H.; Mahendra, S. Encapsulation of Exogenous Proteins in Vault Nanoparticles. In *Protein Scaffolds*, Springer: 2018; pp 25-37.

## HONORS AND AWARDS

- Student Award, Sustainable Nanotechnology Organization (2017)

- MWH/AEESP Outstanding Master's Thesis Award, Association of Environmental Engineering and Science Professors (2016)
- Certificate of Merit, American Chemical Society 251st National Meeting & Exposition (2016)
- Student Paper Competition Honorable Mention, Emerging Contaminants Summit (2016)

# Chapter 1 Introduction

## 1.1. Application of Enzymes in Environmental Remediation

Conventional environmental remediation relies on physical-chemical approaches, such as photooxidation, advanced chemical oxidation, ultrasonication, and electrochemical oxidation, which employ high energy processes or highly active chemicals to breakdown contaminants.[1] These approaches are generally effective and efficient, whereas they are energy-intensive, and potentially cause environmental disruption and generate toxic by-products.[2] As a more environmentally-friendly and less energy-intensive approach, microbial bioremediation is receiving increased attention in recent years.[3] Relying on biological activities, microbial remediation is carried out under mild conditions, and has been successfully employed in treatment of various contaminants, such as halogenated phenols, pesticides, organic dyes, endocrine disruptors, and per- and polyfluoroalkyl substances.[3-5] These contaminants are either metabolized as carbon sources or co-metabolized with additional carbon sources, and are completely mineralized to $CO_2$ or converted to less toxic products.[3]

On the other hand microbial bioremediation also has some disadvantages as compared to conventional physical-chemical processes. Biological activities of microbes strongly depend on microbial viability and growth that are sensitive to various environmental factors such as nutrient concentrations, temperature, oxygen level, co-contaminants, and indigenous microbial community.[2, 3] To create and maintain a suitable condition for microbes, the local environment has to be finely controlled, which will increase the cost of operation and can hardly be achieved in some cases. Additionally, the use of microbes might also cause public concerns as it may cause release of pathogenic organisms.

Enzymes are biological catalysts that are used to accelerate nearly all chemical reactions in cells.[6] Although a few catalytic RNA molecules have enzymatic activity, which are called ribozymes, most of cellular enzymes are proteins. Similar to inorganic catalysts, enzymes are capable of reducing activation energy of chemical reactions, thus enabling biochemical reactions that are too slow to occur under ambient temperature and pressure to take place under physiological conditions. Some isolated and purified enzymes are able to maintain bioactivity and catalyze chemical reactions in the absence of cells, which is called *in vitro* enzymatic catalysis. The use of *in vitro* enzymatic catalysis in industry has been developed over decades, and several enzymes are being used in large-scale industrial processes or commercial products.[7] For example, lipase, which breaks down triglyceride to fatty acids and glycerol, is used in biodiesel production, transesterification of food oils, and chiral resolution of alcohols and amines.[8] Lactase, which breaks down lactose, is used as dairy digestive supplement.[7] Another example could be penicillin G acylase (PGA).[9] PGA catalyzes the hydrolysis of penicillin, and is a very important enzyme used in production of modified antibiotics. The worldwide market for industrial and non-industrial enzymes exceeded $5.5 billion in 2010 and is projected to increase at an annual growth rate of 7-9%.[7]

Sharing similar advantages to microbial bioremediation, using enzymes instead of whole cells is a promising bioremediation alternative as *in vitro* enzyme-catalyzed degradation is not constrained by the requirements for microbial growth, and is less likely to be inhibited by contaminants that are toxic to microbes.[10, 11] Enzymatic bioremediation is also more selective; thus can treat substances over a broad range of concentrations, even at low levels. Due to their high efficiency and turnover numbers, enzyme-based bioremediation is more rapid, so that it can be operated with lower retention times. In addition, the use of enzymes is generally a safer

approach as it avoids potential release of pathogens or genetically modified organisms. To date, several enzymes have been explored in water treatment and soil remediation, and some of the examples are listed in Table 1.1.

**Table 1.1** Enzymes mediated removal of environmental contaminants.

| Enzyme | Contaminant | Matrix | Ref. |
|---|---|---|---|
| Laccase | Azo dyes<br>Phenolic compounds<br>Polycyclic aromatic hydrocarbons<br>Perfluoroalkyl substances | Water | 12-15 |
| Laccase | Estradiol<br>Perfluorooctanoic acid | Soil | 16, 17 |
| Lignin peroxidase (LiP) | Tetracycline<br>Azo dyes<br>Estradiol<br>Chlorinated phenols | Water | 18-21 |
| Manganese peroxidase (MnP) | Azo dyes<br>Phenolic compounds<br>Polycyclic aromatic hydrocarbons | Water | 22-24 |
| Soybean peroxidase (SBP) | Azo dyes<br>Phenolic compounds | Water | 25, 26 |
| Horseradish peroxidase (HRP) | Azo dyes<br>Phenolic compounds<br>Polychlorinated biphenyl | Water | 26-28 |
| Tyrosinase | Phenolic compounds | Water | 29 |
| Atrazine chlorohydrolase | Atrazine | Water | 30 |
| Triazine hydrolase | Atrazine | Water | 31 |

As shown in Table 1.1, while a few enzymes have been explored for bioremediation, peroxidases and laccases are two major enzyme families that are being studied.

Peroxidases catalyze substrate oxidation using peroxide as electron acceptor, and contain ferric heme cofactor as the catalytic center.[32, 33] The catalytic cycle starts with one step of two-electron transfer from heme to peroxide, followed by two steps of one-electron transfer from substrates to oxidized peroxidase enzymes, resulting in oxidized substrates and peroxidase enzymes at ground state. Some peroxidases, such as MnP, require electron shuttles to transfer electrons as they cannot directly gain electrons from substrates.[33] Currently studied peroxidases are from two major sources including fungi and plants.[34-36] LiP and MnP are two enzymes produced and secreted by wood-decay fungus *Phanerochaete chrysosporium*, and have optimum activity at acidic pH. They catalyze various reactions, such as $C_\alpha$-$C_\beta$ cleavage, cleavage of β-O-4, hydroxylation of benzylic methylene groups, oxidation of phenolic groups, and oxidation of benzyl alcohols, in lignin degradation in nature.[35] Plant produced peroxidases (e.g. HRP and SBP) can catalyze similar reaction as fungal peroxidases, but have optimal activity at neutral pH.[26] The working pH ranges of fungal and plant peroxidases are complementary to each other, which enables peroxidase-based bioremediation to work over a wide pH range.

Laccases are a group of copper containing oxidative enzymes that are produced and secreted by white-rot fungi for the degradation of lignin.[37] Similar to fungal peroxidases, laccases have optimal activity at weakly acid pH, and catalyze substrate oxidation. However, laccases utilize molecular oxygen as the terminal electron acceptor rather than peroxide, which gives them a huge advantage over peroxidases in environmental applications as oxygen supplementation is significantly easier than supplementation of peroxide compounds. The laccase redox process is initiated by molecular oxygen oxidizing four copper (I), which form the

catalytic core of laccase enzymes, to copper (II). Subsequently, fully oxidized copper cluster is reduced by gaining electrons from substrates, resulting in substrate oxidation.[37] Although laccases can directly oxidize many substrates, addition of mediators, such as N-hydroxybenzotriazole (HBT), 2,2'-azino-bis-(3-ethylbenzothiazoline-6-sulphonic acid) (ABTS), and 2,2,6,6-tetramethylpiperidine-1-yloxy (TEMPO), which transfer electrons from oxidized laccases to substrates, can significantly enhance laccase catalysis.[37] Some recalcitrant compounds may only be oxidized by laccase in the presence of a mediator.[15]

As non-specific enzymes, peroxidases and laccases are extremely efficient for removing azo dyes and phenolic compounds,[13, 14, 23, 38] and are also found to remove recalcitrant substances, such as polychlorinated biphenyl,[27] per- and polyfluoroalkyl substances,[16] and polyaromatic hydrocarbons[12, 22] in the presence of certain co-substrate or mediator.

What can also be seen from Table 1.1 is that most of the enzymatic bioremediation studies were performed in water system. Application of enzymes in soil decontamination is rarely reported. One of the reasons is that the composition of soil is much more complicated than water. The ubiquitous natural organic matter (NOM), ligands, microbes and metal ions in soil can all possibly lead to enzyme inhibition or inactivation.[39] Enzymes are proteins in nature, and their activities rely on their conformation and three-dimensional structure. Thus, microbes can digest and use enzymes as nutrient source, which results in complete enzyme disruption. The binding of metal ions, ligands, or NOM to enzymatic catalytic core can cause conformational change, which also leads to enzyme inhibition or inactivation. In the relatively simple water systems or even synthetic buffered systems, enzymes can also be inactivated by temperature, pH, or the products formed by their own activities.[40] For example, LiP was totally inactivated within 5 hours at 40°C at pH above 7. At 70°C, complete inactivation was observed in 10 min.[41] Taken

together, these can be concluded as the major limitation of enzymatic bioremediation, which is that enzymes are not stable and requires costly frequent replenishment.

## 1.2. Enzyme Immobilization

### 1.2.1 Introduction to Enzyme Immobilization

To overcome such limitation and develop more stable enzymes for bioremediation, two major approaches have been developed: protein engineering and enzyme immobilization.[42] Protein engineering relies on biotechnologies, such as rational evolution and site-directed mutagenesis, to produce unnatural enzymes with improved stability, activity and other functional properties, often through modification of amino acid sequences of natural enzymes. Although it can generate enzymes with largely improved stability and specific activity, and even with new catalytic properties, it is generally a labor-intensive and time-consuming process, and the outcome is unpredictable and uncontrollable. Enzyme immobilization, on the other hand, does not change enzymes' intrinsic properties, but changes their physical state by attaching or trapping them onto or into solid matrices to increase enzymatic stability. The main advantage of enzyme immobilization over protein engineering is that enzymes immobilized on larger structures can be easily reused, which can significantly lower the cost of enzymatic processes.[40] Immobilization also facilitates enzymatic reactor operation and substrate separation as immobilized enzymes can be packed into columns, which allows continuous influent of substrates and effluent of products.[43]

To evaluate the performance of various immobilization approaches, there are five general considerations: enzyme yield, specific activity yield, overall activity yield, enzyme loading

capacity, and leaching.[43] Enzyme yield is calculated as the percentage of immobilized enzyme from the initial enzyme added:

Enzyme yield = immobilized enzyme/initial enzyme

Some special proteins, such as fluorescent proteins, can be quantified by measuring fluorescence intensities. However, the amount of most enzymes can only be quantified by protein concentration assays, such as BCA assay, Bradford assay, and ELISA. As these assays rely on the interaction between reagents and peptide bonds, functional groups or specific binding sites in enzymes, immobilization supports may affect assay results by shielding enzymes from interacting with assay reagents or by providing extra reagent binding functional groups. Thus, the amount of immobilized enzyme is usually calculated by subtracting enzymes left in supernatant after removing immobilized enzymes from total initial enzymes.

The second consideration is specific activity yield, which is used for evaluating the effect of immobilization process on enzyme specific activity.

Specific activity yield = specific activity of immobilized enzyme/free enzyme

Specific enzyme activity is assessed by two parameters including turnover number ($k_{cat}$) and half-saturation constant ($K_M$). $k_{cat}$ is the maximum number of substrate molecules that can be converted to product per enzyme molecule per second, and it reflects the highest enzyme activity at optimal conditions. $K_M$, on the other hand, equals to the substrate concentration, at which the conversion rate is at half-maximum, and it generally reflects the affinity between substrate and

enzyme. Ideally, immobilized should exhibit the same activity as free enzymes, and specific activity yield should be 100%. However, it has been widely reported that immobilization leads to enzyme inactivation and specific activity decrease of immobilized enzymes, which is reflected as decreased $k_{cat}$ and increased $K_M$.[43] Enzymatic activity depends their three-dimensional structure. Interaction between immobilization support and the enzyme may alter enzymatic conformation, thus leading to a decrease in specific activity. Immobilization reaction condition may not be favorable for the enzyme, which also contributes to the specific activity decrease. Moreover, some immobilization approaches are achieved by burying enzymes in solid matrices, which increases the substrate diffusion resistance and hinder binding between enzyme and substrate molecules, resulting in $K_M$ increase.[43, 44] However, there are also studies showing immobilized enzymes have elevated specific activity. An example would be immobilizing redox enzymes on metal supports, such as copper and iron.[45, 46] Metal supports can act as electron carriers and facilitate electron transfer between the enzyme and substrate, thereby promoting turnover numbers. The other approach to improve specific activity of immobilized enzymes is to immobilize the enzyme in a micro-environment that attracts and concentrates the substrate *via* special interactions like hydrophobic interaction and ionic interaction.[8] By preferentially concentrating the substrate and increasing its local concentration around enzyme molecules, the apparent $K_m$ values will be decreased, leading to an immobilized enzyme with improved specific activity.

The next consideration is overall activity yield that is used to describe the overall efficiency of immobilization techniques.

Overall activity yield = activity of immobilized enzyme/free enzyme

The overall activity yield is comparing total activity of immobilized enzyme to total initial activity of the free enzyme. It can be calculated by multiplying enzyme yield by specific activity yield, and it reflects the overall efficiency of the immobilization process.

The fourth consideration is enzyme loading capacity, describing the amount of enzyme that can be immobilized onto or into per unit mass of immobilization supports.

Enzyme loading capacity = mass of immobilized enzyme/mass of immobilization support

In general, high enzyme loading capacity is preferred, as it decreases the use of immobilization supports and increases enzyme loading density. When being used in fixed-bed columns, immobilized enzymes at higher enzyme loading can be packed in columns at higher enzyme density, thus converting substrate at higher rates.[43, 44]

The last consideration enzyme leaching is used to describe enzymatic physical stability on or in immobilization supports overtime.

Leaching = residual immobilized enzyme/starting immobilized enzyme

Immobilized enzymes can be separated from free enzymes *via* filtration, centrifugation, or sedimentation, as they are attached to large structures. However, the interaction between immobilized enzymes and supports does not last forever, and leaching of immobilized enzymes has been reported in many studies.[47-49] Once released as free enzymes, they can hardly be recycled, leading to activity decrease of immobilized enzymes after reuses. When being used in

fix-bed columns, the continuous water flow also accelerates enzyme leaching, resulting in faster enzyme activity decrease.

### 1.2.2 Immobilization Techniques

As early as 1916, Nelson and Griffin reported the first study of enzyme immobilization, describing the adsorption of invertase on charcoal surfaces.[50] Since then, many physical and chemical immobilization techniques have been developed. In general, these techniques can be divided into three groups: surface binding, entrapment, and crosslinking.[40]

Enzyme binding to solid surface can be achieved *via* three approaches, including physical adsorption, ionic binding, and covalent binding.[40, 43] Physical adsorption results from non-specific interaction between enzyme molecules and solid surface through hydrophobic interaction, Van der Waals attraction, and hydrogen binding. As these interactions are ubiquitous, it makes physical adsorption an easy and universal method for enzyme immobilization. However, low enzyme loading and serious leaching usually come along with physical adsorption, because these interactions are too weak.[43] Ionic binding can be used to attach charged enzyme molecules to counter charged surface. Although the electrostatic interaction is stronger, it still cannot effectively maintain enzyme molecules on the surface. Additionally, as ionic binding is non-specific and reversible, enzyme molecules can be easily replaced by ions with the same charge, resulting in fast enzyme leaching.[47] Covalent binding is stronger than physical adsorption and ionic binding. It is generally not reversible, and fixes enzyme molecules on the surface and prevents leaching. On the contrary, the strong interaction also leads to the major disadvantage of covalent binding, which is enzyme inactivation caused by covalent bonds formed between enzyme molecules and the solid surface.[42] Moreover, for some

inert surfaces, such as glass, chemical modification is often required before immobilization, as they lack functional groups that are used to conjugate with enzyme molecules.[51, 52] This modification process is costly, and uses reactive and toxic chemicals, which contributes to the emission of hazardous waste to the environment. Glass,[51, 52] polyacrylonitrile (PAN),[53] and activated carbon[54] are some common examples used as adsorption surface in enzyme immobilization.

Entrapment is embedding enzymes in polymeric gel or fiber.[40, 43] Different from surface binding that mixes pre-synthesized solid matrices and enzymes, entrapment is usually performed using *in situ* synthesis of solid supports in the presence of enzymes. As polymerization proceeds, enzyme molecules are trapped inside of polymer matrix by covalent or noncovalent bonds. By trapping the enzyme into solid matrices that have smaller size than enzyme molecules, leaching can be prevented completely. However, similar to covalent binding on solid surface, covalent bonds that keep enzyme molecules inside of the solid also cause enzyme inactivation. The other major disadvantage of entrapment is that the dense material surrounding enzyme molecules generate extensive substrate diffusion resistance and prevent the binding between enzymes and substrates, which lead to significant increase of $K_M$ and decrease of enzyme activity. Moreover, the monomers forming gel or fiber are often dissolved in organic solvents and the polymerization is usually carried out at extreme pH and in high content of organic solvents, which also lead to enzyme activity loss. Common polymers used for entrapping enzymes are silica solgel and alginate.[49, 55]

In terms of crosslinking, which also relies on covalent interaction, bonds are not formed between enzyme molecules and solid supports, but between enzymes molecules only.[40] One of the obstacles of crosslinking is that enzyme molecules cannot be efficiently linked to each other

and form packed solids because enzyme molecules are diluted in solution. Inactivation of enzymes in solution is another problem with crosslinking. To overcome such obstacles, two major approaches have been introduced: cross-linked enzyme crystals (CLECs) and cross-linked enzyme aggregates (CLEAs).[40, 43] CLECs starts with growing enzyme crystals, followed by adding cross-linkers (e.g. glutaraldehyde) to react with enzyme molecules.[56] CLEAs are prepared in a similar but easier way. Precipitants, such as ammonium sulfate, polyethylene glycol (PEG), and tert-butyl alcohol, are added to solutions with high enzyme concentration to form enzyme aggregates. Subsequently, the aggregates are collected, and crosslinked by adding cross-linker.[57] Different from surface binding and entrapment that lead to enzyme activity dilution in massive solid matrices, crosslinking generates products containing solely enzyme molecules, which possesses higher spatial density of enzymatic activity than products made through surface binding and entrapment. However, studies on using cross-linked enzymes in bioremediation or in bioengineering application are rarely reported. The possible reason is that the cost and performance of crosslinking cannot be balanced. CLECs generates good templates for crosslinking, but the enzyme crystallization process is sensitive and hard to control.[40, 56] CLEAs provides an easier alternative, but requires large amount of precipitants.[57] Enzymes buried inside of aggregates are also less accessible to substrates, thus resulting in apparent activity loss.

### 1.2.3 Immobilization Supports

Since the first report of adsorption enzymes on solid surface in 1916,[50] many solid supports have been applied for enzyme immobilization. In the early years, researches most focused on large scale immobilization supports, such as glass, polymer, silica sol-gel, alginate beads, and activated carbon. Recent advances in nanotechnology have generated a wide variety

of nanomaterials. Owing to their unique properties, such as large surface area and high reactivity, the use of nanomaterials for enzyme immobilization is getting increased attention.[44]

### *1.2.3.1 Conventional Supports*

Many studies have reported the use of immobilized enzymes on conventional supports in water treatment and bioremediation. Table 1.1 summarizes some examples, and the performance of each solid support used. Glass is one of the most widely used materials for immobilizing enzymes. Chemical functionalization is usually required for attaching enzymes on glass surface, as glass is a relative inert material and lacks of functional groups that can bind to enzyme molecules. Carboxyl groups (-COOH) and amine groups ($-NH_2$) are commonly found in amino acid residues in enzymes, thus introducing amine groups or carboxyl groups on glass surface is a popular modification method. Linkers can also be added to bridge functionalized glass and enzymes. For example, Bódalo et al. immobilized SBP and HRP on modified glass using glutaraldehyde as the linker.[51] Amine groups were introduced on glass surface by reacting it with (3-Aminopropyl) triethoxysilane (APTES), followed by second modification with glutaraldehyde. Subsequently, SRP and HRP were immobilized through the reaction between their amino groups and aldehyde groups on glass surface. For SRP, enzyme yield and specific activity yield were 50.9% and 82.4%, respectively. Enzyme loading was 42.3 mg/g glass. HRP immobilization was not as good as SBP. Both immobilized peroxidases were able to catalyze the remove of chlorophenol and showed better resistance to hydrogen peroxidase inactivation.[51] Another way to use glass as immobilization supports is through silica sol-gel process, which refers to formation of a continuous three-dimensional network of silica within the liquid (gel) from crosslinking of silica nanoparticles in solution (sol).[58] The first step of sol-gel process is

hydrolysis and condensation of silica alkoxide at extreme acidic or basic pH to form sol. Afterwards, solution pH is adjusted to neutral to avoid enzyme inactivation, followed by adding enzyme solution. Polymerization usually happens in minutes, resulting in entrapment of enzymes in the silica gel. Additives, such as PEG, can be added to enlarge the pore size and protect enzyme during polymerization.[55] Qiu and Huang immobilized laccase in silica sol-gel.[55] The authors reported that immobilized laccase exhibited better stability, and applied it to remove chlorophenols.[55] Lloret et al., 2011 also immobilized laccase in silica sol-gel, and packed laccase-sol-gel in a bed-reactor to treat estrogens in continuous flow.[59]

Synthetic polymer is another category of materials that are being commonly used in enzyme immobilization.[53, 60-62] Various polymers, such as polyalanine,[61] polyacrylonitrile,[53] polyvinyl alcohol,[62] and poly(ethylene terephthalate)–poly(aniline)[60] have been used to immobilize enzymes for bioremediation. Similar to glass, due to the lacking of functional groups on some polymers' surface, chemical functionalization is required before performing immobilization.[60] HRP and laccase have been immobilized on polymers and explored for removing various phenolic compounds.[53, 60-62]

Nature also provides a number of polymers, mainly polysaccharides (e.g. chitin, agarose, cellulose, starch, and chitosan), for enzyme immobilization. Chitin is the second abundant natural polymer on earth, and is the primary component of fungal and yeast cell wall and the exoskeleton of arthropods.[63] As the product from partial degradation of chitin under alkaline conditions, chitosan is a linear polysaccharide that has been widely used as an enzyme immobilization support.[63] As compared to synthetic polymers, chitosan can be obtained from shells of shrimp and other crustaceans, thus is inexpensive, non-toxic, and biodegradable.[63] Bayramoglu et al. immobilized laccase on chitosan through covalent binding, and successfully

applied it for organic dye treatment.[64] The authors also conjugated chitosan with magnetic nanoparticles, which simplify the recovery of immobilized enzymes.

Calcium alginate is another example of natural materials applied in enzyme immobilization. Alginic acid is a polysaccharide that commonly found in brown algae cell wall. Sodium salt of alginic acid (sodium alginate) is soluble in water, but not calcium salt. Calcium alginate is obtained by adding calcium ion to sodium alginate solution. By adding enzymes with calcium ion, the enzyme will be co-precipitated and trapped inside of calcium alginate, resulting in calcium alginate immobilized enzyme. Other metals, such as magnesium and copper, can also be used to precipitate alginate ions and immobilize enzymes. Alemzadeh and Nejati entrapped HRP in calcium alginate, and observed near 100% enzyme yield at 5.5% w/v calcium chloride and 1% w/v sodium alginate.[49] The immobilized HRP was proven to effectively remove phenol.[49] Niladevi and Prema compared enzyme yield between using calcium and copper alginate to immobilized laccase, and found that copper showed about 30% higher binding efficiency than calcium.[65] The authors also packed copper alginate immobilized laccase into a column reaction, and showed it successfully removed phenol in a flow system.

Activated carbon is a commonly used adsorbent to remove contaminants from water. Due to its large surface area, it has also been used to immobilize enzymes. Nguyen et al. immobilized laccase on granular activated carbon (GAC) by simply mixing them for 24 hours.[54] The reported enzyme loading was 10 mg/g.[54] GAC immobilized laccase showed improved stability, and still retained 50% activity after 20 reuses.[54] The authors also subjected GAC with bound laccase to degrade various contaminants, including bisphenol A, diclofenac, sulfamethoxazole, and carbamazepine, and showed it performed better than GAC along.[54]

**Table 1.2** Immobilization of Enzymes on Conventional Supports for Bioremediation.

| Solid Support | Immobilization Method | Enzyme | Contaminant | Enzyme yield (%) | Specific activity yield (%) | Enzyme loading (mg enzyme /g support) | Leaching | Ref. |
|---|---|---|---|---|---|---|---|---|
| Aldehyde glass | Covalent | SBP | Chlorophenol | 50.9 | 82.4 | 42.3 | NR | 51 |
| Aldehyde glass | Covalent | HRP | Chlorophenol | 31.5 | 52.5 | 23.1 | NR | 51 |
| Modified glass | Covalent | Laccase | Endocrine disruptors | 45 | 55 | NR | NR | 52 |
| Modified glass | Covalent and cross-linking | Laccase | Endocrine disruptors | 30 | 31 | NR | NR | 52 |
| Silica sol-gel | Entrapment | Laccase | Estrogens | NR | 59.2–82.9 | 2.2-22 | NR | 59 |
| Silica sol-gel | Entrapment | Laccase | Chlorophenol | 99.1 | 70 | NR | NR | 55 |
| Polymer | Covalent and adsorption | HRP | Phenolics | NR | 40 | NR | NR | 60 |
| Calcium alginate | Entrapment | HRP | Phenol | 60-100 | NR | NR | 5-50% in 18 hours | 49 |
| Calcium and copper alginate | Entrapment | Laccase | Phenol | 20-50 | NR | NR | NR | 65 |
| PAN Beads | Covalent | Laccase | Chlorophenol | 10 | NR | 0.25 | NR | 53 |
| Magnetic chitosan | Covalent | Laccase | Dyes | NR | 79.6 | 16.3 | NR | 64 |
| GAC | Physical adsorption | Laccase | Bisphenol A, diclofenac, sulfamethoxazole, carbamazepine | NR | NR | 10 | NR | 54 |

#### *1.2.3.2 Nanomaterials for enzyme immobilization*

As enzyme immobilization supports, nanomaterials have two main advantages over conventional supports. First, nanomaterials have higher surface-to-volume ratios, thus they have more available immobilization sites, leading to higher enzyme loading capacity per mass unit. The second advantage is that using nanomaterials can minimize substrate transfer resistance and diffusional problems, especially for entrapped enzymes. In recent years, a number of nanomaterials have been used to immobilize enzymes for bioremediation applications. Table 1.3 lists some commonly nanomaterials, and their performance in terms of enzyme immobilization.

Nanogel is made by encapsulating the enzyme molecule in a thin and porous polymer layer *via* a two-step procedure, including enzyme surface acryloylation and *in situ* polymerization.[66] In the first step, ethenyl groups are formed on enzyme surface *via* the reacting amines groups in amino acids residuals with N-acryloxysuccinimide. Polymerization at the ethenyl groups occur after adding monomers and crosslinkers, resulting in polymer trapped single enzyme molecules.[66] Enzyme nanogel exhibits high stability under harsh conditions, and also robust activity. Yan et al. reported the preparation of HRP nanogel, which showed significantly improved stability at high temperature and in the presence of organic solvents, without compromising enzyme activity.[66] Organophosphorus hydrolase (OPH), which is an enzyme efficiently detoxify organophosphates (OP), was also successfully stabilized in nanogel, reported by Wei et al.[42] Similar to HRP nanogel, OPH nanogel showed improved resistance to high temperature and organic solvents, and enhanced storage stability. The authors also found OPH nanogel could detoxify OP *in vivo*,[42] but not native OPH, which suggesting OPH nangel can be used to treat OP contamination in filed, and as an antidote to OP poisoning.

Protein-inorganic nanoflowers are formed from co-precipitation of metal salts and proteins. Adding copper ions to phosphate buffer containing proteins, the copper ions first conjugate with protein molecules, providing the nucleation sites for the formation of large agglomerates of primary crystals and protein molecules. Subsequently, anisotropic growth of copper-phosphate crystals that originates at individual copper binding sites forms the complete flower-like structure. When an enzyme is used to bind copper ions, copper-phosphate nanocrystals with enzyme immobilized are formed. In addition to copper, other metal ions, such as iron [46], have also been used to synthesize similar structures. Ge et al. reported the first synthesis of protein-inorganic nanoflower structure in 2012.[45] The authors found laccase immobilized on the nanocrystals exhibited significantly better stability. HRP has also been immobilized on such structures as reported by Ocsoy et al.[46] The major benefit of immobilizing enzyme through protein-inorganic nanoflower approach is that the metal support may serve electron shuttle that facilitate electron transfer between enzymes and substrates, thus improving enzymatic activity. Laccase nanoflower converted phenolic compounds 2-4 times faster than free laccase.[45] HRP incorporated in nanoflowers exhibited activity of ~710% as compared to free HRP enzyme.[46]

Similar to silica sol-gel, mesoporous silica is also formed through hydrolysis and concentration of silica alkoxide, but on templates. Since the M41S family of mesoporous silica sieves was discovered by Mobil scientists in 1992,[67] a number of synthetic method and templates have been reported, such as soft-templating method, in situ templating pathway, and biomaterials.[68, 69] The procedure of immobilizing enzymes on mesoporous silica is similar to that on glass surface, which starts with modification of silica surfaces, followed by formation of covalent bonds between enzyme molecules and functional groups introduced on silica.[67, 70]

Comparing to glass, mesoporous silica has larger surface area, leading to higher enzyme loading capacity.[68] In addition, the high porosity of mesoporous silica also allows efficient substrate diffusion, which minimizes mass transfer resistance in the material.[68] The use of mesoporous silica immobilized enzymes in bioremediation has been reported in several studies.[44] For example, Salis et al. reported the application of functionalized SBA-15 mesoporous silica immobilized laccase in oxidation of phenolic compounds.[70] The enzyme yield reached 100% in 100 minutes, and immobilized laccase retained 60% of initial activity after 14 reuses.[70]

Biosilicification is another way to immobilize enzymes in silica. Biosilicification is a commonly found process in nature, that incorporates silica to live organisms, usually as cell wall composition. Comparing to chemical synthesis of silica materials, which is performed under extreme pH and temperature, biosilicification process is carried out under physiological conditions. Various natural materials, such as cellulose, nucleic acids, peptides, and proteins, have been studies as templates to synthesize silica.[71] Silaffin is a protein discover by Kröger et al. that is able to precipitate silica, forming silica-protein complexes.[72] A short peptide sequence derived from silaffin, named R5 peptide, also showed silica precipitation activity.[72] Immobilization of enzymes in R5 precipitated silica was first reported by Luckarift et al. in 2004.[73] When pre-hydrolyzed tetramethyl orthosilicate (TMOS) was added to the solution containing enzymes and R5 peptides, enzymes were co-precipitated with R5-silica, forming the enzyme-R5-silica complex.[73] The enzyme loading capacity was found to be 220mg/g silica, which is 5-10 times higher than that in sol-gel protocols.[73] Jo et al. developed a modified method, which used R5 peptide fused enzymes to induce silica precipitation.[74] The enzyme carbonic anhydrase (CA), which accelerates $CO_2$ removal from atmosphere by catalyzing $CO_2$ hydration and $CaCO_3$ precipitation, was attached with a R5 peptide sequence.[74] The recombinant

CA-R5 enzyme efficiency mediated silica precipitation, resulting in silica captured CA-R5. Immobilized CA-RA showed 50% specific activity yield and negligible leaching in 24 hours.[74]

Carbon provides another broad category of nanomaterials for enzyme immobilization, such as mesoporous carbon,[75] graphene and graphene oxide,[76, 77] carbon nanotube (CNT),[78] and fullerene.[78] As nanoscale carbon has highly active surface, immobilization is usually achieved via physical adsorption, similar to immobilization on activated carbon. Alternatively, graphene can be chemically modified with functional groups, that covalently bind to enzyme molecules.[77] For example, Zhang et al. immobilized HRP on graphene oxide *via* physical adsorption.[76] Although enzyme yield was only 10%, enzyme loading on graphene oxide reached 100 mg/g [76]. Immobilized HRP showed better activity at extreme pHs and temperature, and better storage stability.[76] Activity of HRP adsorbed on graphene oxide towards removing various phenolic compounds (e.g. phenol, 3-aminophenol, and 2-cholorophenol) was also demonstrated by the authors.[76] Pang et al. compared immobilization of laccase on fullerene, graphene oxide, and non-oxidized and oxidized CNT.[78] Results show that laccase immobilized on graphene oxide had the highest activity, which was about 60% of free enzyme.[78] The carbon immobilized laccases were also found to efficiently treat bisphenol A and catechol via a combination of degradation and adsorption.[78]

Besides these inorganic or organic-inorganic hybrid materials, a new class of materials, protein nanocages, are emerging in recent years. The application of protein nanocages in environmental remediation is rarely reported so far, however, they have been explored in medical applications and biosynthesis.[79] One of the big benefits of protein nanocages is that they are synthesized by cells, the process of which does not require hazardous chemical or harsh condition. By contrast, the synthesis of inorganic nanomaterials usually involves extreme pH,

organic solvents, toxic chemicals, and high temperature.[77, 80-82] The other advantage of protein nanocages is their low toxicity. A number of studies have suggested that inorganic nanomaterials, such as graphene, CNT and metallic nanomaterials, possess cytotoxicity and cause adverse effects to testing organisms. Thus, the potential environmental and health risk of such nanomaterials strongly hinders their application in field. On the contrary, being made from amino acids, protein nanocages are completely biodegradable and possess minimal impact to ecosystem, which makes them plausible enzyme carriers in environmental remediation. In addition, protein nanocages can be easily modified and programed through genetic techniques, which provide different materials that can fulfill various needs. For instance, Azuma et al. synthesized a supercharged protein cage by engineering lumazine synthase (LS).[83] The cage displays high negative charge on the interior, which attacks positively charged substrates and repels negatively charged substrates.[83] Protease was encapsulated inside of the LS cage through the electrostatic interaction between the cage interior and positively charged GFP attached to the protease.[83] The encapsulated protease preferentially cleaved positively charged polypeptides, and showed high selectivity.[83] In terms of bioremediation, protein cages can be engineered to selectively concentrate contaminants inside of the cage, which will increase the rate and efficiency of contaminants removal, especially for those at low environmental concentrations. Thus, protein cages have great potential as enzyme carriers for bioremediation applications, and may turn into more environmentally friendly and efficient alternatives to currently used inorganic enzyme immobilization supports.

**Table 1.3** Immobilization of Enzymes on Nanomaterials for Bioremediation

| Solid Support | Immobilization Method | Enzyme | Contaminant | Enzyme yield (%) | Specific activity yield (%) | Enzyme loading (mg enzyme /g support) | Leaching | Ref. |
|---|---|---|---|---|---|---|---|---|
| Nanogel | Entrapment | OPH | Organo-phosphate | NR | 95 | NR | NR | 42 |
| Nanogel | Entrapment | HRP | NR | NR | 100 | NR | NR | 66 |
| Iron nanoflower | Covalent | HRP | Phenolics | NR | 500-700 | NR | NR | 46 |
| Copper nanoflower | Covalent | Laccase | Chlorophenol | NR | 200-600 | NR | NR | 45 |
| Silica | Entrapment | CA | $CO_2$ | 40-100 | ~50 | 230 | <10% in 24 hours | 48 |
| Silica | Entrapment | CA | $CO_2$ | 40-100 | ~50 | NR | <1% in 24 hours | 74 |
| Porous silica bead | Covalent | Laccase | Organic dyes | NR | NR | NR | NR | 84 |
| Mesoporous silica | Covalent | Laccase | Phenolics | 100 | NR | NR | NR | 70 |
| Magnetic bimodal mesoporous carbon | Physical adsorption | Laccase | Phenolics | NR | 20-91 | 491.7 | NR | 75 |
| Graphene oxide | Physical adsorption | HRP | Phenolics | ~10 | NR | 100 | NR | 76 |

**Table 1.3** Immobilization of Enzymes on Nanomaterials for Bioremediation (continued)

| | | | | | | | | |
|---|---|---|---|---|---|---|---|---|
| CNT | Physical adsorption | Laccase | Phenolics | NR | 52 | NR | NR | 78 |
| Chitosan–halloysite hybrid | Physical adsorption | Laccase | Phenolics | NR | 123.1 | NR | NR | 87 |
| Lumazine synthase protein cage | Ionic binding | TEV proteases | NR | NR | ~500 | NR | NR | 83 |
| Ferritin cage | Ionic binding | Anhydrase, aldolase, | NR | NR | 90-110 | NR | NR | 86 |
| CCMV nanocages | Entrapment | Lipase | NR | NR | 70 | NR | NR | 85 |

## 1.3 Vault Nanoparticle

### 1.3.1 Natural vaults and recombinant vaults

Vaults are the largest cytoplasmic ribonucleoprotein particles occurring in nature. First discovered in 1986 at UCLA,[88] vault nanoparticles have been purified from a number of eukaryotes, such as humans, sea urchins, torpedo electric eels, bullfrogs, rabbits, mouse, and slime mode *Dictyostelium discoideum*,[89] whose structure is highly conserved and have a unique barrel-like morphology (Figure 1.1).[88, 90] Although the biological function of natural vault particles is still mysterious, vaults have been shown to involve in several cellular functions including multi-drug resistance, cell signaling, nuclear-cytoplasmic transport, mRNA localization, innate immunity, and nuclear pore assembly.[91, 92] Natural vaults are composed of three types of proteins and 1 or more copies of a small untranslated vault RNA. The Major Vault Protein (MVP) forms the outer shell of vaults, and makes up about 75% of the total protein mass in the particle.[93] Nucleic acid sequence analysis reveals the unique MVP coding sequence is highly conserved among eukaryotic species, which explains the conservation of vault structure. Multiple copies of two other protein components, vault poly(ADP-ribose) polymerase (VPARP) and telomerase-associated protein-1 (TEP1), and untranslated vault RNA fragments were located inside of vault lumen *via* Cryo-EM reconstruction of ribonuclease treated rat liver vaults and vaults purified from VPARP and TEP1 knockout mice.[94, 95] Vaults purified from rat liver have a mass about 13 MDa, and dimensions of 41 x 41 x 72.5 nm.[90] Each vault particle is assembled from seventy-eight copies of MVP, and contains two identical half-vaults.[90]

Although vaults are found in numerous eukaryotic species, no MVP homologues have been identified in insects, yeast, worms, or plants. When expressing MVP coding sequence in insect cells through the baculovirus system, formation of vault-like particles is observed. The

recombinant vaults have typical vaults' morphology and size, and are virtually undistinguishable from natural vaults when viewed under transmission electron microscope (TEM) (Figure 1.1). Formation of vault structures from MVP peptides is found to be mediated by polyribosomes, and the assembly and MVP translation take place simultaneously on singe MVP mRNA.[96] Differential Cryo-EM mapping of engineered recombinant vaults with modification at MVP N-terminal or C-terminal showed that the N-termini of 78 copies MVP joined at the particle waist and sequences attached to N-termini were buried in the vault lumen.[97, 98] C-termini of thirty-nine copies of MVP conjugate at one end of the particle, and sequences attached to MVP C-termini were localized on the particle surface.[97, 99]

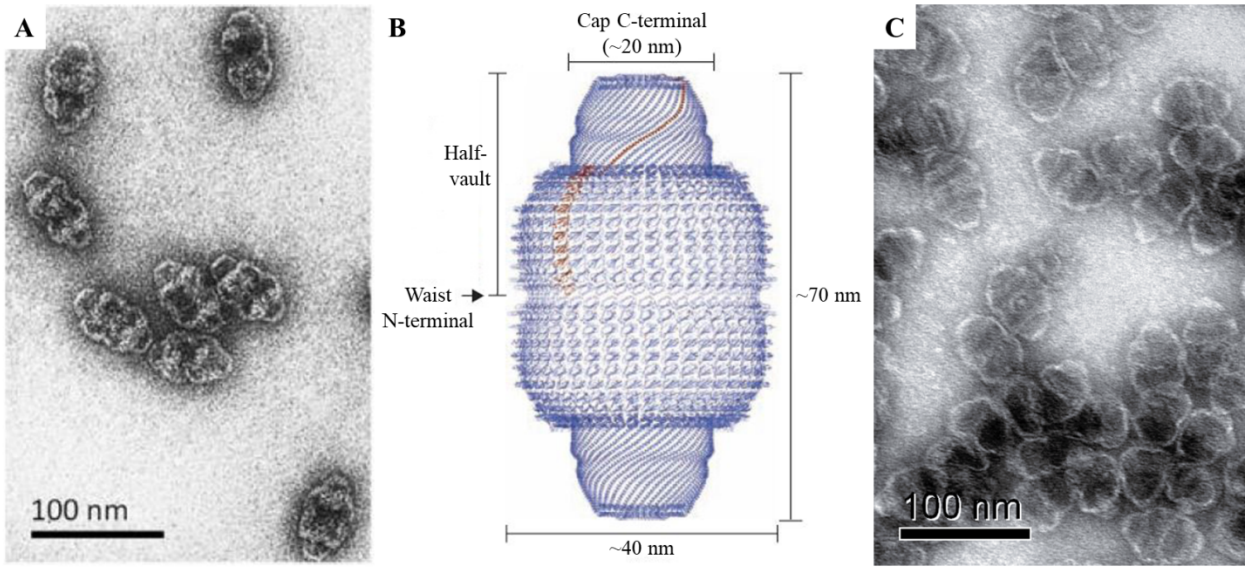


**Figure 1.1** Natural and Recombinant Vault Particles. (A) TEM image of natural vaults purified from rat liver.[92] (B) Overall structure of the MVP shell of vault.[90] (C) TEM image of recombinant vaults synthesized in insect Sf9 culture.

### 1.3.2 Vaults engineering

Modification of vault particles were mainly performed on recombinant vaults, as they are made solely from MVP peptides. Different from natural vaults that enclose VPARP, TEP1 and

RNA fragments, the interior of recombinant vaults is empty, which provides decent space for anchoring heterologous components, including but not limited to proteins,[100] lipids,[101] and nucleic acids.[102] In general, three approaches have been developed to engineer recombinant vaults (Figure 1.2).

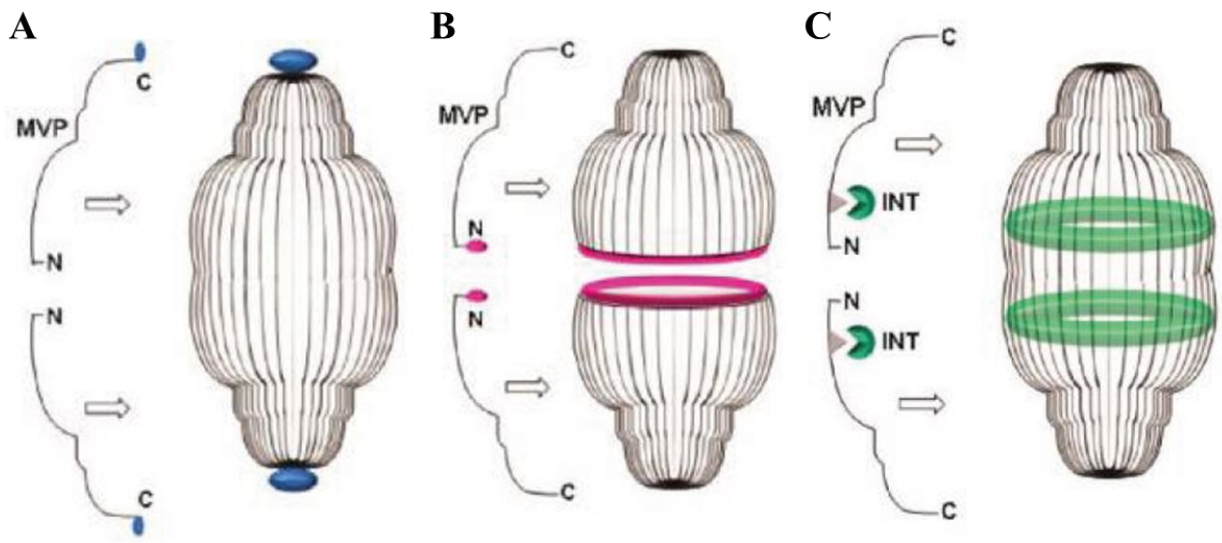


**Figure 1.2** Three Approaches Used to Engineer Vault Particles. (A) Modification at the C-terminal of MVP. C-terminal extensions (shown in blue) are displayed on the particle surface at the end of the caps. (B) Modification at the N-terminal of MVP. C-terminal extensions (shown in red) are buried inside of the particles at the waist. (C) INT strategy to engineer vaults. INT binding sites on MVP locate on the interior of vaults, and are below and above the waist, where INT fused components are anchored.[103]

The first approach is to directly modify MVP peptide, often through adding peptide or protein sequences to N- or C- terminal of MVP. As mentioned above, depending on which terminal the sequence is attached to, it can be displayed on vaults' surface, or buried inside the lumen, which endows recombinant vaults with different properties. For example, Kickhoefer et al. attached a 55 amino acid epidermal growth factor (EGF) tag to the C-terminus of MVP, and the modified vaults displayed epithelial cancer cells binding affinity due to the interaction between EGF peptides on vaults and EGF receptor (EGFR) on cell surface.[99] Han et al. reported the synthesis of recombinant vaults with N-termini modification.[103] The authors added a

membrane lytic peptide derived from adenovirus protein VI (pVI) to the N-terminal of MVP peptide.[103] The resultant pVI-vaults encapsulated 78 copies of membrane lytic peptides per particle, and efficiently disrupted the endosomal membrane, which facilitated the delivery of biomaterials to the cell cytoplasm.[103]

INT strategy is another vault engineering approach. The INT domain is defined as a 162 amino acid fragment at the C-terminal of VPARP (residues 1563-1724), which was the shortest MVP interacting region in VPARP identified in a yeast two-hybrid analysis using MVP as the bait.[94, 100] Acting as a zip code, INT domain can direct heterologous components that are fused to INT into vaults. INT conjugated components can be packaged into vaults either by co-expressing them with MVP or by simply mixing them with pre-synthesized recombinant vault particles. The dynamic structure of vaults allows incorporating of heterologous components even after the intact structure of vaults is formed. The first study of using INT domain to engineer vaults was reported by Kickhoefer et al. in 2005. The authors demonstrated that INT domain modified luciferase and green fluorescent protein (GFP) were uptaken by recombinant vaults and maintained their bioactivities.[100] Thus far, various biological components, such as proteins and peptides,[104] phospholipid bilayer nanodisk,[101] mRNA,[102] and chemokine,[105] have been packaged into vaults *via* the INT strategy.

Recently, chemical modification has been developed as a new approach to engineer vaults. As protein particles with a mass of 7.8 MDa, vaults have numerous derivatizable amino acid residues, displaying functional groups, such as amine groups, hydroxyl groups, carboxyl groups, thiol groups, pyrrolidine groups, and benzene groups, which can be chemically modified. For example, Benner et al. engineered vaults with fluorescein reporter probes and cell-penetrating peptides, through selective modification of lysine and cysteine residues on particle

surface.[106] The resultant engineered vaults showed enhanced uptake into cells of interest and assisted cell imaging.[106]

### 1.3.3 Vault Application

Applications of engineered vaults have been explored, mainly in medical field. Unlike many nanoparticles, vaults are biocompatible and non-immunogenic, and monodispersed even at high concentrations. The lumen of recombinant vaults is also large enough to anchor hundreds of protein molecules, and numerous small chemical molecules. Additionally, MVP terminal modification, INT strategy, and chemical modification have been developed as powerful tools to engineer and program vaults. All these properties together, make vaults great vessels for therapeutic delivery.

Mucosal immune responses offer superior protection against diseases, and are optimally produced by stimulating mucosal associated lymphoid tissue (MALT) with immunogenic proteins.[107] It has been proposed that delivery to dendritic cells in MALT through the Fc receptor of immunoglobulin (Ig) is an effective vaccination strategy for stimulating cell-mediated immune responses against many pathogens.[107] Champion et al. engineered the C-terminal of MVP with a Fc domain binding peptide Z, and packaged INT domain fused major outer membrane protein (MOMP) of *Chlamydia muridarum*.[107] MOMP is a highly immunogenic protein that is able to lessen development of infertility after *Chlamydia* infection.[107] MOMP-INT/MVP-Z was efficiently uptaken by dendritic cells, and intranasal dose of the engineered vaults to mice induced anti-chlamydial immunity and reduced bacterial burden following chlamydial genital infection.[107] These results suggest engineered vaults can serve as vaccine delivery vessel to induce protective immunity against microbial infection.[92, 107]

The other potential application of engineered vaults is as tumor immunotherapy. CCL21 is a lymphoid chemokine that can attract immune cells including dendritic cells and T cells.[105] Kar et al. constructed CCL21-INT, which was then packaged into vaults.[105] The engineered vaults were shown to attract T cells and elevate dendritic cells APC activity *in vitro*, and reduce lung tumor growth in mice through intratumoral delivery of CCL21 *in vivo*,[105] underlining the potential of using engineered vault particles to deliver antitumor cytokines.

Delivery of hydrophobic drugs is another reported therapeutic application of engineered vaults. Buehler et al. engineered the N-terminal of MVP with a lipophilic peptide AH derived from the cell membrane interaction region of hepatitis C virus.[101] The incorporation of AH peptides to vaults created a lipophilic microenvironment in the vault lumen, which enabled reversible encapsulation of lipophilic compounds in vaults.[101] The resultant AH-vaults were shown to preferentially uptake lipophilic therapeutics and deliver them to cells *in vitro* and *in vivo*.[101] These findings further contribute to the development of vaults-based platform for therapeutic delivery.

### 1.4 Summary

As environment-friendly and efficient biocatalysts, enzymes are being widely used in industrial processes to replace inorganic catalysts. In environmental field, enzymatic bioremediation is also a promising alternative to microbial remediation and conventional physicochemical processes. However, due to the vulnerable nature of proteins, enzymes are usually not stable, can be inactivated by inhibitors, unfavorable operating conditions, and the products formed by their own activities, thus leading to high cost of enzyme usage. The

immobilization of enzymes appears to be an effective approach to overcome this economical drawback, as immobilized enzymes are more stable and can be easily reused.

To date, although numerous solid supports have been developed for enzyme immobilization, there still remain several unresolved issues, especially towards bioremediation applications. Conventional solid supports for enzymes immobilization are usually large matrices, which cause substrate diffusional limitation and mass transfer resistance, thus leading to reduced enzyme activity. Enzyme loading capacity on these large matrices is also low. Recent advances in nanotechnology leads to development of numerous inorganic nanomaterials, which appear to be superior alternatives to those large enzyme supports. Due to their small dimensions, mass transfer limitation is minimalized, and the large surface area of nanomaterials also provides abundant enzyme binding sites, resulting in higher loading capacity. However, in respect of environmental application, these nanomaterials are not perfect candidates for immobilizing biodegradative enzymes, primarily due to two reasons. First, the synthesis of inorganic organic materials often require harsh conditions, organic solvent, and other toxic chemicals, which results in extra emission of hazardous wastes. Second, many studies have shown that these nanomaterials induce cytotoxicity and cause adverse effects in testing organism. Application of such nanomaterials as supports in enzymatic bioremediation may cause unforeseen environmental and health impact. Thus, developing eco-friendly, safe and effective approaches to immobilize enzymes for environmental applications remains challenging.

Protein nanocages appear to be a plausible enzyme carrier for environmental remediation, as they are synthesized by cells under physiological condition and are completely biodegradable. Vaults are the largest ribonucleoprotein particles found in nature. Derived from natural vaults, recombinant vaults are assembled from seventy-eight copies of MVP peptide, and possess large

lumen for anchoring heterologous enzyme molecules. As compared to other protein nanocages, vaults are non-immunogenic and biocompatible. Moreover, the antigen-antibody like interaction between INT domain and vaults also enables efficient simultaneous purification and encapsulation of enzymes from raw extracts, which significantly lower the immobilization cost. Taken together, the unique properties of vaults and vault-encapsulation suggest that vault particles would be great enzyme immobilization supports, especially for environmental applications.

My Ph.D. research projects mainly focused on the development of vaults-based enzyme immobilization platform for environmental applications. In this dissertation, researches on the following aspects are discussed in detail accordingly.

- Develop vaults encapsulated MnP, and demonstrate its enhanced stability and catalytic performance (Chapter 2)
- Evaluate the performance of vaults encapsulated MnP in removing and detoxifying bisphenolic contaminants (Chapter 3)
- Develop yeast as the host for economical production of recombinant vaults (Chapter 4)
- Develop vault-based silica support, and evaluate its application in enzyme immobilization (Chapter 5)

## 1.5 References


1. Hamby, D. M. Site remediation techniques supporting environmental restoration activities - A review. *Science of the Total Environment* **1996,** *191* (3), 203-224.
2. Kumar, A.; Bisht, B. S.; Joshi, V. D.; Dhewa, T. Review on Bioremediation of Polluted Environment: A Management Tool. *International Journal of Environmental Sciences* **2011,** *1* (6), 1079.
3. Watanabe, M. E. Can bioremediation bounce back? *Nature Biotechnology* **2001,** *19* (12), 1111-1115.
4. Farhadian, M.; Vachelard, C.; Duchez, D.; Larroche, C. In situ bioremediation of monoaromatic pollutants in groundwater: A review. *Bioresource Technology* **2008,** *99* (13), 5296-5308.
5. Atlas, R. M. Bioremediation of Petroleum Pollutants. *International Biodeterioration & Biodegradation* **1995,** *35* (1-3), 317-327.
6. Robinson, P. K. Enzymes: principles and biotechnological applications. *Understanding Biochemistry: Enzymes and Membranes* **2015,** *59*, 1-41.
7. DiCosimo, R.; McAuliffe, J.; Poulose, A. J.; Bohlmann, G. Industrial use of immobilized enzymes. *Chemical Society Reviews* **2013,** *42* (15), 6437-6474.
8. Kalantari, M.; Yu, M. H.; Yang, Y. N.; Strounina, E.; Gu, Z. Y.; Huang, X. D.; Zhang, J.; Song, H.; Yu, C. Z. Tailoring mesoporous-silica nanoparticles for robust immobilization of lipase and biocatalysis. *Nano Research* **2017,** *10* (2), 605-617.
9. Srirangan, K.; Orr, V.; Akawi, L.; Westbrook, A.; Moo-Young, M.; Chou, C. P. Biotechnological advances on Penicillin G acylase: Pharmaceutical implications, unique

expression mechanism and production strategies. *Biotechnology Advances* **2013,** *31* (8), 1319-1332.

10. Sutherland, T. D.; Horne, I.; Weir, K. M.; Coppin, C. W.; Williams, M. R.; Selleck, M.; Russell, R. J.; Oakeshott, J. G. Enzymatic bioremediation: From enzyme discovery to applications. *Clinical and Experimental Pharmacology and Physiology* **2004,** *31* (11), 817-821.
11. Karigar, C. S.; Rao, S. S. Role of microbial enzymes in the bioremediation of pollutants: a review. *Enzyme research* **2011,** *2011*, 805187.
12. Majcherczyk, A.; Johannes, C.; Huttermann, A. Oxidation of polycyclic aromatic hydrocarbons (PAH) by laccase of Trametes versicolor. *Enzyme and Microbial Technology* **1998,** *22* (5), 335-341.
13. Pointing, S. B.; Vrijmoed, L. L. P. Decolorization of azo and triphenylmethane dyes by Pycnoporus sanguineus producing laccase as the sole phenoloxidase. *World Journal of Microbiology & Biotechnology* **2000,** *16* (3), 317-318.
14. Fukuda, T.; Uchida, H.; Takashima, Y.; Uwajima, T.; Kawabata, T.; Suzuki, M. Degradation of bisphenol a by purified laccase from Trametes villosa. *Biochemical and Biophysical Research Communications* **2001,** *284* (3), 704-706.
15. Luo, Q.; Lu, J. H.; Zhang, H.; Wang, Z. Y.; Feng, M. B.; Chiang, S. Y. D.; Woodward, D.; Huang, Q. G. Laccase-Catalyzed Degradation of Perfluorooctanoic Acid. *Environmental Science & Technology Letters* **2015,** *2* (7), 198-203.
16. Luo, Q.; Liang, S.; Huang, Q. Laccase induced degradation of perfluorooctanoic acid in a soil slurry. *Journal of Hazardous Materials* **2018,** *359*, 241-247.

17. Singh, R.; Cabrera, M. L.; Radcliffe, D. E.; Zhang, H.; Huang, Q. G. Laccase mediated transformation of 17 beta-estradiol in soil. *Environmental Pollution* **2015,** *197*, 28-35.

18. Wen, X. H.; Jia, Y. N.; Li, J. X. Degradation of tetracycline and oxytetracycline by crude lignin peroxidase prepared from *Phanerochaete chrysosporium* - A white rot fungus. *Chemosphere* **2009,** *75* (8), 1003-1007.

19. Hammel, K. E.; Tardone, P. J. The Oxidative 4-Dechlorination of Polychlorinated Phenols Is Catalyzed by Extracellular Fungal Lignin Peroxidases. *Biochemistry* **1988,** *27* (17), 6563-6568.

20. Mao, L. A.; Huang, Q. G.; Luo, Q.; Lu, J. H.; Yang, X.; Gao, S. X. Ligninase-mediated removal of 17 beta-estradiol from water in the presence of natural organic matter: Efficiency and pathways. *Chemosphere* **2010,** *80* (4), 469-473.

21. Paszczynski, A.; Crawford, R. L. Degradation of Azo-Compounds by Ligninase from *Phanerochaete chrysosporium* - Involvement of Veratryl Alcohol. *Biochemical and Biophysical Research Communications* **1991,** *178* (3), 1056-1063.

22. Sack, U.; Hofrichter, M.; Fritsche, W. Degradation of polycyclic aromatic hydrocarbons by manganese peroxidase of Nematoloma frowardii. *Fems Microbiology Letters* **1997,** *152* (2), 227-234.

23. Hirano, T.; Honda, Y.; Watanabe, T.; Kuwahara, M. Degradation of bisphenol A by the lignin-degrading enzyme, manganese peroxidase, produced by the white-rot basidiomycete, *Pleurotus ostreatus*. *Bioscience, Biotechnology, and Biochemistry* **2000,** *64* (9), 1958-1962.

24. Harazono, K.; Watanabe, Y.; Nakamura, K. Decolorization of azo dye by the white-rot basidiomycete Phanerochaete sordida and by its manganese peroxidase. *Journal of Bioscience and Bioengineering* **2003,** *95* (5), 455-459.

25. Ali, L.; Algaithi, R.; Habib, H. M.; Souka, U.; Rauf, M. A.; Ashraf, S. S. Soybean peroxidase-mediated degradation of an azo dye- a detailed mechanistic study. *BMC Biochemistry* **2013,** *14*.

26. Li, J. H.; Peng, J. B.; Zhang, Y.; Ji, Y. F.; Shi, H. H.; Mao, L.; Gao, S. X. Removal of triclosan via peroxidases-mediated reactions in water: Reaction kinetics, products and detoxification. *Journal of Hazardous Materials* **2016,** *310*, 152-160.

27. Colosi, L. M.; Burlingame, D. J.; Huang, Q. G.; Weber, W. J. Peroxidase-mediated removal of a polychlorinated biphenyl using natural organic matter as the sole cosubstrate. *Environmental Science & Technology* **2007,** *41* (3), 891-896.

28. Mohan, S. V.; Prasad, K. K.; Rao, N. C.; Sarma, P. N. Acid azo dye degradation by free and immobilized horseradish peroxidase (HRP) catalyzed process. *Chemosphere* **2005,** *58* (8), 1097-1105.

29. Bayramoglu, G.; Akbulut, A.; Arica, M. Y. Immobilization of tyrosinase on modified diatom biosilica: Enzymatic removal of phenolic compounds from aqueous solution. *Journal of Hazardous Materials* **2013,** *244*, 528-536.

30. Reategui, E.; Reynolds, E.; Kasinkas, L.; Aggarwal, A.; Sadowsky, M. J.; Aksan, A.; Wackett, L. P. Silica gel-encapsulated AtzA biocatalyst for atrazine biodegradation. *Applied Microbiology and Biotechnology* **2012,** *96* (1), 231-240.

31. Scott, C.; Lewis, S. E.; Milla, R.; Taylor, M. C.; Rodgers, A. J. W.; Dumsday, G.; Brodie, J. E.; Oakeshott, J. G.; Russell, R. J. A free-enzyme catalyst for the bioremediation of environmental atrazine contamination. *Journal of Environmental Management* **2010,** *91* (10), 2075-2078.

32. Tien, M.; Kirk, T. K. Lignin peroxidase of *Phanerochaete chrysosporium*. *Methods in Enzymology* **1988,** *161*, 238-249.

33. Hofrichter, M. Review: lignin conversion by manganese peroxidase (MnP). *Enzyme and Microbial Technology* **2002,** *30* (4), 454-466.

34. Tien, M.; Kirk, T. K. Lignin Peroxidase of *Phanerochaete chrysosporium*. *Methods in Enzymology* **1988,** *161*, 238-249.

35. Gold, M. H.; Wariishi, H.; Renganathan, V.; Valli, K. Lignin Peroxidase and Manganese Peroxidase - Extracellular Ligninases from *Phanerochaete chrysosporium*. *Abstracts of Papers of the American Chemical Society* **1988,** *196*, 388-INOR.

36. Gold, M. H.; Glenn, J. K. Manganese Peroxidase from *Phanerochaete chrysosporium*. *Methods in Enzymology* **1988,** *161*, 258-264.

37. Riva, S. Laccases: blue enzymes for green chemistry. *Trends in Biotechnology* **2006,** *24* (5), 219-226.

38. Spadaro, J. T.; Renganathan, V. Peroxidase-catalyzed oxidation of azo dyes: mechanism of Disperse Yellow 3 degradation. *Archives of Biochemistry and Biophysics* **1994,** *312* (1), 301-307.

39. Pereira, J. R.; Mendez, J. Inhibition of Peroxidase by Algal Humic and Fulvic Acids. *Biologia Plantarum* **1976,** *18* (3), 179-182.

40. Franssen, M. C. R.; Steunenberg, P.; Scott, E. L.; Zuilhof, H.; Sanders, J. P. M. Immobilised enzymes in biorenewables production. *Chemical Society Reviews* **2013,** *42* (15), 6491-6533.

41. Tuisel, H.; Sinclair, R.; Bumpus, J. A.; Ashbaugh, W.; Brock, B. J.; Aust, S. D. Lignin Peroxidase H2 from *Phanerochaete chrysosporium* - Purification, Characterization and

Stability to Temperature and Ph. *Archives of Biochemistry and Biophysics* **1990,** *279* (1), 158-166.

42. Wei, W.; Du, J. J.; Li, J.; Yan, M.; Zhu, Q.; Jin, X.; Zhu, X. Y.; Hu, Z. M.; Tang, Y.; Lu, Y. F. Construction of Robust Enzyme Nanocapsules for Effective Organophosphate Decontamination, Detoxification, and Protection. *Advanced Materials* **2013,** *25* (15), 2212-2218.
43. Sheldon, R. A.; van Pelt, S. Enzyme immobilisation in biocatalysis: why, what and how. *Chemical Society Reviews* **2013,** *42* (15), 6223-6235.
44. Cipolatti, E. P.; Valerio, A.; Henriques, R. O.; Moritz, D. E.; Ninow, J. L.; Freire, D. M. G.; Manoel, E. A.; Fernandez-Lafuente, R.; de Oliveira, D. Nanomaterials for biocatalyst immobilization - state of the art and future trends. *RSC Advances* **2016,** *6* (106), 104675-104692.
45. Ge, J.; Lei, J. D.; Zare, R. N. Protein-inorganic hybrid nanoflowers. *Nature Nanotechnology* **2012,** *7* (7), 428-432.
46. Ocsoy, I.; Dogru, E.; Usta, S. A new generation of flowerlike horseradish peroxides as a nanobiocatalyst for superior enzymatic activity. *Enzyme and Microbial Technology* **2015,** *75-76*, 25-29.
47. Liese, A.; Hilterhaus, L. Evaluation of immobilized enzymes for industrial applications. *Chemical Society Reviews* **2013,** *42* (15), 6236-6249.
48. Forsyth, C.; Yip, T. W. S.; Patwardhan, S. V. CO2 sequestration by enzyme immobilized onto bioinspired silica. *Chemical Communications* **2013,** *49* (31), 3191-3193.

49. Alemzadeh, I.; Nejati, S. Removal of Phenols with Encapsulated Horseradish Peroxidase in Calcium Alginate. *Iranian Journal of Chemistry & Chemical Engineering-International English Edition* **2009,** *28* (2), 43-49.

50. Nelson, J. M.; Griffin, E. G. Adsorption of invertase. *Journal of the American Chemical Society* **1916,** *38*, 1109-1115.

51. Bodalo, A.; Bastida, J.; Maximo, M. F.; Montiel, M. C.; Gomez, M.; Murcia, M. D. A comparative study of free and immobilized soybean and horseradish peroxidases for 4-chlorophenol removal: protective effects of immobilization. *Bioprocess and Biosystems Engineering* **2008,** *31* (6), 587-593.

52. Cabana, H.; Alexandre, C.; Agathos, S. N.; Jones, J. P. Immobilization of laccase from the white rot fungus Coriolopsis polyzona and use of the immobilized biocatalyst for the continuous elimination of endocrine disrupting chemicals. *Bioresource Technology* **2009,** *100* (14), 3447-3458.

53. Menale, C.; Nicolucci, C.; Catapane, M.; Rossi, S.; Bencivenga, U.; Mita, D. G.; Diano, N. Optimization of operational conditions for biodegradation of chlorophenols by laccase-polyacrilonitrile beads system. *Journal of Molecular Catalysis B: Enzymatic* **2012,** *78*, 38-44.

54. Nguyen, L. N.; Hai, F. I.; Dosseto, A.; Richardson, C.; Price, W. E.; Nghiem, L. D. Continuous adsorption and biotransformation of micropollutants by granular activated carbon-bound laccase in a packed-bed enzyme reactor. *Bioresource Technology* **2016,** *210*, 108-116.

55. Qiu, L. F.; Huang, Z. X. The treatment of chlorophenols with laccase immobilized on sol-gel-derived silica. *World Journal of Microbiology & Biotechnology* **2010,** *26* (5), 775-781.

56. Stclair, N. L.; Navia, M. A. Cross-Linked Enzyme Crystals as Robust Biocatalysts. *Journal of the American Chemical Society* **1992,** *114* (18), 7314-7316.

57. Cao, L.; van Rantwijk, F.; Sheldon, R. A. Cross-linked enzyme aggregates: a simple and effective method for the immobilization of penicillin acylase. *Organic Letters* **2000,** *2* (10), 1361-4.

58. Dave, B. C.; Dunn, B.; Valentine, J. S.; Zink, J. I. Sol-Gel Encapsulation Methods for Biosensors. *Analytical Chemistry* **1994,** *66* (22), A1120-A1127.

59. Lloret, L.; Eibes, G.; Feijoo, G.; Moreira, M. T.; Lema, J. M.; Hollmann, F. Immobilization of laccase by encapsulation in a sol-gel matrix and its characterization and use for the removal of estrogens. *Biotechnology Progress* **2011,** *27* (6), 1570-1579.

60. Caramori, S. S.; Fernandes, K. F. Covalent immobilisation of horseradish peroxidase onto poly (ethylene terephthalate)-poly (aniline) composite. *Process Biochemistry* **2004,** *39* (7), 883-888.

61. Fernandes, K. F.; Lima, C. S.; Pinho, H.; Collins, C. H. Immobilization of horseradish peroxidase onto polyaniline polymers. *Process Biochemistry* **2003,** *38* (9), 1379-1384.

62. Liu, Y. C.; Qian, J. H.; Fu, X. L.; Liu, H. Y.; Deng, J. Q.; Yu, T. Y. Immobilization of horseradish peroxidase onto a composite membrane of regenerated silk fibroin and polyvinyl alcohol and its application to a new methylene blue-mediating sensor for hydrogen peroxide. *Enzyme and Microbial Technology* **1997,** *21* (3), 154-159.

63. Rinaudo, M. Chitin and chitosan: Properties and applications. *Progress in Polymer Science* **2006,** *31* (7), 603-632.

64. Bayramoglu, G.; Yilmaz, M.; Arica, M. Y. Preparation and characterization of epoxy-functionalized magnetic chitosan beads: laccase immobilized for degradation of reactive dyes. *Bioprocess and Biosystems Engineering* **2010,** *33* (4), 439-448.

65. Niladevi, K. N.; Prema, P. Immobilization of laccase from Streptomyces psammoticus and its application in phenol removal using packed bed reactor. *World Journal of Microbiology & Biotechnology* **2008,** *24* (7), 1215-1222.

66. Yan, M.; Ge, J.; Liu, Z.; Ouyang, P. K. Encapsulation of single enzyme in nanogel with enhanced biocatalytic activity and stability. *Journal of the American Chemical Society* **2006,** *128* (34), 11008-11009.

67. Beck, J. S.; Vartuli, J. C.; Roth, W. J.; Leonowicz, M. E.; Kresge, C. T.; Schmitt, K. D.; Chu, C. T. W.; Olson, D. H.; Sheppard, E. W.; Mccullen, S. B.; Higgins, J. B.; Schlenker, J. L. A New Family of Mesoporous Molecular-Sieves Prepared with Liquid-Crystal Templates. *Journal of the American Chemical Society* **1992,** *114* (27), 10834-10843.

68. Li, W.; Liu, J.; Zhao, D. Y. Mesoporous materials for energy conversion and storage devices. *Nature Reviews Materials* **2016,** *1* (6).

69. Mao, C. B.; Wang, F. K.; Cao, B. R. Controlling Nanostructures of Mesoporous Silica Fibers by Supramolecular Assembly of Genetically Modifiable Bacteriophages. *Angewandte Chemie International Edition* **2012,** *51* (26), 6411-6415.

70. Salis, A.; Pisano, M.; Monduzzi, M.; Solinas, V.; Sanjust, E. Laccase from Pleurotus sajor-caju on functionalised SBA-15 mesoporous silica: Immobilisation and use for the oxidation of phenolic compounds. *Journal of Molecular Catalysis B: Enzymatic* **2009,** *58* (1-4), 175-180.

71. Liu, B.; Cao, Y. Y.; Huang, Z. H.; Duan, Y. Y.; Che, S. N. Silica Biomineralization via the Self-Assembly of Helical Biomolecules. *Advanced Materials* **2015,** *27* (3), 479-497.

72. Kroger, N.; Deutzmann, R.; Sumper, M. Polycationic peptides from diatom biosilica that direct silica nanosphere formation. *Science* **1999,** *286* (5442), 1129-1132.

73. Luckarift, H. R.; Spain, J. C.; Naik, R. R.; Stone, M. O. Enzyme immobilization in a biomimetic silica support. *Nature Biotechnology* **2004,** *22* (2), 211-213.

74. Jo, B. H.; Seo, J. H.; Yang, Y. J.; Baek, K.; Choi, Y. S.; Pack, S. P.; Oh, S. H.; Cha, H. J. Bioinspired Silica Nanocomposite with Autoencapsulated Carbonic Anhydrase as a Robust Biocatalyst for $CO_2$ Sequestration. *ACS Catalysis* **2014,** *4* (12), 4332-4340.

75. Liu, Y. Y.; Zeng, Z. T.; Zeng, G. M.; Tang, L.; Pang, Y.; Li, Z.; Liu, C.; Lei, X. X.; Wu, M. S.; Ren, P. Y.; Liu, Z. F.; Chen, M.; Xie, G. X. Immobilization of laccase on magnetic bimodal mesoporous carbon and the application in the removal of phenolic compounds. *Bioresource Technology* **2012,** *115*, 21-26.

76. Zhang, F.; Zheng, B.; Zhang, J. L.; Huang, X. L.; Liu, H.; Guo, S. W.; Zhang, J. Y. Horseradish Peroxidase Immobilized on Graphene Oxide: Physical Properties and Applications in Phenolic Compound Removal. *Journal of Physical Chemistry C* **2010,** *114* (18), 8469-8473.

77. Jiang, B.; Yang, K. G.; Zhang, L. H.; Liang, Z.; Peng, X. J.; Zhang, Y. K. Dendrimer-grafted graphene oxide nanosheets as novel support for trypsin immobilization to achieve fast on-plate digestion of proteins. *Talanta* **2014,** *122*, 278-284.

78. Pang, R.; Li, M. Z.; Zhang, C. D. Degradation of phenolic compounds by laccase immobilized on carbon nanomaterials: Diffusional limitation investigation. *Talanta* **2015,** *131*, 38-45.

79. Patterson, D. P.; Prevelige, P. E.; Douglas, T. Nanoreactors by Programmed Enzyme Encapsulation Inside the Capsid of the Bacteriophage P22. *ACS Nano* **2012,** *6* (6), 5000-5009.

80. Mohamad, N. R.; Buang, N. A.; Mahat, N. A.; Lok, Y. Y.; Huyop, F.; Aboul-Enein, H. Y.; Wahab, R. A. A facile enzymatic synthesis of geranyl propionate by physically adsorbed Candida rugosa lipase onto multi-walled carbon nanotubes. *Enzyme and Microbial Technology* **2015,** *72*, 49-55.

81. Xu, C.; Xu, X.; Su, J.; Ding, Y. Research on unsupported nanoporous gold catalyst for CO oxidation. *Journal of Catalysis* **2007,** *252* (2), 243-248.

82. Zhu, J.; Sun, G. Lipase immobilization on glutaraldehyde-activated nanofibrous membranes for improved enzyme stabilities and activities. *Reactive & Functional Polymers* **2012,** *72* (11), 839-845.

83. Azuma, Y.; Bader, D. L. V.; Hilvert, D. Substrate Sorting by a Supercharged Nanoreactor. *Journal of the American Chemical Society* **2018,** *140* (3), 860-863.

84. Champagne, P. P.; Ramsay, J. A. Dye decolorization and detoxification by laccase immobilized on porous glass beads. *Bioresource Technology* **2010,** *101* (7), 2230-2235.

85. Schoonen, L.; Nolte, R. J. M.; van Hest, J. C. M. Highly efficient enzyme encapsulation in a protein nanocage: towards enzyme catalysis in a cellular nanocompartment mimic. *Nanoscale* **2016,** *8* (30), 14467-14472.

86. Tetter, S.; Hilvert, D. Enzyme Encapsulation by a Ferritin Cage. *Angewandte Chemie International Edition* **2017,** *56* (47), 14933-14936.

87. Yao, J. L.; Wang, Q. R.; Wang, Y. Y.; Zhang, Y. T.; Zhang, B.; Zhang, H. S. Immobilization of laccase on chitosan-halloysite hybrid porous microspheres for phenols removal. *Desalination and Water Treatment* **2015,** *55* (5), 1293-1301.

88. Kedersha, N. L.; Rome, L. H. Isolation and characterization of a novel ribonucleoprotein particle: large structures contain a single species of small RNA. *Journal of Cell Biology* **1986,** *103* (3), 699-709.

89. Kedersha, N. L.; Miquel, M. C.; Bittner, D.; Rome, L. H. Vaults. II. Ribonucleoprotein structures are highly conserved among higher and lower eukaryotes. *Journal of Cell Biology* **1990,** *110* (4), 895-901.

90. Tanaka, H.; Kato, K.; Yamashita, E.; Sumizawa, T.; Zhou, Y.; Yao, M.; Iwasaki, K.; Yoshimura, M.; Tsukihara, T. The structure of rat liver vault at 3.5 angstrom resolution. *Science* **2009,** *323*, 384-388.

91. Berger, W.; Steiner, E.; Grusch, M.; Elbling, L.; Micksche, M. Vaults and the major vault protein: novel roles in signal pathway regulation and immunity. *Cellular and Molecular Life Sciences* **2009,** *66* (1), 43-61.

92. Rome, L. H.; Kickhoefer, V. A. Development of the vault particle as a platform technology. *ACS Nano* **2013,** *7* (2), 889-902.

93. Kedersha, N. L.; Heuser, J. E.; Chugani, D. C.; Rome, L. H. Vaults. III. Vault ribonucleoprotein particles open into flower-like structures with octagonal symmetry. *Journal of Cell Biology* **1991,** *112* (2), 225-235.

94. Kickhoefer, V. A.; Siva, A. C.; Kedersha, N. L.; Inman, E. M.; Ruland, C.; Streuli, M.; Rome, L. H. The 193-kD vault protein, VPARP, is a novel poly(ADP-ribose) polymerase. *Journal of Cell Biology* **1999,** *146* (5), 917-928.

95. Kickhoefer, V. A.; Stephen, A. G.; Harrington, L.; Robinson, M. O.; Rome, L. H. Vaults and telomerase share a common subunit, TEP1. *Journal of Biological Chemistry* **1999,** *274* (46), 32712-32717.

96. Mrazek, J.; Toso, D.; Ryazantsev, S.; Zhang, X.; Zhou, Z. H.; Fernandez, B. C.; Kickhoefer, V. A.; Rome, L. H. Polyribosomes are molecular 3D nanoprinters that orchestrate the assembly of vault particles. *ACS Nano* **2014,** *8* (11), 11552-11559.

97. Mikyas, Y.; Makabi, M.; Raval-Fernandes, S.; Harrington, L.; Kickhoefer, V. A.; Rome, L. H.; Stewart, P. L. Cryoelectron microscopy imaging of recombinant and tissue derived vaults: localization of the MVP N termini and VPARP. *Journal of Molecular Biology* **2004,** *344* (1), 91-105.

98. Ding, K.; Zhang, X.; Mrazek, J.; Kickhoefer, V. A.; Lai, M.; Ng, H. L.; Yang, O. O.; Rome, L. H.; Zhou, Z. H. Solution Structures of Engineered Vault Particles. *Structure* **2018,** *26* (4), 619-+.

99. Kickhoefer, V. A.; Han, M.; Raval-Fernandes, S.; Poderycki, M. J.; Moniz, R. J.; Vaccari, D.; Silvestry, M.; Stewart, P. L.; Kelly, K. A.; Rome, L. H. Targeting vault nanoparticles to specific cell surface receptors. *ACS Nano* **2009,** *3* (1), 27-36.

100. Kickhoefer, V. A.; Garcia, Y.; Mikyas, Y.; Johansson, E.; Zhou, J. C.; Raval-Fernandes, S.; Minoofar, P.; Zink, J. I.; Dunn, B.; Stewart, P. L.; Rome, L. H. Engineering of vault nanocapsules with enzymatic and fluorescent properties. *Proceedings of the National Academy of Sciences of the United States of America* **2005,** *102*, 4348-4352.

101. Buehler, D. C.; Toso, D. B.; Kickhoefer, V. A.; Zhou, Z. H.; Rome, L. H. Vaults engineered for hydrophobic drug delivery. *Small* **2011,** *7*, 1432-1439.

102. Pupols, M.; Kickhoefer, V. A.; Rome, L. H. Nucleic acid nanocapsules: packaging mRNA into the vault particle. *Faseb Journal* **2010,** *24*.

103. Han, M.; Kickhoefer, V. A.; Nemerow, G. R.; Rome, L. H. Targeted vault nanoparticles engineered with an endosomolytic peptide deliver biomolecules to the cytoplasm. *ACS Nano* **2011,** *5*, 6128-6137.

104. Lai, C. Y.; Wiethoff, C. M.; Kickhoefer, V. A.; Rome, L. H.; Nemerow, G. R. Vault nanoparticles containing an adenovirus-derived membrane lytic protein facilitate toxin and gene transfer. *ACS Nano* **2009,** *3* (3), 691-699.

105. Kar, U. K.; Srivastava, M. K.; Andersson, A.; Baratelli, F.; Huang, M.; Kickhoefer, V. A.; Dubinett, S. M.; Rome, L. H.; Sharma, S. Novel CCL21-vault nanocapsule intratumoral delivery inhibits lung cancer growth. *PLoS ONE* **2011,** *6* (5), e18758.

106. Benner, N. L.; Zang, X. Y.; Buehler, D. C.; Kickhoefer, V. A.; Rome, M. E.; Rome, L. H.; Wender, P. A. Vault Nanoparticles: Chemical Modifications for Imaging and Enhanced Delivery. *ACS Nano* **2017,** *11* (1), 872-881.

107. Champion, C. I.; Kickhoefer, V. A.; Liu, G. C.; Moniz, R. J.; Freed, A. S.; Bergmann, L. L.; Vaccari, D.; Raval-Fernandes, S.; Chan, A. M.; Rome, L. H.; Kelly, K. A. A Vault Nanoparticle Vaccine Induces Protective Mucosal Immunity. *PLoS ONE* **2009,** *4* (4).

## Chapter 2 Vault Nanoparticles Packaged with Enzymes as an Efficient Pollutant Biodegradation Technology

### 2.1 Introduction

Biological remediation is a cost effective *in situ* treatment technology for cleaning contaminated soil and water, and has been successfully applied to treat a wide range of inorganic and organic contaminants.[1-3] Current bioremediation research and practice mostly focuses on processes using microbial whole cells, which rely on microbial growth and are highly constrained by local biogeochemical conditions including oxygen levels, nutrient availability, pH, temperature, dissolved ions, soil permeability, and co-contaminants. In addition, the application of microbial cells has the potential of releasing pathogens to the environment and affecting local microbial community. As an alternative approach, enzymatic bioremediation has been proposed because *in vitro* enzymes are not constrained by the requirements for microbial growth and public health concerns. Additionally, due to their high catalytic efficiency, enzymatic remediation is generally more rapid, and can be accomplished in days or weeks.[4, 5] Manganese peroxidase (MnP), which has been isolated from several fungi,[6-9] has been previously applied in environmental bioremediation due to its ability to mediate oxidation and removal of a broad range of contaminants including polycyclic aromatic hydrocarbons,[6] phenolic compounds,[9, 10] and azo dyes,[11] using $H_2O_2$ as the terminal electron acceptor.

In spite of these advantages, the application of free enzymes for remediation is restricted by their limited stability under natural environments. Macro-sized enzyme immobilization, including surface binding and encapsulation, has been previously used for enhancing enzymatic stability.[12, 13] Through covalently binding to solid surfaces or physically packaging in solid matrices, immobilized enzymes present higher stability against a variety of inhibitors, such as

organic solvents and thermal inactivation. However, due to strong covalent binding and extra substrate diffusion resistance from solid matrices, immobilized enzymes generally show lower efficiency and much higher Michaelis half-saturation constant ($K_m$) values, which result in longer remediation times.[14, 15] Several nano-sized encapsulation methods have been developed to improve enzymatic stability without significantly affecting catalytic efficiency.[14-20] Nevertheless, to date, most of these techniques require multiple reaction steps and well-controlled conditions.

Vault nanoparticles, which are classified as ribonucleoprotein particles, are commonly found in various eukaryotic organisms[21-25] with a highly conserved barrel shape. Most natural vaults are comprised of four components, including 78 copies of the major vault protein (MVP), which forms the outer vault shell and makes up over 70% of the total mass of the vault. Inside naturally-occurring vaults isolated from higher eukaryotes are multiple copies of vault poly(ADP-ribose) polymerase (VPARP), which has a few domains tightly bound to vault shells, several copies of telomerase-associated protein-1 (TEP1), and small untranslated RNAs (vRNA).[26-30] Two identical half vaults, each consisting of 39 MVP chains, are bound together with their N-termini at the barrel waist to form vault nanoparticles with dimensions of 70 x 40 x 40 nm.[31, 32] The C-terminals of MVP chains come together at the two vault ends to form a cap structure. Recombinant vaults, which are assembled from heterologously expressed MVP in insect cells without VPARP, TEP1, or vRNA, have similar morphology as natural vaults and have no contents.[33] By expressing MVPs with N- and C-terminal peptide extensions, exogenous peptides can be immobilized on the exterior or interior of the assembled vault nanoparticles.[34] In addition, due to their hollow structure, the interior space of recombinant vaults is large enough to hold macromolecules, such as proteins and lipids. The INT domain, which is the strongest MVP interacting domain in VPARP, serves as a packaging signal due to its high affinity with the vault MVP shell, and this

allows the incorporation of exogenous components into vault nanoparticles. Various macromolecules, including luciferase,[35] green fluorescent protein,[35] lipid bilayer nanodisk,[36] and the chemokine CCL21,[37] have been successfully bound to the interior sites of vaults by INT domain fusion.

Recombinant vault nanoparticles, packaging various components or being modified at cap and waist, have been mainly investigated in therapeutic applications, such as cell targeting,[34, 38] vaccines,[39] tumor therapy[37], and drug delivery.[40, 41] This study explored a novel application of vault nanoparticles in improving enzymatic stability and enhancing biodegradation rates. The compact MVP shells prevent packaged enzymes from conformational changes, and possibly enhance enzymatic stability against thermal inactivation. In addition, the vault shell serves as a shield and provides a stable interior environment to protect immobilized enzymes from being affected by various environmental factors, such as natural organic matter, inorganic ligands, or proteolytic enzymes. In contrast from traditional encapsulation approaches with macro-sized materials, the thin and dynamic MVP shell and nanoscale size of vault particles render them unlikely to increase substrate diffusion resistance or decrease catalytic rates of packaged enzymes. As compared to other nanostructure-based immobilizations requiring serial chemical reaction steps and fully controlled conditions, such as mesoporous silicas,[16, 17] carbon nanotubes,[18, 19] and nanogels,[14] the vaults are naturally synthesized nanoparticles like virus capsids,[20, 42-44] which makes them attractive as a green, energy- and cost-efficient technologies with potential for large-scale implementation. The high affinity between INT domain and vault interior also allows packaging in vaults more efficient and flexible for encapsulating diverse components. As such, this study was performed to package manganese peroxidase (MnP) into vault nanoparticles, and examine whether packaged vaults enhanced MnP stability as well as MnP catalytic efficiency.

## 2.2 Materials and Methods

### 2.2.1 Recombinant MnP-INT Plasmids

MnP coding sequence was isolated from the wood-decaying fungus *Phanerochaete chrysosporium* (ATCC: 24725). The fungal culture was grown in nitrogen-limiting Kirk medium[45], and collected 1 day before MnP activity reached its maximum level. Total RNA was extracted and purified using phenol-chloroform extraction. Afterwards, cDNA was synthesized using Thermo Scientific Maxima First Strand cDNA Synthesis Kit for RT-qPCR, followed by PCR amplification using the following primers: 5′- ATGGCCTTCGGTTCTCTCCTC-3′ and 5′-TTAGGCAGGGCCATCGAACT-3′. PCR products were separated on agarose gel, purified, and inserted into pCR4-TOPO vector (Invitrogen). Subsequently, Mach1-T1 Competent *E. coli* (Invitrogen) was transferred with recombinant vectors using heat shock and plated on LB agar containing 50 $\mu$g/mL ampicillin. A few ampicillin resistant colonies were selected, and re-grown in LB medium (Amp(+)) for plasmid extraction. Purified plasmids were sequenced to confirm MnP coding sequence.

Isolated MnP coding sequence has 1149 bp with a 72 bp long signal sequence. For construction of sMnP-INT expression cassette, *mnp* was amplified with a forward primer 5′-CTAGTCCATGGCCTTCGGTTCTCTCCTCG-3′, containing an *Nco*1 restriction site, and a reverse primer, 5′-GTGTGCAGCTAGCAGGGCCATCGAACTGAACACCAG-3′, containing an *Nhe*1 restriction site. PCR amplified fragments were double digested with *Nco*1-*Nhe*1, and inserted upstream of INT sequence in INT-pFastBac vector treated with the same restriction enzymes. MnP signal sequence was removed to make nsMnP-INT expression construct. The following primers were used: forward primer with a *BamH*1 restriction site 5′-

CCCCGGATCCATGGCAGTCTGTCCAGACGGTAC-3′, and reverse primer with an *Nhe*1 restriction site 5′-CATGCTAGCAGGGCCATCGAACTGAA-3′. *BamH*1-*Nhe*1 digested PCR fragments were ligated upstream of INT-6xHis sequence in INT-6xHis-pFastBac. All constructs were confirmed by DNA sequencing.

### 2.2.2 Expression and Packaging of INT Fused MnP

Recombinant baculovirus for expressing sMnP-INT and nsMnP-INT were generated as described in Bac-to-Bac protocol (Invitrogen). Fifty milliliters of Sf9 cell culture (2 x $10^6$ cells/mL, in Sf-900 II SFM media (Life Technologies)) was infected with 5 $\mu$L baculovirus, and incubated at $27^0$C. Seventy-two hours after infection, the cell pellet was collected for nsMnP-INT analysis and the culture supernatant was collected for analysis of sMnP-INT infections. Culture supernatant from sMnP-INT was centrifuged at 100,000 x g for 1 hour to remove the baculovirus particles followed by concentrating 5-fold using an Amicon Ultracel 30K centrifugal filter. Afterwards, nsMnP-INT cell lysate was mixed with CP-rMVP vaults,[30] and purified as previously described.[33] To package sMnP-INT into recombinant vaults, partially purified empty human MVP vaults in buffer A (50 mM Tris, pH 7.4, 75 mM NaCl, 0.5 mM $MgCl_2$) with 1% Triton X-100 were mixed with the 5-fold concentrated sMnP-INT culture supernatant, and incubated on ice for 30 minutes. This was followed by centrifuging the mixture at 100,000 x g for 1 hour at $4^0$C. Recombinant sMnP associated with human vault nanoparticles pellets (P100), while free INT fused sMnP would stay in the supernatant S100. The P100 pellet containing the recombinant MnP-vaults, was then resuspended in buffer A (without Triton X-100), and analyzed by SDS-PAGE fractionation followed by both Coomassie staining and Western blot with anti-INT antibody.

Packaged vaults were then assessed by negative stain TEM to confirm its morphology as previously described.[33]

### 2.2.3 Purification of nMnP from *Phanerochaete chrysosporium*

*P. chrysosporium*, which is a well-characterized MnP producing fungus, was used as a source of nMnP. *P. chrysosporium* was grown and maintained on ME agar plates containing 5 g/L glucose, 5 g/L malt extract, 1 g/L peptone, 1 g/L yeast extract, 0.5 g/L asparagine, 1 g/L $KH_2PO_4$, 0.5 g/L $MgSO4_7 \cdot H_2O$, 0.5 mg/L thiamin-HCl, and 10 g/L agar at 30 ºC. Spores were collected and resuspended in sterile DI water, followed by filtration through sterilized glass wool. Filtered spore suspension was inoculated into nitrogen limiting Kirk medium, and grown in 30 ºC incubator at 150 rpm for accumulating biomass. After 3 days of growth, fungal culture was blended to make homogenous suspension and collected through centrifugation, followed by 3 times sterile DI water wash. Subsequently, 1 mL resuspended fungal culture was inoculated into 300 mL nitrogen limiting Kirk medium in 1 L Erlenmeyer flask, and incubated at 30 ºC, 150 rpm with 30 min aeration every day. Two peroxidases, including MnP and lignin peroxidase (LiP), were produced at different times. MnP, which has $Mn^{2+}$ dependent activity, is produced two days earlier than LiP, whose activity is not $Mn^{2+}$ dependent. By collecting the culture at early stage, the purified nMnP contained negligible LiP. After purification, the activity of nMnP was confirmed to be $Mn^{2+}$ dependent. At day 5, culture medium was collected, and concentrated using ammonium sulfate precipitation (85% saturation at 4 ºC). Subsequently, precipitates were resuspended in sterile DI water, and centrifuged at 7,197 x g to remove undissolved constituents. The supernatant containing nMnP was then desalted using GE PD-10 desalting column. Finally,

nMnP was confirmed with SDS-PAGE, $Mn^{2+}$ oxidation activity,[8] and $Mn^{2+}$ dependent ABTS oxidation activity assay.

### 2.2.4 Activity Test of INT Fused MnP and Vaults Packaged MnP-INT

ABTS assay was performed to assess peroxidase activity of INT fused MnP and vaults packaged MnP-INT. In MnP-catalyzed reactions, ABTS is oxidized by $H_2O_2$, and the oxidation products have strong absorbance at 420 nm ($\varepsilon_{420\ nm}$ = 36000 $L \cdot mol^{-1} \cdot cm^{-1}$) and generate green color. MnP activity or ABTS oxidation rate was determined by measuring absorbance change rate at 420 nm after addition of $H_2O_2$,[46-48] and one unit of enzyme activity was defined as the amount of enzyme required to react/produce 1 $\mu$mol/min of substrate/product. Initial activity confirmation tests were performed in microplates. Assay mixture constituted 150 $\mu$L MnP assay buffer (pH 4.0, 50 mM malonate buffer), 15 $\mu$L 1.4 mM ABTS, 15 $\mu$L 20 mM $MnCl_2$, and 15 $\mu$L enzyme (cell lysate, or cell supernatant, or packaged vaults suspension in buffer A), and was initiated by adding 15 $\mu$L 4 mM $H_2O_2$. Each reaction stood for up to 5 minutes to allow for the green color development. Three controls, including manganese ion-deplete ($Mn^{2+}$(-)), hydrogen peroxide-deplete ($H_2O_2$(-)), and enzyme-deplete (enzyme (-)), were also carried out by removing corresponding component from the reaction mixture.

The leakage of sMnP-INT from vault nanoparticles was evaluated by separating free sMnP-INT from vault-packaged sMnP-INT through ultracentrifugation. After 1 h spin at 100,000 x g, vault nanoparticles were pelleted at the bottom, which was then resuspended in buffer A, while leaked sMnP-INT stayed in the supernatant. ABTS peroxidation assay was performed to assess the activities in resuspended pellet and supernatant, which were then used calculated to the

recovery by normalizing them to the enzymatic activity in uncentrifuged sample. Unpacakged sMnP-INT was included as the negative control.

### 2.2.5 Kinetics of Vault-Packaged sMnP-INT and Unpackaged sMnP-INT

The sMnP-INT was purified from Sf9 culture before use in further experiments. The culture supernatant was centrifuged at 100,000 x g for 1 hour to remove baculovirus particles, and concentrated with 30 kDa filter. Concentrated supernatant was then subjected to ammonium sulfate precipitation (85% saturation at 4 ºC), and resuspended in buffer A. Finally, the solution was desalted with GE PD-10 desalting column, and eluted and stored in buffer A.

The $K_m$ values for different types of MnP were determined from Lineweaver-Burk plots by transforming ABTS oxidation rates at various substrate concentrations to double reciprocal plots (1/[ABTS] vs. 1/V). Triplicate reactions were performed in 400 $\mu$L mixtures containing one type of MnP, MnP assay buffer, 2 mM $MnCl_2$, 0.4 mM $H_2O_2$, and different concentrations of ABTS, including 0.2 mM, 0.1 mM, 0.05 mM, 0.025 mM, and 0.0125 mM. $A_{420nm}$ was collected every 2 s for 30 s after initiating the reaction to calculate the initial oxidation rate.

To test the effect of vault shells on ABTS diffusion, 5 $\mu$L vaults containing sMnP-INT were pre-incubated with 40 $\mu$L ABTS for 5 min, 20 min, and 60 min. Two ABTS concentrations were assessed, including 2 mM and 0.2 mM, which gave final concentrations of 0.2 mM and 0.02 mM, respectively. After incubation, 275 $\mu$L MnP assay buffer and 40 $\mu$L 20 mM $MnCl_2$ were added, and 40 $\mu$L 4 mM $H_2O_2$ was added to initiate the reactions. For 0 minute pre-incubation control, 5 $\mu$L vaults was added to reaction mixture just before $H_2O_2$ initiation. All conditions were performed in triplicates.

### 2.2.6 Thermal Inactivation

Vault-packaged sMnP-INT, free sMnP-INT, and nMnP in buffer A were incubated at 20$^{0}$C for 1 h, and then incubated at 30 $^{0}$C, followed by another 1 h incubation at 40$^{0}$C. Samples were collected at 1, 2, 2.5, and 3 h, and analyzed for ABTS oxidation activities. Assay mixture contained 100 $\mu$L MnP assay buffer, 10 $\mu$L enzyme, 10 $\mu$L 20 mM $MnCl_2$, 10 $\mu$L 1.4 mM ABTS, and 10 $\mu$L 4 mM $H_2O_2$. Residual activities were normalized to their initial activities, which were 147 U/L, 142 U/L, and 131 U/L for sMnP-INT-vault, sMnP-INT, and nMnP, respectively.

For detailed thermal inactivation study, three types of MnP in buffer A were incubated at 25$^{0}$C for about 70 hours, and samples were collected at 1, 2.5, 4, 6, 8, 22, 32.5, 47, and 70.5 h. Activity assays were performed in 400 $\mu$L mixtures consisting of MnP assay buffer, MnP enzyme, 0.5 mM ABTS, 2 mM $MnCl_2$, and 0.4 mM $H_2O_2$. $A_{420}$ was recorded for 30 s with 2 s intervals to calculate residual activities, which were further normalized to their corresponding initial activities. Data obtained were fitted to the Henley series-type enzyme inactivation model by predicting $k_1$, $k_2$, and $\alpha$ that yielded the minimum sum of squared residuals.

### 2.2.7 Biodegradation of Phenol

Phenol degradation was performed in MnP assay buffer at 28$^{0}$C in a shaking incubator (250 rpm), and the reaction mixture contained MnP enzyme, 1.5 mM $MnCl_2$, 150 $\mu$M phenol, and 0.4 mM $H_2O_2$, which was added last to initiate the reaction. Initial enzyme activities were 55.7 U/L for all three types of MnP, including sMnP-INT-vault, sMnP-INT, and nMnP. Enzyme free reaction was included as the negative control to correct for any non-enzymatic losses of phenol. Samples were collected at 0 h and 24 h. Prior to collection of samples, one equal volume methanol was added to terminate the reaction, and phenol concentration was determined using a Hewlett

Packard high-performance liquid chromatograph (HP 1050 HPLC system) with UV detection at 269 nm. A range of phenol-50% water-50% methanol mixtures was used for generating phenol calibration curves. For 48 hours degradation test, the reaction mixture contained 10.7 U/L enzyme (sMnP-INT-vault or sMnP-INT), 300 $\mu$M phenol, 1.5 mM $MnCl_2$, and 0.4 mM $H_2O_2$. Three volumes of methanol were added to terminate the reactions, and phenol concentrations were determined as described above. To assess the activity of sMnP-INT under turnover conditions, 10 $\mu$L of 1.4 mM ABTS was added to sacrificed reactions at 0, 4, 7.5, and 16 h, and mixtures stood for 5 minutes to allow for the development of green color.

### 2.2.8 Activity Test at Various pH Values

Activities of sMnP-INT-vault and sMnP-INT were tested using ABTS assay at pH ranging from 2.5 to 6.0 (0.5 gradient). Assay mixtures contained 270 $\mu$L 50 mM malonate buffer at various pH, 10 $\mu$L enzyme solution (sMnP-INT-vault or sMnP-INT), 40 $\mu$L 1 mM ABTS, 40 $\mu$L 20 mM $MnCl_2$, and 40 $\mu$L 4 mM $H_2O_2$. Results were normalized to corresponding activity at optimum pH.

## 2.3 Results and Discussion

### 2.3.1 Expression and Packaging of INT Domain-fused MnP in Vaults

VPARP protein, which is present in naturally occurring vaults, is tightly bound non-covalently to the inside of the vault shell. The INT domain (162 amino acid residues 1563-1724 in VPARP) is responsible for VPARP binding to vaults *via* an interaction with MVP near the barrel waist.[30] Previous studies have demonstrated that INT domain maintains its binding properties when fused to heterologous proteins. Addition of these INT fusion proteins to vaults results in their

packaging into vaults near the nanoparticle's interior waist. In addition, the vault structure has been shown to be dynamic which allows particles to transiently and reversibly open allowing the packaging of INT fused components into empty vaults.[49] We hypothesized that INT fused MnP would be packaged into vaults *via* incubating MnP-INT with empty vaults. The synthesis processes of INT domain-fused MnP and vault nanoparticles packaging procedures are illustrated in Figure 2.1, and further details are described in Materials and Methods section.

Since MnP is produced as a secreted protein in fungi, two recombinant INT fusion proteins with MnP were constructed: non-secreted MnP (nsMnP-INT) and secreted MnP (sMnP-INT). Expression of nsMnP-INT and sMnP-INT in Sf9 cells was confirmed with Western blot analysis using anti-INT antibody. While nsMnP-INT was detected in cell pellet lysate, major sMnP-INT was detected in cell culture supernatant suggesting successful secretion of INT fused sMnP. Vaults packaged with nsMnP-INT or sMnP-INT were isolated using a gradient ultracentrifuge, and analyzed with Coomassie stain and immunoblot (Figure 2.2 A&C). The formation of nsMnP-INT vault complex and sMnP-INT vault complex indicated that both nsMnP-INT and sMnP-INT were incorporated into vault particles. To further confirm the formation of vault nanoparticles, purified vaults containing nsMnP-INT or sMnP-INT were examined with negative stain transmission electron microscopy (TEM). Intact vault structures, which were identical to the previously observed morphology of vault nanoparticles binding to INT fused proteins,[35] were observed (Figure 2.2 B&D), indicating that the incorporation of nsMnP-INT or sMnP-INT did not affect the stability of vault nanoparticles.

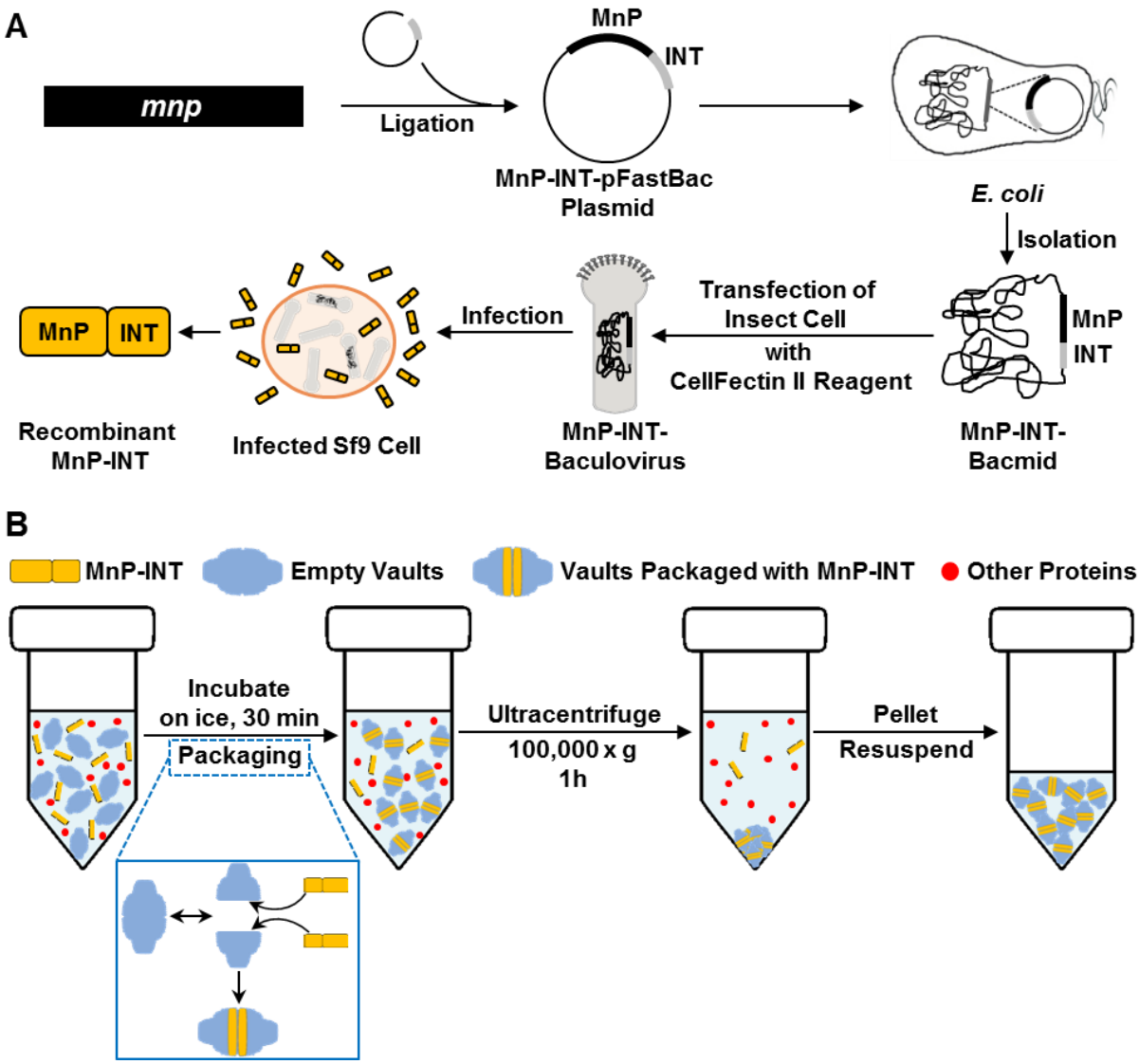


**Figure 2.1** A Schematic for the Synthesis of Vault Nanoparticles Packaged with MnP. (A) The expression of INT domain fused MnP. MnP coding sequence was isolated from *Phanerochaete chrysosporium*, and inserted upstream of INT sequence in a pFastBac plasmids. Afterwards, recombinant plasmid was transformed into *E. coli* to generate MnP-INT-Bacmid through transposition, which was then used to generate insect cell baculovirus. Finally, insect Sf9 cells were infected by MnP-INT virus to produce recombinant INT fused MnP. (B) Single-step Vault Nanoparticles Packaging. Recombinant MnP-INT was mixed with empty vaults, which were synthesized in Sf9 cells, and the mixture was incubated on ice for 30 minutes. Due to the affinity of INT domain with vaults' interior and its dynamic structure, MnP-INT was spontaneously sequestered by vault nanoparticles. Subsequently, ultracentrifugation was performed to separate vault-associated MnP from the mixture.

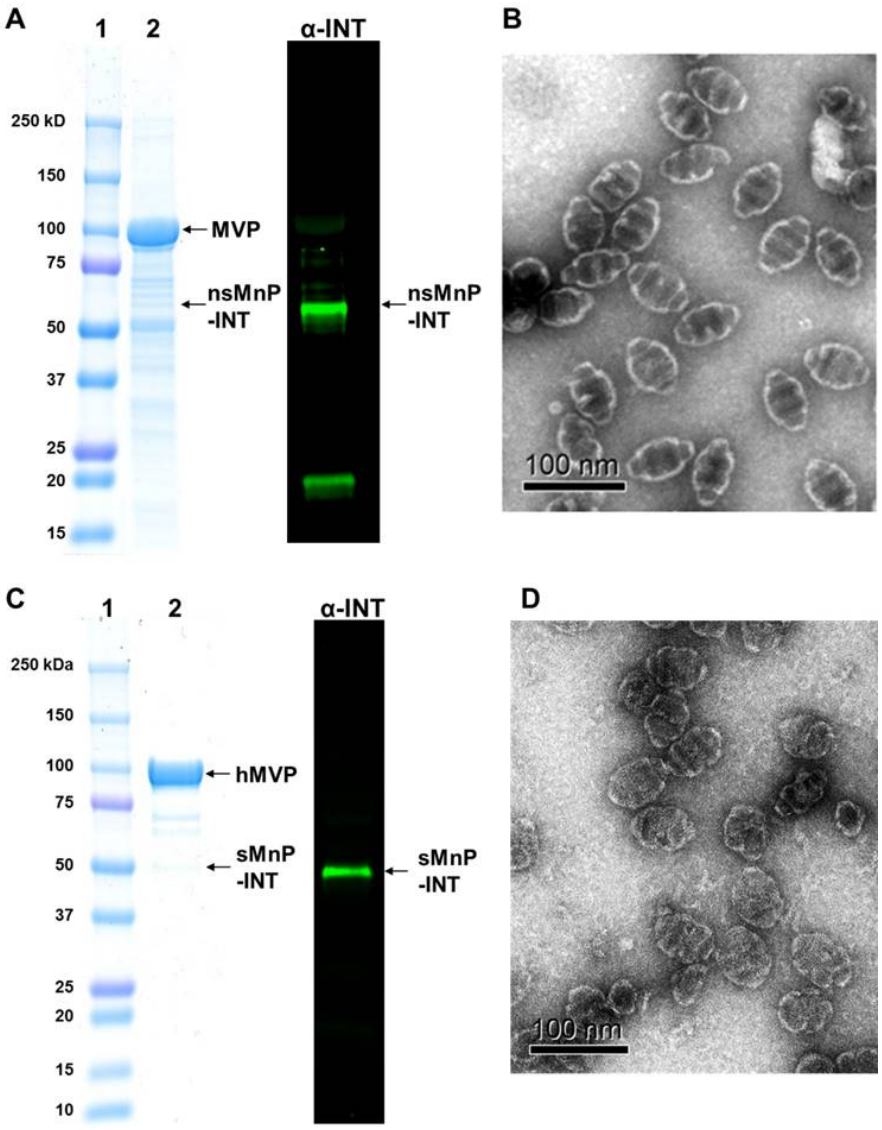


**Figure 2.2** Evaluation of Recombinant MnP-Vaults. A & C. Coomassie stains of purified vaults [nsMnP-INT-vault (A) and sMnP-INT-vault (C)] fractionated on a 4-15% SDS-PAGE (left panels). Lane 1, protein molecular weight markers in kDa. Lane 2, nsMnP-INT vaults (A) and sMnP-INT vault (C). The MVP and (ns or s)-MnP-INT bands are indicated by arrows. Western Blot analysis confirmed the presence of (ns or s)-MnP-INT (right panels) in the purified vaults. B & D. Negative-stained electron micrographs of purified nsMnP-INT vaults (B) and sMnP-INT vaults (D).

### 2.3.2 Kinetics of MnP-INT and Vault-Packaged MnP-INT

Once nsMnP-INT and sMnP-INT were successfully expressed and packaged into vault nanoparticles, it was important to verify that MnP maintained its activity when fused to the INT domain and expressed in Sf9 cells, and that the enzyme was functional when packaged into vaults. The activity of recombinant and packaged MnP was tested using 2,2'-azino-bis(3-ethylbenzothiazoline-6-sulphonic acid) (ABTS) peroxidation assay. Under catalysis by MnP, the oxidation product from ABTS generates a green chromophore that has strong absorbance at 420 nm. The enzymatic activity was calculated using the rate of change in absorbance.

Oxidation of ABTS was observed for sMnP-INT (Figure 2.3), while nsMnP-INT did not exhibit any ABTS oxidation. Since natural MnP is produced as secreted enzyme, we reason that signal peptide processing might contribute to correct folding of MnP and might be required to activate MnP. Additionally, INT fused hCCL21 (human secondary lymphoid chemokine) did not show any peroxidase activity (Figure 2.S1), suggesting that extracellularly expressed INT domain did not contribute to ABTS oxidation.

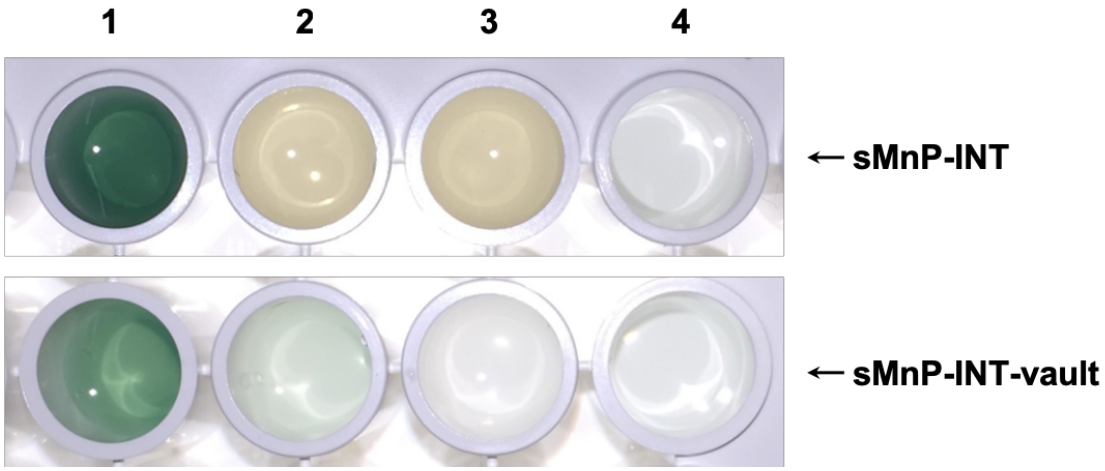


**Figure 2.3** Peroxidase Activity Tests of sMnP-INT (top panel) and Vault-packaged sMnP-INT (bottom panel) using ABTS Oxidation under Different Conditions. Lane 1 represents reactions containing $Mn^{2+}$, $H_2O_2$, and recombinant MnP. The rest are $Mn^{2+}$(-) control (lane 2), $H_2O_2$ (-) control

(lane 3), and peroxidase(-) control (lane 4). Color change to green indicates ABTS oxidation mediated by recombinant MnP.

We next examined ABTS oxidation by vaults packaged with sMnP-INT or nsMnP-INT. Empty vault particles did not show any oxidation of ABTS, and vaults containing nsMnP-INT did not exhibit any activity either since nsMnP-INT itself was not active at oxidizing ABTS. In contrast, a significant ABTS color change was observed for sMnP-INT sequestered in vaults, which indicated that vault nanoparticles containing sMnP-INT could catalyze the oxidation of ABTS. To further confirm that the ABTS oxidation activity was contributed from sMnP-INT, $Mn^{2+}$ deplete and $H_2O_2$ deplete controls were performed. Natural MnP is strongly $Mn^{2+}$ dependent and totally $H_2O_2$ dependent. The divalent manganese ions act as electron shuttles between MnP and substrate, while $H_2O_2$ acts as the terminal electron acceptor. Ground state MnP donates electrons to oxidant $H_2O_2$, and then gets electrons from $Mn^{2+}$. Subsequently, oxidized manganese gains electrons from substrate and drives the substrate oxidation. In the absence of $Mn^{2+}$, the substrate cannot directly donate electrons to the oxidized enzyme, which results in little or no substrate oxidation. Consistent results were observed for both of sMnP-INT and vault packaged sMnP-INT (Figure 2.3). In the absence of $Mn^{2+}$, no ABTS oxidation was detected for sMnP-INT and much lower oxidation was detected for vault-packaged sMnP-INT. Meanwhile, neither sMnP-INT nor sMnP-INT-vault showed any ABTS oxidation in $H_2O_2$ depleted controls. The yield of enzyme activity in vaults packaged sMnP-INT was about 80%, which was significantly higher than previously reported packaging approaches, for example, 30% recovery of horseradish peroxidase on mesoporous silicas[16] and 38% - 73% enzyme activity yield in single-enzyme nanoparticles.[50] Approximately 10% of total enzyme activity was identified as secreted sMnP-INT on day 2, and no further secretion was observed between day 2 and day 7 at 4°C (Table 2.S1), suggesting that the strong interaction between INT domain and vault interior could maintain

enzymes inside, although the vault shell is dynamic (Table 2.S1). Overall, these findings indicate that extracellularly expressed sMnP-INT retained its ABTS oxidation ability even after fusion to the INT domain, and could maintain most of its activity when packaged into vault nanoparticles. Since secreted MnP-INT was the only active enzyme form, it was employed for further experiments.

The presence of the vault shell might act as a barrier that impacts the diffusion of substrates, and hinders packaged enzymes from contacting with substrate, which would decrease catalytic rates and increase $K_m$ values. A previous study found that vault-packaged luciferase showed a lag in luminescence intensity after initiating with ATP, while ATP preincubated luciferase-vaults displayed a fast emission intensity rise,[35] suggesting that the vault MVP shell slows down the diffusion of ATP molecule and limits the availability of sequestered luciferase. To evaluate the effect of vaults packaging on MnP catalysis, $K_m$ values of ABTS oxidation were measured for sMnP-INT and vault-packaged sMnP-INT (Figure 2.S2, Table 2.1). Naturally produced MnP (nMnP) was included as a control. Unexpectedly, sMnP-INT displayed lower $K_m$ than nMnP, which means that sMnP-INT had a higher affinity for substrate ABTS. This result indicates that INT domain fusion enhances the affinity of MnP to ABTS. More importantly, unlike traditional enzyme packaging, which results in marked rise of $K_m$ values,[51, 52] vault-packaged sMnP-INT exhibited a $K_m$ of 70 $\mu$M, which was only slightly higher than that of unpackaged sMnP-INT (21 $\mu$M). The small increase of $K_m$ was likely due to the dynamic nature of the MVP shell of the vaults, which did not provide much resistance to substrate diffusion. To confirm if it was the ABTS diffusion resistance from the vault shell that led to the small increase of $K_m$, we examined the oxidation of ABTS preincubated with sMnP-INT-vault. No significant difference in oxidation rates was observed between sMnP-INT-vault and ABTS preincubated sMnP-INT-vault (Figure

2.S3), which implies that ABTS diffusion does not limit sMnP-INT-vault catalyzed oxidation rate. Perhaps the slight increase of $K_m$ is attributed to the binding of sMnP-INT to vaults.

**Table 2.1** $K_m$ Values of sMnP-INT, sMnP-INT-vault, and naturally-produced MnP from the fungus *Phanerochaete chrysosporium*. All values were calculated from linear regression of Lineweaver-Burk Plot ($r^2 \geq 0.99$).

| | $K_m$ ($\mu$M) |
|---|---|
| sMnP-INT-vault | 69.5±9.7 |
| sMnP-INT | 21.0±2.0 |
| nMnP | 102.9±9.8 |

### 2.3.3 Thermal Stability of Vault-Packaged sMnP-INT

We next examined the stability of packaged and unpackaged sMnP-INT against thermal inactivation. Vault-packaged sMnP-INT, sMnP-INT, and nMnP were sequentially incubated at $20^0$C, $30^0$C, and $40^0$C for one hour each, and residual activity was analyzed using ABTS oxidation (Figure 2.4). Vault-packaged sMnP-INT underwent much slower heat-induced activity losses when compared to unpackaged sMnP-INT and nMnP. At $20^0$C, sMnP-INT lost 20% activity in 1-hour incubation; however, vault-packaged sMnP-INT and nMnP maintained 100% of their initial activity. After 1-hour incubation at $30^0$C, compared with 45% activity retention of nMnP, vault-packaged sMnP-INT still preserved 75% of its initial activity. Subsequently, the three MnPs were incubated at $40^0$C, and neither unpackaged sMnP-INT nor nMnP showed any ABTS oxidation activity at the end. In contrast to the complete loss of activity by the nMnP and the sMnP-INT, sMnP-INT packaged in vaults still conserved 16% of its original activity. These data suggested that under the protection of the vault MVP shell, the packaged sMnP-INT has much higher thermal

stability than unpackaged sMnP-INT and nMnP. The stability enhancement might be attributed to constraints from the vault shell, which prevents enzyme conformational changes during the heat inactivation process.

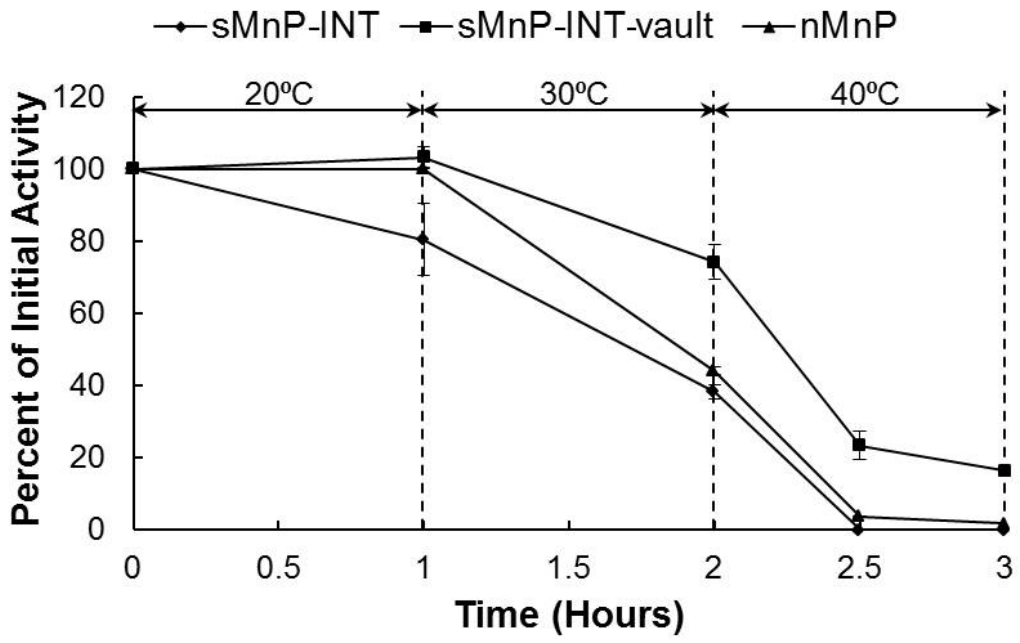


**Figure 2.4** Enhanced Thermal Stability of Vault-packaged sMnP-INT. sMnP-INT-vault, sMnP-INT, and nMnP were incubated at 20$^0$C for 1 hour, followed by 1-hour incubation at 30$^0$C, and one more hour at 40$^0$C. Samples were collected and analyzed over time, and activity was normalized to their initial activity.

To further understand how vault packaging impacts thermal inactivation, a detailed inactivation study was performed at 25$^0$C for 70 hours (Figure 2.S4B). Among three types of enzymes, vault-packaged sMnP-INT showed best stability, followed by nMnP. The activity of sMnP-INT decreased by half in 2.5 hours, it was nearly completely deactivated in 50 hours. The half-life of nMnP was about 14 hours, which is 6 times longer than that of sMnP-INT, and it still maintained 35% of its original activity after 70 hours of incubation. The activity of vault-packaged sMnP-INT leveled off at 65% of the initial activity after about 12 hours without any further

inactivation. To explain this, the collected data were fit into the series-type enzyme inactivation model.[53-55] Model equation is shown as following:

$$\frac{E_{obs}}{E_0} = a = \left[1 + \frac{\alpha k_1}{k_2 - k_1}\right] e^{-k_1 t} - \frac{\alpha k_1}{k_2 - k_1} e^{-k_2 t}$$

In general, enzyme inactivation could be divided into two steps (Figure 2.S4A). $E_0$ is the initial active enzyme, and it is deactivated to $E_1$, which is the less active form of the enzyme, in the first inactivation step. Subsequently, $E_1$ is inactivated to $E_D$, which is the non-active form of the enzyme. The rate constants of two inactivation steps are $k_1$ and $k_2$, and the ratio of specific activity of $E_1$ to the specific activity of $E_0$ is $\alpha$, which is less than 1 in most cases. Data were fitted into the proposed model, and three parameters ($k_1$, $k_2$, and $\alpha$) were calculated for vault packaged sMnP-INT, free sMnP-INT, and nMnP (Table 2.2). The sMnP-INT exhibited approximately 7 times higher $k_1$ and $k_2$ than nMnP, which suggests that INT fusion leads to less stable MnP folding, and sMnP-INT underwent faster inactivation. Thus, it could be concluded that heterologously expressed INT fused MnP is less stable. It was also found that $k_1$ of vault-packaged sMnP-INT was slightly lower than that of sMnP-INT, and $\alpha$ value of sMnP-INT-vault was larger than that of sMnP-INT. Moreover, vault-packaged sMnP-INT had a 200 times smaller $k_2$ than free sMnP-INT. These findings demonstrate that packaging in vault nanoparticles slightly decreases the first step inactivation rate and enhances activity of intermediate enzyme sMnP-INT. More importantly, vault packaging significantly decreases the second step inactivation rate $k_2$, which is the reason why vault-packaged sMnP-INT activity reaches a plateau.

**Table 2.2** Values of $k_1$, $k_2$ and $\alpha$ for sMnP-INT, sMnP-INT-vault, and Naturally-produced MnP from the fungus *Phanerochaete chrysosporium*.

| | $k_1$ ($hr^{-1}$) | $k_2$ ($hr^{-1}$) | $\alpha$ |
|---|---|---|---|
| sMnP-INT-vault | 0.60 | 0.00021 | 0.67 |
| sMnP-INT | 0.86 | 0.043 | 0.45 |
| nMnP | 0.20 | 0.0056 | 0.48 |

### 2.3.4 Catalytic Performance of Vault-Packaged sMnP-INT

With the goal of developing an effective enzymatic biodegradation approach, we evaluated the catalytic performance of vault-packaged sMnP-INT for removing contaminants and determine whether vault packaging could enhance removal efficiency. As vault packaging significantly improves thermal stability and keeps the enzyme functional over longer times, we reasoned that the contaminant removal efficiency would also be enhanced with vault-packaged enzyme. Consequently, the effectiveness of vault-packaged sMnP-INT was examined using phenol as a model water contaminant. Phenol, which is a common environmental pollutant, is degraded in biochemical reactions catalyzed by nMnP.[56] Twenty-four hour-long degradation tests were performed using three types of MnP, including vault-packaged sMnP-INT, free sMnP-INT, and nMnP, with same initial ABTS oxidation activities (Figure 2.5). In contrast to the negligible degradation in enzyme-free control, all three types of MnP could catalyze the degradation of phenol within 24 hours, which further confirmed that MnP maintained its catalytic ability when fused to INT domain and packaged into vaults. After 24 hours' reaction, phenol removal mediated by sMnP-INT-vault, free sMnP-INT, and nMnP was 98%, 30%, and 87% of the initial concentration, respectively. This result is consistent with the thermal stability pattern, where vault-

packaged sMnP-INT showed the best performance among three types of MnP, while free sMnP-INT gave the lowest performance. Additionally, phenol degradation was performed over 48 hours to compare the stability of sMnP-INT-vault and sMnP-INT under turnover conditions (Figure 2.S5A). About 12% phenol degradation was observed for vault-packaged sMnP-INT from 24 to 48 hours, indicating that sMnP-INT-vault maintained some activity after 24 hours of reaction. Since unpackaged sMnP-INT did not exhibit significant phenol degradation in 48 hours, ABTS oxidation test was performed to monitor its activity under turnover conditions. As shown in Figure 2.S5B, sMnP-INT would be completely deactivated in 7.5 hours, which is at least 3 times shorter than the life of vault-packaged sMnP-INT.

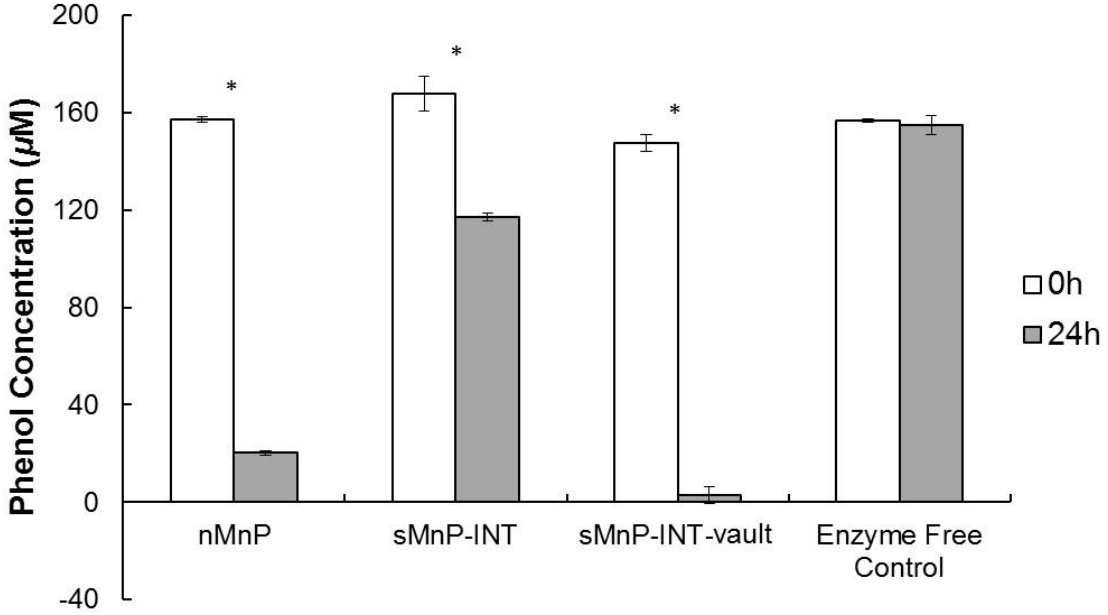


**Figure 2.5** Biodegradation of Phenol Catalyzed by sMnP-INT-vault, sMnP-INT, and nMnP. For each type of MnP, equal ABTS based activity was added in the beginning, and reactions were performed at $28^0$C for 24 hours. Triplicate samples were collected at 0 h and 24 h. Phenol degradation under enzyme-free condition was included as negative control. Asterisk indicates statistical difference compared to time 0 h at $p < 0.05$.

Moreover, water chemistries vary among diverse environments. For example, pH of surface water and groundwater ranges from 4.5 to 10, which affects the *in situ* enzymatic activities.

To understand the performance of vault packaged sMnP-INT under realistic conditions, we examined the activity of sMnP-INT-vault and sMnP-INT under various pHs, and results were normalized to their activity at optimal pH (Figure 2.6). Both sMnP-INT and vault-packaged sMnP-INT gave the best performance at pH 4.01. When pH increased to 5.01, sMnP-INT-vault retained 92% of its optimal activity, while the relative activity of unpackaged sMnP-INT decreased to 68%. At pH 5.51, compared to the 47% relative activity of sMnP-INT, vault packaged sMnP-INT still maintained 61% of its activity at optimal pH. However, when pH decreased to 3.0 or lower, no significant activity enhancement was observed with sMnP-INT-vault, which is probably due to the disassociation of vault nanoparticles at low pH.[57] It has been previously reported that MnP activity is favored in weakly acidic environments (pH 4.0-5.0).[58] Thus, our results show that intact vault nanoparticles enhance the activity of packaged sMnP-INT against large pH changes.

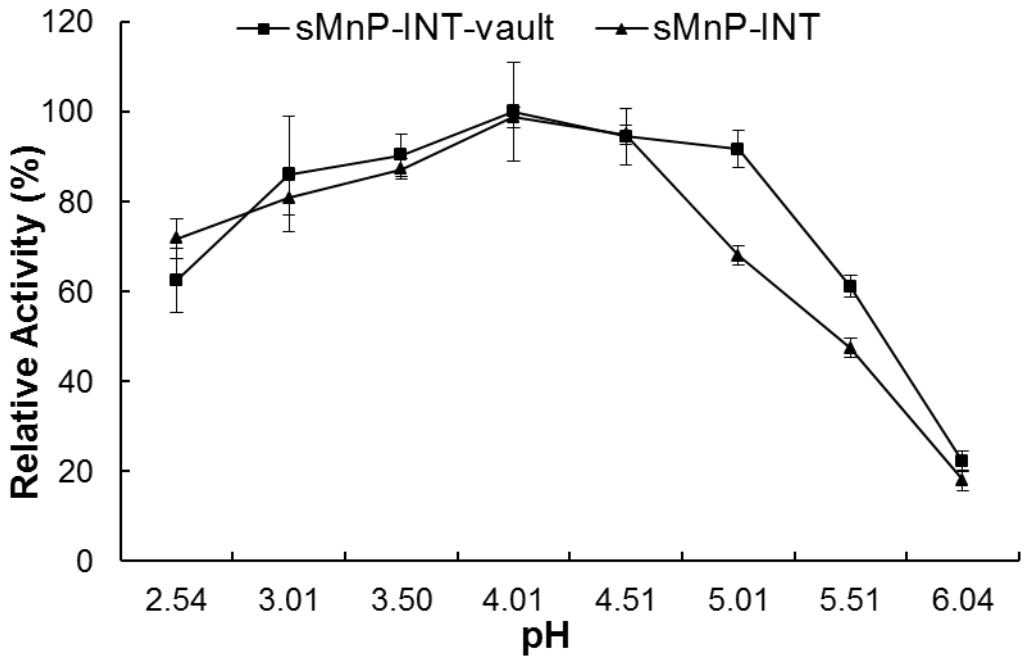


**Figure 2.6** Relative Activity of sMnP-INT-vault and sMnP-INT at Various pH Normalized to Their Activities at pH 4. ABTS oxidation assay was performed in buffers of different pH (2.5-6.0), and both of sMnP-INT-vault and sMnP-INT showed optimal activity at pH 4.01

## 2.4 Conclusions and Prospects

The results from the present study indicate that MnP activity is maintained after fusion to the INT domain and extracellular expression in Sf9 cells. Furthermore, vault nanoparticles containing sMnP-INT also exhibit MnP activity. In contrast to the significant $K_m$ increases observed in traditional immobilization methods, vaults packaged sMnP-INT showed just slightly higher $K_m$ than free sMnP-INT. More importantly, vaults packaging exhibited significant enhancement of sMnP-INT thermal stability and catalytic performance. This study serves as the foundation for integration of vault particles with specific biodegradative enzymes in a transformative step towards effective bioremediation of environmental contaminants with the potential for more customized enzyme catalyzed solutions for water treatment and contaminated sites.

## 2.5 Supporting Information

**Table 2.S1** Leakage of sMnP-INT from vault nanoparticles. Recoveries were calculated based on the activities in resuspended vault pellets and supernatants. The unpackaged sMnP-INT control showed that the free sMnP-INT was not pelleted, and did not lose activity during centrifugation. About 10% activity was detected in the supernatants, indicating a minor leakage of the enzymes. The recoveries in resuspended pellets were only around 70%, which was probably due to losses in resuspension.

| | Activity Recovery | |
|---|---|---|
| | Supernatant | Resuspended Pellet |
| Day 2 | 8.7 – 12.1% | 66.7 – 72.5% |
| Day 7 | 8.7 – 9.1 % | 63.6 – 72.5% |

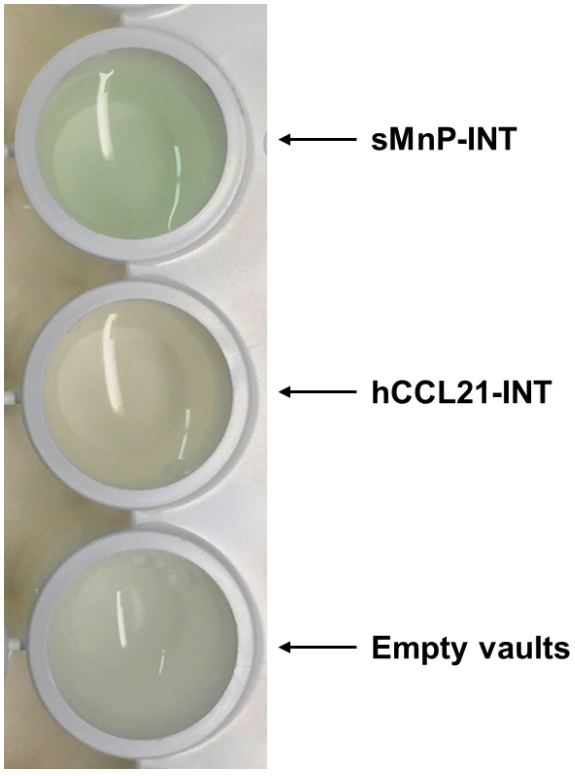


**Figure 2.S1** Peroxidase Activity Test of sMnP-INT, hCCL21-INT, and Empty Vaults. Neither hCCL21-INT nor empty vaults showed ABTS oxidation, indicating that INT domain and vaults did not contribute to the peroxidase activity observed in sMnP-INT and sMnP-INT-vault assays.

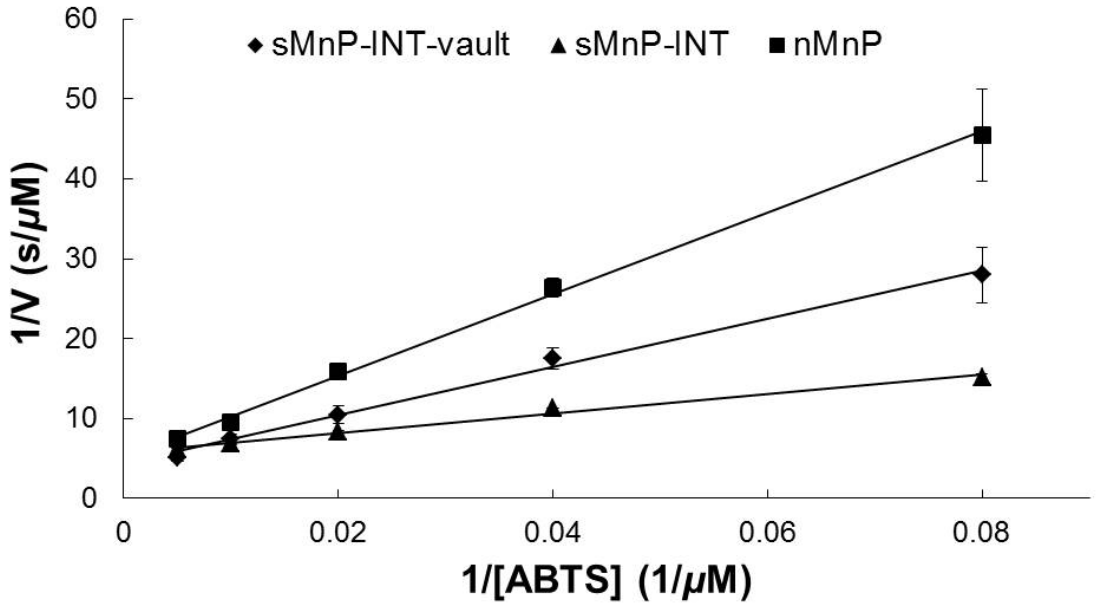


**Figure 2.S2** Double Reciprocal Plots of ABTS Concentrations versus their Oxidation Rates. Reaction rates were measured with various ABTS concentrations, including 0.2 mM, 0.1 mM, 0.05 mM, 0.025 mM and 0.0125 mM. $K_m$ values were calculated from the x-intercepts of linear regressions.

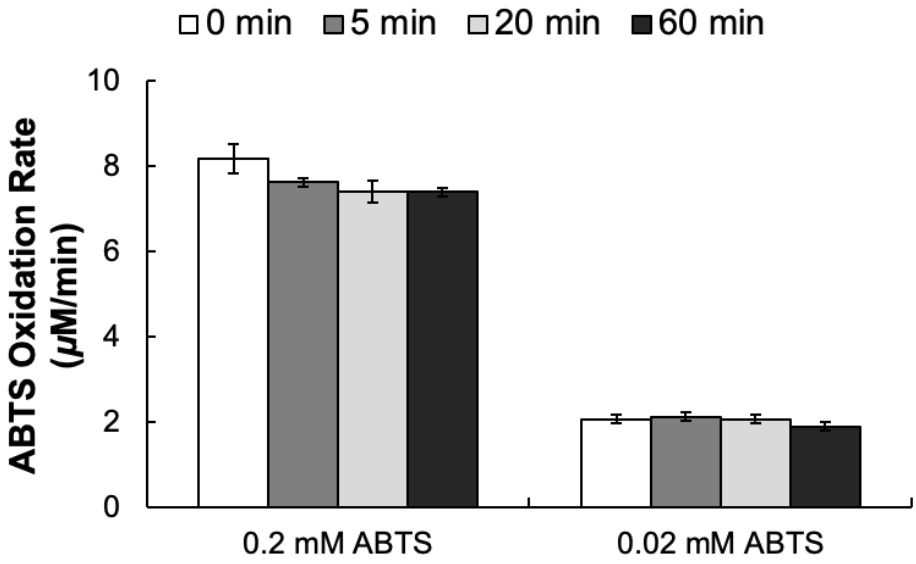


**Figure 2.S3** ABTS Diffusion Analysis. Oxidation rates were compared between ABTS-preinucbated sMnP-INT-vault (5 min, 20 min, and 60 min) and non-preincubated sMnP-INT-vault (0 min). Two ABTS concentrations were tested, including 0.2 mM and 0.02 mM.

A

$$E_0 \xrightarrow{k_1} E_1 \xrightarrow{k_2} E_D$$

B

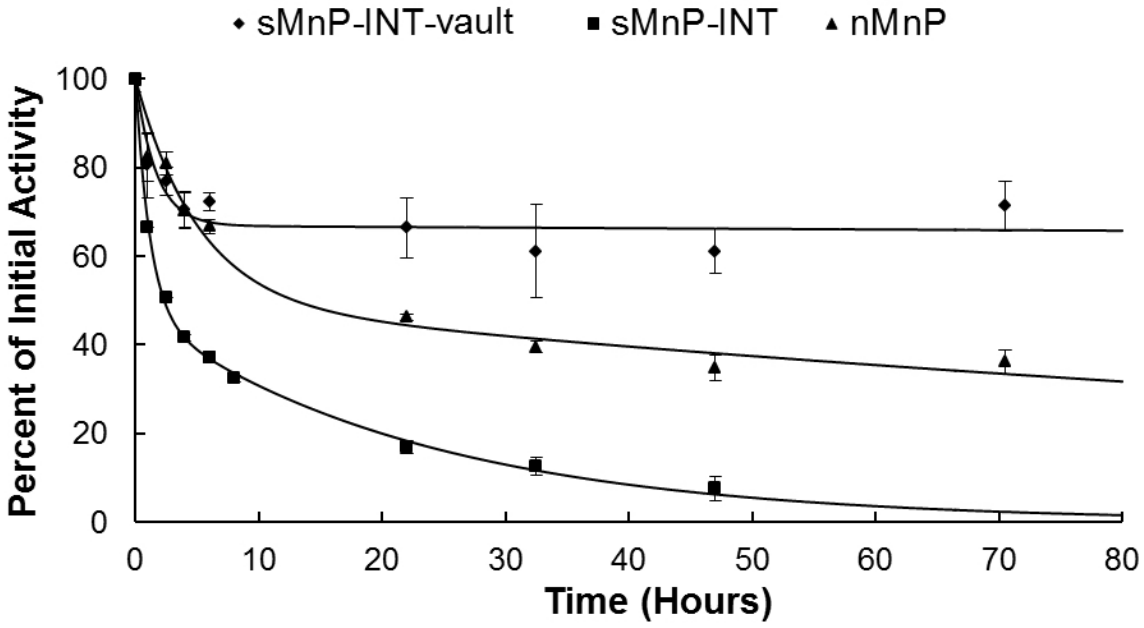


**Figure 2.S4** Enzyme Activity Decay Modeling. (A) Two-step inactivation model. Initial state enzyme ($E_0$) is first deactivated to $E_1$, which has lower specific activity than $E_0$, and subsequently, $E_1$ is inactivated to $E_D$, which is totally inactive. The reaction rate constants for two steps are $k_1$ and $k_2$, respectively. (B) Non-linear regression fit of Henley model for three types of MnP. Markers represent experimental data points, and solid lines are fitted curves.

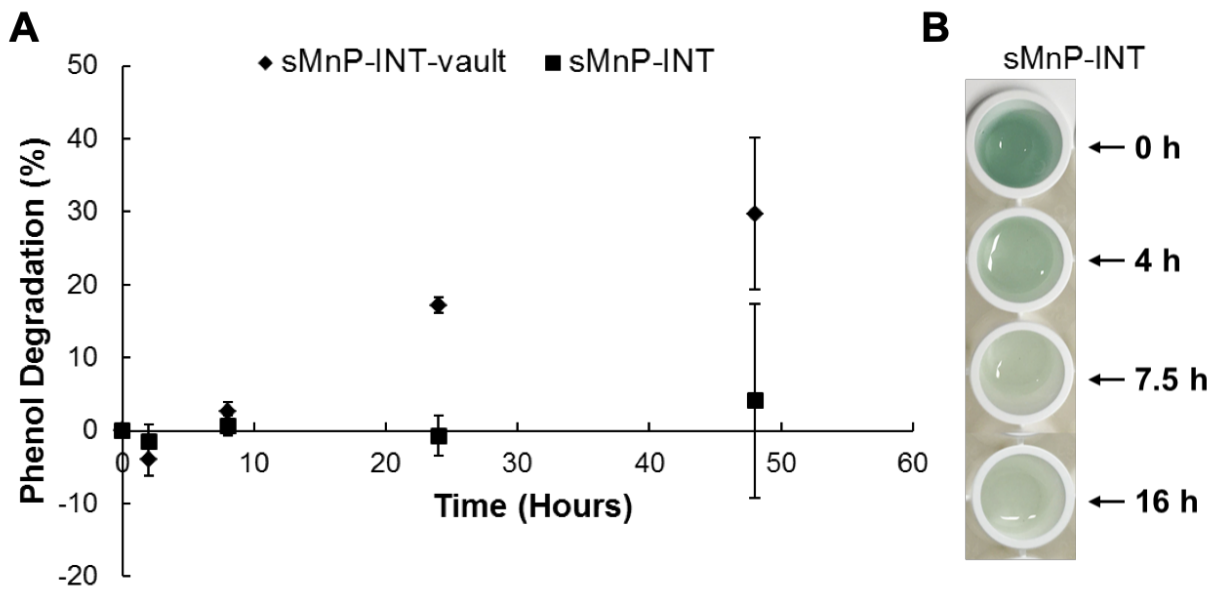


**Figure 2.S5** Enhanced Stability of Vault-packaged sMnP-INT under Turnover Conditions. (A) Degradation of phenol by sMnP-INT-vault and sMnP-INT in 48 hours. (B) Activity test of sMnP-INT in phenol degradation reactions. The activity of sMnP-INT was depleted within 7.5 hours, but the phenol degrading capacity of sMnP-INT-vault was maintained.

## 2.6 References


1. Atlas, R. M. Bioremediation of Petroleum Pollutants. *International Biodeterioration & Biodegradation* **1995,** *35* (1-3), 317-327.
2. Ellis, D. E.; Lutz, E. J.; Odom, J. M.; Buchanan, R. J.; Bartlett, C. L.; Lee, M. D.; Harkness, M. R.; Deweerd, K. A. Bioaugmentation for Accelerated *in situ* Anaerobic Bioremediation. *Environmental Science & Technology* **2000,** *34* (11), 2254-2260.
3. Barkay, T.; Schaefer, J. Metal and Radionuclide Bioremediation: Issues, Considerations and Potentials. *Current Opinion in Microbiology* **2001,** *4* (3), 318-323.
4. Sutherland, T. D.; Horne, I.; Weir, K. M.; Coppin, C. W.; Williams, M. R.; Selleck, M.; Russell, R. J.; Oakeshott, J. G. Enzymatic bioremediation: From enzyme discovery to applications. *Clinical and Experimental Pharmacology and Physiology* **2004,** *31* (11), 817-821.
5. Scott, C.; Lewis, S. E.; Milla, R.; Taylor, M. C.; Rodgers, A. J. W.; Dumsday, G.; Brodie, J. E.; Oakeshott, J. G.; Russell, R. J. A free-enzyme catalyst for the bioremediation of environmental atrazine contamination. *Journal of Environmental Management* **2010,** *91* (10), 2075-2078.
6. Baborova, P.; Moder, M.; Baldrian, P.; Cajthamlova, K.; Cajthaml, T. Purification of a New Manganese Peroxidase of the White-Rot Fungus *Irpex Lacteus*, and Degradation of Polycyclic Aromatic Hydrocarbons by the Enzyme. *Research in Microbiology* **2006,** *157* (3), 248-253.
7. Lackner, R.; Srebotnik, E.; Messner, K. Oxidative Degradation of High Molecular Weight Chlorolignin by Manganese Peroxidase of *Phanerochaete chrysosporium*. *Biochemical and Biophysical Research Communications* **1991,** *178* (3), 1092-1098.

8. Sack, U.; Hofrichter, M.; Fritsche, W. Degradation of polycyclic aromatic hydrocarbons by manganese peroxidase of Nematoloma frowardii. *Fems Microbiology Letters* **1997,** *152* (2), 227-234.

9. Hirano, T.; Honda, Y.; Watanabe, T.; Kuwahara, M. Degradation of Bisphenol A by the Lignin-Degrading Enzyme, Manganese Peroxidase, Produced by the White-Rot Basidiomycete, *Pleurotus Ostreatus*. *Bioscience, Biotechnology, and Biochemistry* **2000,** *64* (9), 1958-1962.

10. Tuor, U.; Wariishi, H.; Schoemaker, H. E.; Gold, M. H. Oxidation of Phenolic Arylglycerol Beta-Aryl Ether Lignin Model Compounds by Manganese Peroxidase from *Phanerochaete chrysosporium*: Oxidative Cleavage of an Alpha-Carbonyl Model Compound. *Biochemistry* **1992,** *31* (21), 4986-4995.

11. Mielgo, I.; Lopez, C.; Moreira, M. T.; Feijoo, G.; Lema, J. M. Oxidative Degradation of Azo Dyes by Manganese Peroxidase under Optimized Conditions. *Biotechnology Progress* **2003,** *19* (2), 325-331.

12. Olsson, B.; Ogren, L. Optimization of Peroxidase Immobilization and of the Design of Packed-Bed Enzyme Reactors for Flow Injection Analysis. *Analytica Chimica Acta* **1983,** *145* (Jan), 87-99.

13. Azevedo, A. M.; Prazeres, D. M. F.; Cabral, J. M. S.; Fonseca, L. P. Stability of Free and Immobilised Peroxidase in Aqueous-Organic Solvents Mixtures. *Journal of Molecular Catalysis B: Enzymatic* **2001,** *15* (4-6), 147-153.

14. Yan, M.; Ge, J.; Liu, Z.; Ouyang, P. K. Encapsulation of single enzyme in nanogel with enhanced biocatalytic activity and stability. *Journal of the American Chemical Society* **2006,** *128* (34), 11008-11009.

15. Wei, W.; Du, J. J.; Li, J.; Yan, M.; Zhu, Q.; Jin, X.; Zhu, X. Y.; Hu, Z. M.; Tang, Y.; Lu, Y. F. Construction of Robust Enzyme Nanocapsules for Effective Organophosphate Decontamination, Detoxification, and Protection. *Advanced Materials* **2013,** *25* (15), 2212-2218.

16. Chouyyok, W.; Panpranot, J.; Thanachayanant, C.; Prichanont, S. Effects of pH and Pore Characters of Mesoporous Silicas on Horseradish Peroxidase Immobilization. *Journal of Molecular Catalysis B: Enzymatic* **2009,** *56* (4), 246-252.

17. Ravindra, R.; Shuang, Z.; Gies, H.; Winter, R. Protein Encapsulation in Mesoporous Silicate: The Effects of Confinement on Protein Stability, Hydration, and Volumetric Properties. *Journal of the American Chemical Society* **2004,** *126* (39), 12224-12225.

18. Zhang, J. L.; Zhang, F.; Yang, H. J.; Huang, X. L.; Liu, H.; Zhang, J. Y.; Guo, S. W. Graphene Oxide as a Matrix for Enzyme Immobilization. *Langmuir* **2010,** *26* (9), 6083-6085.

19. Feng, W.; Ji, P. J. Enzymes Immobilized on Carbon Nanotubes. *Biotechnology Advances* **2011,** *29* (6), 889-895.

20. Patterson, D. P.; Prevelige, P. E.; Douglas, T. Nanoreactors by Programmed Enzyme Encapsulation Inside the Capsid of the Bacteriophage P22. *ACS Nano* **2012,** *6* (6), 5000-5009.

21. Kedersha, N. L.; Miquel, M. C.; Bittner, D.; Rome, L. H. Vaults. II. Ribonucleoprotein structures are highly conserved among higher and lower eukaryotes. *Journal of Cell Biology* **1990,** *110* (4), 895-901.

22. Hamill, D. R.; Suprenant, K. A. Characterization of the Sea Urchin Major Vault Protein: A Possible Role for Vault Ribonucleoprotein Particles in Nucleocytoplasmic Transport. *Developmental Biology* **1997,** *190* (1), 117-128.

23. Herrmann, C.; Volknandt, W.; Wittich, B.; Kellner, R.; Zimmermann, H. The Major Vault Protein (MVP100) Is Contained in Cholinergic Nerve Terminals of Electric Ray Electric Organ. *Journal of Biological Chemistry* **1996,** *271* (23), 13908-13915.

24. Vasu, S. K.; Kedersha, N. L.; Rome, L. H. cDNA Cloning and Disruption of the Major Vault Protein Alpha Gene (mvpA) in *Dictyostelium Discoideum*. *Journal of Biological Chemistry* **1993,** *268* (21), 15356-15360.

25. Rome, L. H.; Kickhoefer, V. A. Development of the Vault Particle as a Platform Technology. *ACS Nano* **2013,** *7*, 889-902.

26. Kickhoefer, V. A.; Stephen, A. G.; Harrington, L.; Robinson, M. O.; Rome, L. H. Vaults and Telomerase Share a Common Subunit, TEP1. In *Journal of Biological Chemistry*, 1999; Vol. 274, pp 32712-32717.

27. Kickhoefer, V. A.; Siva, A. C.; Kedersha, N. L.; Inman, E. M.; Ruland, C.; Streuli, M.; Rome, L. H. The 193-kD vault protein, VPARP, is a novel poly(ADP-ribose) polymerase. *Journal of Cell Biology* **1999,** *146* (5), 917-928.

28. Kickhoefer, V. A.; Liu, Y.; Kong, L. B.; Snow, B. E.; Stewart, P. L.; Harrington, L.; Rome, L. H. The telomerase/vault-associated protein TEP1 is required for vault RNA stability and its association with the vault particle. *Journal of Cell Biology* **2001,** *152* (1), 157-164.

29. Kickhoefer, V. A.; Searles, R. P.; Kedersha, N. L.; Garber, M. E.; Johnson, D. L.; Rome, L. H. Vault ribonucleoprotein particles from rat and bullfrog contain a related small RNA that

is transcribed by RNA polymerase III. *Journal of Biological Chemistry* **1993,** *268* (11), 7868-7873.

30. Mikyas, Y.; Makabi, M.; Raval-Fernandes, S.; Harrington, L.; Kickhoefer, V. A.; Rome, L. H.; Stewart, P. L. Cryoelectron microscopy imaging of recombinant and tissue derived vaults: localization of the MVP N termini and VPARP. *Journal of Molecular Biology* **2004,** *344* (1), 91-105.
31. Tanaka, H.; Kato, K.; Yamashita, E.; Sumizawa, T.; Zhou, Y.; Yao, M.; Iwasaki, K.; Yoshimura, M.; Tsukihara, T. The structure of rat liver vault at 3.5 angstrom resolution. *Science* **2009,** *323* (5912), 384-388.
32. Kedersha, N. L.; Heuser, J. E.; Chugani, D. C.; Rome, L. H. Vaults. III. Vault ribonucleoprotein particles open into flower-like structures with octagonal symmetry. *Journal of Cell Biology* **1991,** *112* (2), 225-235.
33. Stephen, A. G.; Raval-Fernandes, S.; Huynh, T.; Torres, M.; Kickhoefer, V. A.; Rome, L. H. Assembly of vault-like particles in insect cells expressing only the major vault protein. *Journal of Biological Chemistry* **2001,** *276* (26), 23217-23220.
34. Han, M.; Kickhoefer, V. A.; Nemerow, G. R.; Rome, L. H. Targeted vault nanoparticles engineered with an endosomolytic peptide deliver biomolecules to the cytoplasm. *ACS Nano* **2011,** *5*, 6128-6137.
35. Kickhoefer, V. A.; Garcia, Y.; Mikyas, Y.; Johansson, E.; Zhou, J. C.; Raval-Fernandes, S.; Minoofar, P.; Zink, J. I.; Dunn, B.; Stewart, P. L.; Rome, L. H. Engineering of vault nanocapsules with enzymatic and fluorescent properties. *Proceedings of the National Academy of Sciences of the United States of America* **2005,** *102*, 4348-4352.

36. Buehler, D. C.; Toso, D. B.; Kickhoefer, V. A.; Zhou, Z. H.; Rome, L. H. Vaults engineered for hydrophobic drug delivery. *Small* **2011,** *7*, 1432-1439.

37. Kar, U. K.; Srivastava, M. K.; Andersson, A.; Baratelli, F.; Huang, M.; Kickhoefer, V. A.; Dubinett, S. M.; Rome, L. H.; Sharma, S. Novel CCL21-vault nanocapsule intratumoral delivery inhibits lung cancer growth. *PLoS ONE* **2011,** *6* (5), e18758.

38. Kickhoefer, V. A.; Han, M.; Raval-Fernandes, S.; Poderycki, M. J.; Moniz, R. J.; Vaccari, D.; Silvestry, M.; Stewart, P. L.; Kelly, K. A.; Rome, L. H. Targeting Vault Nanoparticles to Specific Cell Surface Receptors. *ACS Nano* **2009,** *3* (1), 27-36.

39. Champion, C. I.; Kickhoefer, V. A.; Liu, G. C.; Moniz, R. J.; Freed, A. S.; Bergmann, L. L.; Vaccari, D.; Raval-Fernandes, S.; Chan, A. M.; Rome, L. H.; Kelly, K. A. A Vault Nanoparticle Vaccine Induces Protective Mucosal Immunity. *PLoS One* **2009,** *4* (4), e5409.

40. Buehler, D. C.; Marsden, M. D.; Shen, S.; Toso, D. B.; Wu, X.; Loo, J. A.; Zhou, Z. H.; Kickhoefer, V. A.; Wender, P. A.; Zack, J. A.; Rome, L. H. Bioengineered Vaults: Self-Assembling Protein Shell–Lipophilic Core Nanoparticles for Drug Delivery. *ACS Nano* **2014,** *8*, 7723-7732.

41. Lai, C. Y.; Wiethoff, C. M.; Kickhoefer, V. A.; Rome, L. H.; Nemerow, G. R. Vault nanoparticles containing an adenovirus-derived membrane lytic protein facilitate toxin and gene transfer. *ACS Nano* **2009,** *3* (3), 691-699.

42. Douglas, T.; Young, M. Host-Guest Encapsulation of Materials by Assembled Virus Protein Cages. *Nature* **1998,** *393* (6681), 152-155.

43. Douglas, T.; Young, M. Viruses: Making Friends with Old Foes. *Science* **2006,** *312* (5775), 873-875.

44. Sanchez-Sanchez, L.; Tapia-Moreno, A.; Juarez-Moreno, K.; Patterson, D. P.; Cadena-Nava, R. D.; Douglas, T.; Vazquez-Duhalt, R. Design of a VLP-Nanovehicle for CYP450 Enzymatic Activity Delivery. *Journal of Nanobiotechnology* **2015,** *13* (1), 66.

45. Tien, M.; Kirk, T. K. Lignin peroxidase of *Phanerochaete chrysosporium*. *Methods in Enzymology* **1988,** *161*, 238-249.

46. Hofrichter, M.; Vares, K.; Scheibner, K.; Galkin, S.; Sipila, J.; Hatakka, A. Mineralization and solubilization of synthetic lignin by manganese peroxidases from *Nematoloma frowardii* and *Phlebia radiata*. *Journal of Biotechnology* **1999,** *67* (2-3), 217-228.

47. Hofrichter, M.; Fritsche, W. Depolymerization of Low-Rank Coal by Extracellular Fungal Enzyme Systems. III. *In vitro* Depolymerization of Coal Humic Acids by a Crude Preparation of Manganese Peroxidase from the White-Rot Fungus *Nematoloma Frowardii* b19. *Applied Microbiology and Biotechnology* **1997,** *47* (5), 566-571.

48. Hofrichter, M.; Lundell, T.; Hatakka, A. Conversion of Milled Pine Wood by Manganese Peroxidase from *Phlebia Radiata*. *Applied and Environmental Microbiology* **2001,** *67* (10), 4588-93.

49. Poderycki, M. J.; Kickhoefer, V. A.; Kaddis, C. S.; Raval-Fernandes, S.; Johansson, E.; Zink, J. I.; Loo, J. A.; Rome, L. H. The Vault Exterior Shell Is a Dynamic Structure that Allows Incorporation of Vault-Associated Proteins into Its Interior. *Biochemistry* **2006,** *45* (39), 12184-12193.

50. Kim, J.; Grate, J. W. Single-Enzyme Nanoparticles Armored by a Nanometer-Scale Organic/Inorganic Network. *Nano Letters* **2003,** *3* (9), 1219-1222.

51. Taqieddin, E.; Amiji, M. Enzyme Immobilization in Novel Alginate-Chitosan Core-Shell Microcapsules. *Biomaterials* **2004,** *25* (10), 1937-1945.

52. Cho, Y. K.; Bailey, J. E. Immobilization of Enzymes on Activated Carbon: Properties of Immobilized Glucoamylase, Glucose Oxidase, and Gluconolactonase. *Biotechnology and Bioengineering* **1978,** *20* (10), 1651-1665.

53. Henley, J. P.; Sadana, A. Categorization of enzyme deactivations using a series-type mechanism. *Enzyme and Microbial Technology* **1985,** *7* (2), 50-60.

54. Henley, J. P.; Sadana, A. Series-type enzyme deactivations: influence of intermediate activity on deactivation kinetics. *Enzyme and Microbial Technology* **1984,** *6* (1), 35-41.

55. Sadana, A.; Henley, J. P. Single-Step Unimolecular Non-First-Order Enzyme Deactivation Kinetics. *Biotechnology and Bioengineering* **1987,** *30* (6), 717-723.

56. Wariishi, H.; Valli, K.; Gold, M. H. Manganese(II) Oxidation by Manganese Peroxidase from the Basidiomycete *Phanerochaete chrysosporium*. Kinetic Mechanism and Role of Chelators. *Journal of Biological Chemistry* **1992,** *267*, 23688-23695.

57. Esfandiary, R.; Kickhoefer, V. A.; Rome, L. H.; Joshi, S. B.; Middaugh, C. R. Structural Stability of Vault Particles. *Journal of Pharmaceutical Sciences* **2009,** *98*, 1376–1386.

58. Urek, R. O.; Pazarlioglu, N. K. Purification and Partial Characterization of Manganese Peroxidase from Immobilized *Phanerochaete chrysosporium*. *Process Biochemistry* **2004,** *39* (12), 2061-2068.

## Chapter 3 A Vault-encapsulated Enzyme Approach for Efficient Degradation and Detoxification of Bisphenol A and its Analogues

### 3.1 Introduction

Enzymatic bioremediation, which utilizes enzymatic catalysis to degrade or transform contaminants in the environment, has been explored for several decades.[1-4] Benefiting from high efficiency and specificity of enzymes, enzymatic treatment is therefore considered effective and, because of its reduced chemical and energy use, congruent with the principles of environmental sustainability.[1, 4, 5] However, as many enzymes are not stable outside living cells, and can be inactivated by heat, co-contaminants, and products formed by their own activities, the use of enzymes in water treatment requires high dosage and frequent replenishment, which raises cost and limits their applications in large scale systems.[1] A potential solution is to entrap enzymes in solid supports, such as alginate beads, hollow fiber membranes, and magnetic particles,[1] to lower dosage and prevent inactivation, thus reduce the cost. But entrapped enzymes usually become less active due to substrate diffusion resistance caused by the solid supports.[1, 5, 6] Recent advances in nanotechnology have provided a wide variety of nanomaterials that are potential alternatives to conventional entrapment supports. Owing to their small dimensions, substrate diffusion problems can be minimized in nano-immoblization, which benefit enzyme catalytic efficiency.[5, 6] However, most of these materials, such as carbon nanotubes, polymeric nanoparticles, and mesoporous metal oxides, require harsh synthesis conditions and generate hazardous wastes.[6]

The use of bio-nanomaterials in enzyme stabilization is gaining more attention, as they are synthesized under physiological conditions and create less waste streams.[7] We recently reported a protein scaffold based stabilization approach by encapsulating enzymes in vault

nanoparticles.[8] Vaults are the largest natural ribonucleoprotein particle with dimensions of 41 x 41 x 72.5 nm, which are synthesized in humans and many other eukaryotes.[9] Each native vault consists of 78 copies of major vault protein (MVP), which assemble into the outer shell of the particle, and several copies of two different vault-associated proteins and small, untranslated RNAs.[9] Synthesized from heterologously expressed MVP in insect cells, recombinant vaults are empty protein shells that are morphologically identical to native vault particles, and do not cause any adverse public health effects.[10] Recombinant vaults have a core cavity of around 3.87 x $10^4$ nm,[3 11] which enable it to be a plausible carrier for encapsulating large macromolecules. The INT domain, a protein sequence that was derived from one of the vault-associated proteins, has a strong non-covalent interaction with vault interior binding sites, and can direct and sequester fusion proteins containing this domain inside vaults.[12] Using the INT fusion strategy, manganese peroxidase (MnP) was encapsulated in vaults, and the resulted vault-encapsulated MnP exhibited better stability during storage and higher resistance against heat inactivation than free MnP.[8] However, the effectiveness of vault encapsulation towards enhancing enzymatic treatment of various water contaminants is still unknown.

Bisphenol A (BPA), a chemical commonly used in plastic, paper, and food packaging industries, is one of the most prevalent endocrine disrupting compounds (EDC) in the environment.[13] A large number of studies have epidemiologically and mechanistically linked BPA exposure to a variety of significant adverse health effects including, most notably, a strong impact on reproduction and fertility.[14] In recent years, these health risk concerns associated with its exposure have led to a substitution of BPA with structural analogues, such as bisphenol F (BPF), bisphenol S (BPS) and bisphenol AP (BPAP) (Figure 3.S1). Such analogues are now being used in numerous commercial products and, consequently, they are now also found in

different water systems, such as surface water,[15] wastewater,[16] and sediments.[13] However, due to their high degree of structural similarities with BPA, many of these substitutes have been shown to possess similar endocrine disrupting activity and reproductive toxicity as BPA.[17, 18]

Several oxidative enzymes, such MnP, horseradish peroxidase, and laccase, have been demonstrated to mediate transformation of BPA *via* coupling reactions or scission reactions.[2, 19] However, similar to many other oxidation processes, enzymatic catalysis does not completely mineralize bisphenols (BPs), leaving a wide range of intermediates.[2, 20, 21] Since their chemical structure is similar to that of their parent compounds, such intermediates are also likely to pose health risks, especially the reproductive effects, which are considered as hallmarks of BPs' toxicity.[17, 22-27] Several studies have assessed toxicity of BPA oxidative transformation products, but focused on acute toxicity only.[20, 21] Evaluation of reproductive toxicity of such intermediates will provide deeper understandings of detoxification processes of BPs and benefit efficiency assessment of various remediation strategies.

The aim of this study was to develop a vault encapsulated enzymatic system as an effective and sustainable approach towards contaminants removal and detoxification. First, the effect of vault encapsulation on MnP enzyme kinetics was assessed. Then, we investigated the transformation of BPA and its analogues BPS, BPF, and BPAP by vault-encapsulated MnP (hereafter vMnP) at low enzyme dosage, and compared it with unencapsulated MnPs. Finally, we used a combination of *in vitro* and *in vivo* assays to assess whether the degradation of the parent compound led to the production of transformation products that caused lower estrogenic and reproductive effects.

## 3.2 Material and Methods

### 3.2.1 Preparation of Vault Nanoparticles Encapsulated With MnP

Vaults and recombinant MnP-INT (rMnP) were expressed in *Spodoptera frugiperda* (Sf9) insect cells infected with baculoviruses encoding either hMVP or rMnP as previously described.[8] The rMnP was encapsulated in vaults and purified following standard vault processing protocols.[8, 28] Purified vMnP was fractionated on a 4-15% SDS-PAGE gel and analyzed by Coomassie staining and Western blotting using primary rabbit anti-INT antibody and secondary goat anti-rabbit IgG (H+L) (IRDye 800CW, LI-COR). Negative-stain Transmission Electron Microscopy (TEM) was then performed to confirm the intactness, shape, and size of encapsulated vault particles. Number-based particle size distributions and zeta potentials of empty and encapsulated vaults were determined using PALS (ZetaPALS, Brookhaven Instruments).

### 3.2.2 Enzymatic Kinetics Studies

Concentrations of non-encapsulated rMnP or vMnP were determined by enzyme-linked immunosorbent assay (ELISA). Antibodies for ELISA were primary rabbit anti-INT antibody and secondary goat anti-rabbit IgG HRP antibody (BioRad), which were quantified by using the chromogenic reaction of TMB (Dako) according to the manufacturer's instructions. Native MnP (nMnP) was purified from *Phanerochaete chrysosporium* culture as described previously,[8] and quantified by measuring its absorbance at 406 nm which is maximum absorption wavelength of native MnP enzyme ($\varepsilon_{406nm}$ = 129.3 $mM^{-1}$ $cm^{-1}$).[29]

Manganese divalent ion substrate assays were performed in 200 µL mixture containing pH 4.0 50 mM malonate buffer, MnP, $MnCl_2$ (50 – 1000 µM), and 100 µM $H_2O_2$. Assays for

$H_2O_2$ substrate were performed in the similar system but containing 1000 μM $MnCl_2$ and 5 – 100 μM $H_2O_2$. For the substrates ABTS (2,2'-azino-bis(3-ethylbenzothiazoline-6-sulphonic acid)) and guaiacol, the assays were carried in 50 mM malonate buffer containing MnP enzyme, 2 mM $MnCl_2$, 100 μM $H_2O_2$ with either ABTS (2.5 – 500 μM) or guaiacol (5 – 125 μM) (details in SI). All kinetics assays were carried out at room temperature in triplicate. Initial reaction rates of each substrate were plotted against corresponding concentrations, which were fit to Michaelis-Menten kinetics model using non-linear regression.

### 3.2.3 Transformation of BPs

All BPs removal reactions were performed at 25°C in a shaking incubator (250 rpm). For each BP, the reaction mixture was composed of 80.3 μL of pH 4.5 50 mM malonate buffer, 10 μL of each type of MnP, 0.74 μL of 20 mM BP dissolved in methanol, 7.5 μL of 20 mM $MnCl_2$ and 1.5 μL of 20 mM $H_2O_2$, with a final volume of 100 μL. MnP enzyme was dosed at 19.3, 15.3, 23.3, and 23.3 U/L for BPA, BPS, BPF, and BPAP reactions, respectively. The enzyme activity assays were carried out in a pH 4.5 50 mM malonate buffer containing 2 mM $MnCl_2$, 400 μM $H_2O_2$, and 100 μM ABTS. Absorbance increases at 420 nm were recorded for 30 seconds with a 2-second interval for calculating initial ABTS oxidation rates. Enzyme free conditions were included to correct for any non-enzymatic losses of BPs. At each pre-specified time point, triplicate samples were terminated by adding three volumes of methanol, followed by filtration through 0.2 μm syringe filters. The residual BP concentrations were measured using a HPLC as described in the SI. BPA removal was also tested at pH values ranging from 4.0 to 5.5 with a gradient of 0.5. Reaction mixtures were set up as described above in 50 mM malonate

buffers at various pHs, each with an initial enzyme activity of 15.3 U/L. Samples were collected at 0 and 24 hours in triplicates, and analyzed using HPLC.

### 3.2.4 Characterization of Products

Eleven-milliliter reactions in pH 4.5 50 mM malonate buffers, containing 4.97 x $10^{-2}$ μM MnP (vMnP or nMnP), 1.5 mM $MnCl_2$, 300 μM $H_2O_2$, and 150 μM BP (BPA, BPF, or BPAP), were incubated at 25 °C, 250 rpm. Matrix tests containing all components except for MnP and BPs were performed as background negative controls, and enzyme-free assays containing all components except for MnP were performed as positive controls. Recoveries of BPA, BPF, and BPAP were also evaluated in the system only contained malonate buffer and 150 μM of BP (Table 3.S1). After 24-hour reaction, 1 mL of solution was collected from each sample and mixed with 2 mL of methanol, and stored prior to determining residual BP concentrations using HPLC. The remaining 10 mL solution was subjected to solid-phase extraction (SPE) and processed as described in SI. The final concentrated SPE eluate in 10 μL ethanol was used for product characterization and toxicity tests. Two microliters of final concentrated SPE eluate were diluted in 50 μL of methanol, and the diluted samples were then subjected to UPLC/MS analyses to characterize products (details in SI). Qualitative and quantitative analyses of UPLC/MS data were carried out using MZmine 2. Detailed data processing methods and parameters are listed in Table 3.S2.

### 3.2.5 Toxicity Evaluation Studies

#### *3.2.5.1 Estrogen receptor competitive binding assay*

The binding affinities of each BP and its transformation products towards estrogen receptors α and β were examined by ThermoFisher Scientific performing a time-resolved Förster resonance energy transfer (TR-FRET) based ER competitive binding assay according to the manufacturer's instructions. Briefly, BPs or their metabolites compete with a fluorescent ER ligand (tracer) for binding to the human ER α or β. The displacement of the tracer from the ER reduces fluorescent signal emission triggered by the excitation of conjugated terbium on the receptor. Based on the fluorescence loss, a dose-response curve was generated for each tested chemicals and the half maximal inhibitory concentration ($IC_{50}$) was then calculated.

#### *3.2.5.2 Nematode chemical exposure*

*Caenorhabditis elegans* nematodes were exposed to numbered and blinded samples of BPA, BPF, and BPAP as well as their degradation products following the protocol described previously.[30] Briefly, worm embryos were collected from the sensitized strain carrying the yIs34[*Pxol-1::GFP, rol-6*] reporter construct[30] by hypochlorite sodium treatment followed by L1 synchronization. L4 stage larvae were then transferred to M9 liquid culture buffer mixed with 100 μM of each BP or their degradation products for 24 hours for germline apoptosis assay (peak of germline morphology and function), and 48 hours for fertility assessment (to maximize the number of impacted germ cells becoming embryos). Worms were cultured with heat-inactivated bacteria as food in order to avoid potential bacterial metabolism of the compounds. New concentrated heat-inactivated bacteria were added at 24 hours when performing a 48 hour exposure to prevent food depletion.

#### *3.2.5.3 Germline apoptosis assay*

After 24 hours exposure as described above, worms were incubated with 25 μg/mL of acridine orange in M9 solution at room temperature for 2 hours to stain the apoptotic nuclei in the germline as described previously.[31] After staining, the worms were transferred to new NGM plates for a 30 mins recovery and healthy worms were selected for microscopic examination. The total number of apoptotic nuclei in the posterior gonad of each worm was counted by fluorescence microscopy.

#### *3.2.5.4 Fertility assessment*

After 48 hours exposure, worms from each treatment group were individually transferred to new NGM plates without cholesterol and transferred every 12 hours to a new plate. The numbers of eggs laid by each worm, larvae hatched from these eggs (i.e. embryonic lethality), and larvae successfully reaching adulthood (i.e. larval lethality) were tallied in the three days after exposure.

## 3.3 Results

### 3.3.1 Characterization of vMnP

We first assessed whether MnP and vault complexes were properly formed *in vitro* by Western blot analysis, Coomassie staining, and TEM images (Figure 3.S2A and 3.S2B). Vaults containing rMnP exhibited similar morphology and zeta potentials as empty vaults, but showed a slightly up-shifted distribution of hydrodynamic diameter (Figure 3.S2C and 3.S2D, Details in SI).

Previously, we found that encapsulation in vaults elevated the apparent Michaelis-Menten half saturation constants ($K_m$) for ABTS,[8] but the mechanism was not established. To fully understand the effect of vault encapsulation on MnP kinetics, we further evaluated $K_m$ and turnover numbers ($k_{cat}$) of four substrates including $Mn^{2+}$, $H_2O_2$, ABTS, and guaiacol. Results are summarized in Table 3.1, and the plots are shown in Figure 3.S3. For all substrates under study, $K_m$ values of recombinant rMnP ranged from 30% higher for guaiacol (80±15 vs. 61±7 μM) to 17% lower for ABTS (75±3 vs. 90±6 μM) than the numbers for nMnP, indicating that heterologous expression in Sf9 cells and fusion of INT domain did not substantially alter the affinity between the MnP enzyme and its substrates. Comparing $K_m$ values between rMnP and vMnP, no significant change was observed for $H_2O_2$ and guaiacol, but a decrease and increase were noted for $Mn^{2+}$ and ABTS respectively. It is also observed that rMnP displayed about 3-fold lower $k_{cat}$ relative to the nMnP for each of the substrates tested, which is commonly found for recombinant enzymes.[32] When comparing $k_{cat}$ of vMnP and rMnP, the changes ranged from about 20% decrease for $Mn^{2+}$ (20.3±0.5 vs. 26.4±0.5 $s^{-1}$, respectively) to no significant change in the case of guaiacol (13.3±1.2 vs. 14.0±1.3 $s^{-1}$, respectively). The changes in overall catalytic efficiency ($k_{cat}/K_m$) followed similar pattern as $k_{cat}$. Native MnP showed about 3-fold higher efficiency than encapsulated or free INT-fused MnP for all four tested substrates, which is most likely attributed to its higher $k_{cat}$ numbers. Comparing the catalytic efficiencies of vMnP and rMnP, these two MnPs showed close $k_{cat}/K_m$ values (less than 10% difference) for the substrates studied in this experiment except for ABTS. The ABTS $k_{cat}/K_m$ value of rMnP was about 1.6-fold higher than that of vMnP, which mostly resulted from the lower ABTS $K_m$ value for rMnP. Together, these experiments confirm that encapsulation in vault particles has limited effect on the enzyme's kinetic properties.

**Table 3.1** Michaelis-Menten Kinetics Parameters of Three Types of MnPs for Substrates $Mn^{2+}$, $H_2O_2$, ABTS, and Guaiacol.

| | | [a]$K_M$ (μM) | [a]$k_{cat}$ ($s^{-1}$) | $k_{cat}/K_M$ ($s^{-1}$ $\mu M^{-1}$) |
|---|---|---|---|---|
| [b]$Mn^{2+}$ | vMnP | 285±19 | 20.3±0.5 | 0.0712±0.005 |
| | rMnP | 331±14 | 26.4±0.5 | 0.0798±0.004 |
| | nMnP | 271±13 | 72.3±1.4 | 0.267±0.014 |
| [c]$H_2O_2$ | vMnP | 28±3 | 10.5±0.4 | 0.38±0.04 |
| | rMnP | 34±3 | 13.8±0.5 | 0.41±0.04 |
| | nMnP | 31±3 | 38.6±1.5 | 1.2±0.13 |
| [d]ABTS | vMnP | 103±8 | 29.6±0.8 | 0.29±0.02 |
| | rMnP | 75±3 | 35.2±0.4 | 0.47±0.02 |
| | nMnP | 90±6 | 118±3 | 1.3±0.09 |
| [d]Guaiacol | vMnP | 67±12 | 13.3±1.2 | 0.20±0.04 |
| | rMnP | 80±15 | 14.0±1.3 | 0.18±0.04 |
| | nMnP | 61±7 | 58±3 | 0.95±0.12 |

a. Data are presented as the mean ± one standard error from 3 replicates of 5-6 substrate concentrations.

b. Reactions were conducted in the presence of 100 μM $H_2O_2$.

c. Reactions were conducted in the presence of 1 mM $Mn^{2+}$. $k_{cat}$ for $H_2O_2$ was calculated according to the reported stoichiometry of 2 mol of $Mn^{3+}$ produced per mole of $H_2O_2$ consumed.

d. Reactions were conducted in the presence of 2 mM $Mn^{2+}$ and 100 μM $H_2O_2$.

### 3.3.2 Transformation of BPA

Several 24-hour time-course removal tests were performed using vMnP, rMnP, and nMnP, each with a low initial enzyme dosage at 19.3 U/L, which is 10-100 times lower than the dosage employed in previous peroxidase-catalyzed degradation studies.[2, 19] As shown in

Figure 3.1A, BPA concentration quickly dropped by 20-38% in the first 30 minutes. Afterwards, nMnP and rMnP mediated BPA conversion stopped, and no further significant removal was observed. In contrast, BPA transformation under vMnP catalysis lasted for at least another 4 hours. After 24 hours, vMnP achieved approximately 96% removal of BPA, whereas only 42% and 25% BPA removals were observed for rMnP and nMnP, respectively (Figure 3.1A).

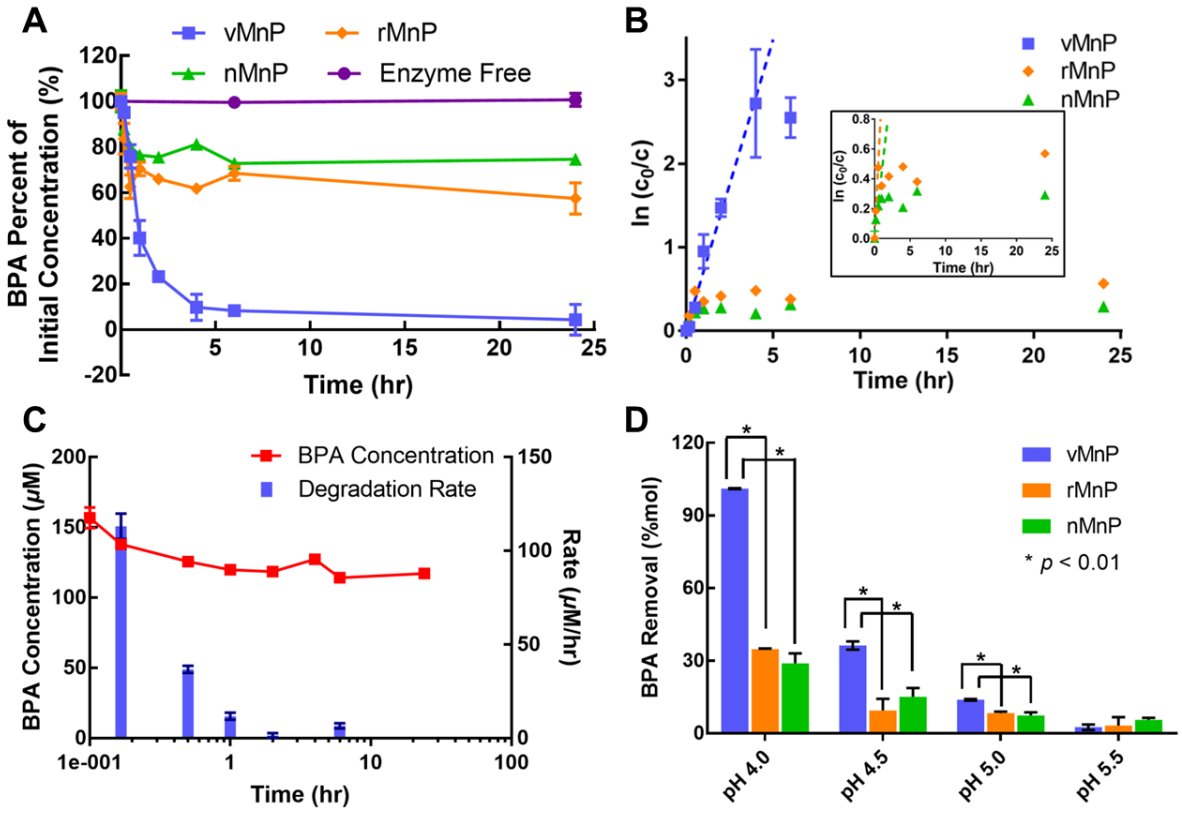


**Figure 3.1** Enhanced BPA Removal by MnP Encapsulated in Vaults. (A) Removal of BPA Mediated by vMnP, rMnP and nMnP. In 24 hours, vMnP degraded nearly 100% BPA, as compared with only 30-40% BPA degradation by rMnP and nMnP enzymes. (B) Pseudo-first order kinetics of BPA transformation. vMnP mediated BPA transformation followed pseudo-first order kinetics in the first four hours, but nMnP and rMnP driven BPA conversion only obeyed the kinetics for the first 30 minutes. (C) nMnP mediated BPA conversion rates. The rate of nMnP catalyzed BPA removal immediately decreased after initiating reaction. (D) Vault-packaging Enhanced BPA Removal at Various pHs. Error bars represent one standard error of the mean (n=3).

BPA conversion mediated by vMnP followed a pseudo-first order kinetics for the first 4 hours (Figure 3.1B), indicating there was no enzyme activity loss during this period. Between 4

and 24 hours, the concentration of BPA further decreased from 10% to 4% of the initial concentration, indicating that vMnP still maintained activity. However, reactions no longer followed the pseudo-first order kinetics. The alteration of BPA transformation kinetics was probably due to the competitive inhibition of vMnP by products formed by its activities, as over 90% of BPA was converted after 4 hours and the resulting products were also favorable substrates of MnP enzymes.[2] For rMnP and nMnP, the pseudo-first order conversion of BPA was only maintained for 30 minutes or less (Figure 3.1B). Figure 3.1C shows the change of nMnP mediated BPA conversion rates, which are calculated by normalizing concentration decreases to the intervals between two time points over the 24-hour testing period. The rate peaked in the first ten minutes to 113.0 μM/h, and then rapidly decreased to near-zero in two hours. Similar results were also observed for rMnP, suggesting that both unencapsulated enzymes quickly lost their activities after initiating reactions, and had significantly shorter lives under experimental conditions.

Next, we compared the performance of the three MnPs for removing BPA at different pHs in 24 hours (Figure 3.1D). The results indicate that vMnP consistently showed better performance than unencapsulated rMnP and nMnP at pH 4.0, 4.5, and 5.0. However, due to fact that optimum pH for MnP is around 4, very low BPA removal was observed at pH 5.5. Therefore, these results suggest that vMnP has longer functional longevity than nMnP, and can still efficiently remove BPA at low enzyme dosage.

### 3.3.3 Transformation of BPA Analogues

Although BPA has been progressively replaced away from some commercial products, most of its substitutes are analogues that share a high degree of structural similarities, suggesting

these alternatives may also be treatable by peroxidases. Therefore, we evaluated the effectiveness of vMnP for removing three widely used BPA analogues including BPS, BPF, and BPAP.[13]

Significant BPF and BPAP degradation was observed in the presence of each type of MnP tested, with BPF following very similar degradation kinetics compared to BPA (Figure 3.2A). After 24 hours of reaction, the concentration of BPF decreased to 10.4% of its initial concentration for the vMnP treatment, while it only reached 53.7% and 64.4% after rMnP and nMnP treatments, respectively. For unencapsulated MnPs, most of the BPF removal occurred in the first hour and no further concentration decrease was seen between 1 and 24 hours, while vMnP-mediated BPF conversion increased from 50.2% to 64.8% between 1 and 3 hours and finally reached 89.6% at 24 hours. In the case of BPAP, only 19.0% degradation occurred by nMnP treatment, which is much lower than that of BPA and BPF, the rMnP mediated BPAP degradation reached 85.1% in 24 hours (Figure 3.2B). Interestingly, vMnP exhibited slower BPAP conversion than rMnP in the first 6 hours. About 81.0% BPAP removal was observed for rMnP after 6-hour reaction, while only 43.5% BPAP degradation was observed for vMnP. Due to its low solubility, BPAP forms small aggregates when added into reaction solutions. These aggregates have larger size than the space between MVP peptides forming vaults' shell and have limited diffusion, thus the concentration of BPAP inside of the vaults is lower than when in solution and very limited amount of BPAP is accessible to vMnP. Consistent with the lower diffusion of BPAP, we observed that over longer incubation period (beyond 6 hours) 74.7% removal was achieved. For rMnP, the degradation rate only increased by 4.1% between 6 and 24 hours, indicating most of the enzyme lost its activity after 6-hour reaction. BPS was not degraded by all three MnPs within 24 hours (Figure 3.S4). Thus, the results of BPF and BPAP

degradation further demonstrate that encapsulation of MnP in vaults significantly extends enzyme life in reactions and improves contaminant transformation efficiency.

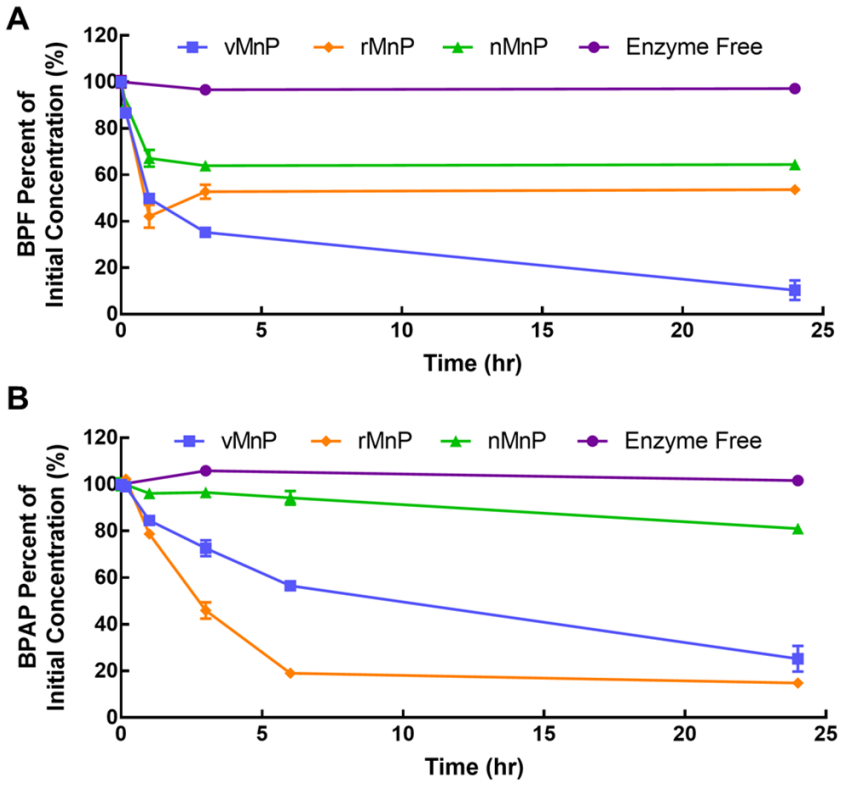


**Figure 3.2** Removal Kinetics of BPF (A) and BPAP (B) by MnPs. For BPF, vMnP catalysis reached nearly 90% removal, while rMnP and nMnP only achieved 46% and 35% removal, respectively. In the case of BPAP, vMnP showed lower removal than rMnP in the first 6 hours, but eventually caught up at 24 hours. Error bars represent one standard error of the mean (n=3).

### 3.3.4 Enzymatic Transformation Product Profiles

Since vMnP and rMnP exhibited different degradation kinetics, we next characterized and compared the product profiles after vMnP and nMnP treatments for each BP using UPLC/MS. Products were separated by their retention times and mass to charge ratios (Figure 3.3). This preliminary analysis indicates that vMnP and nMnP treatments generated significantly different product species as the reactions progressed. Referring to previously reported

mechanisms of peroxidase catalyzed BPs transformations,[2, 19] the proposed MnP mediated reaction pathways for BPA, BPF, and BPAP are presented in Figure 3.S5, 3.S6, and 3.S7, respectively. In general, the parent BPs undergo scission reactions that breakdown BPs to small-mass products, followed by coupling reactions that generate oligomeric BPs.

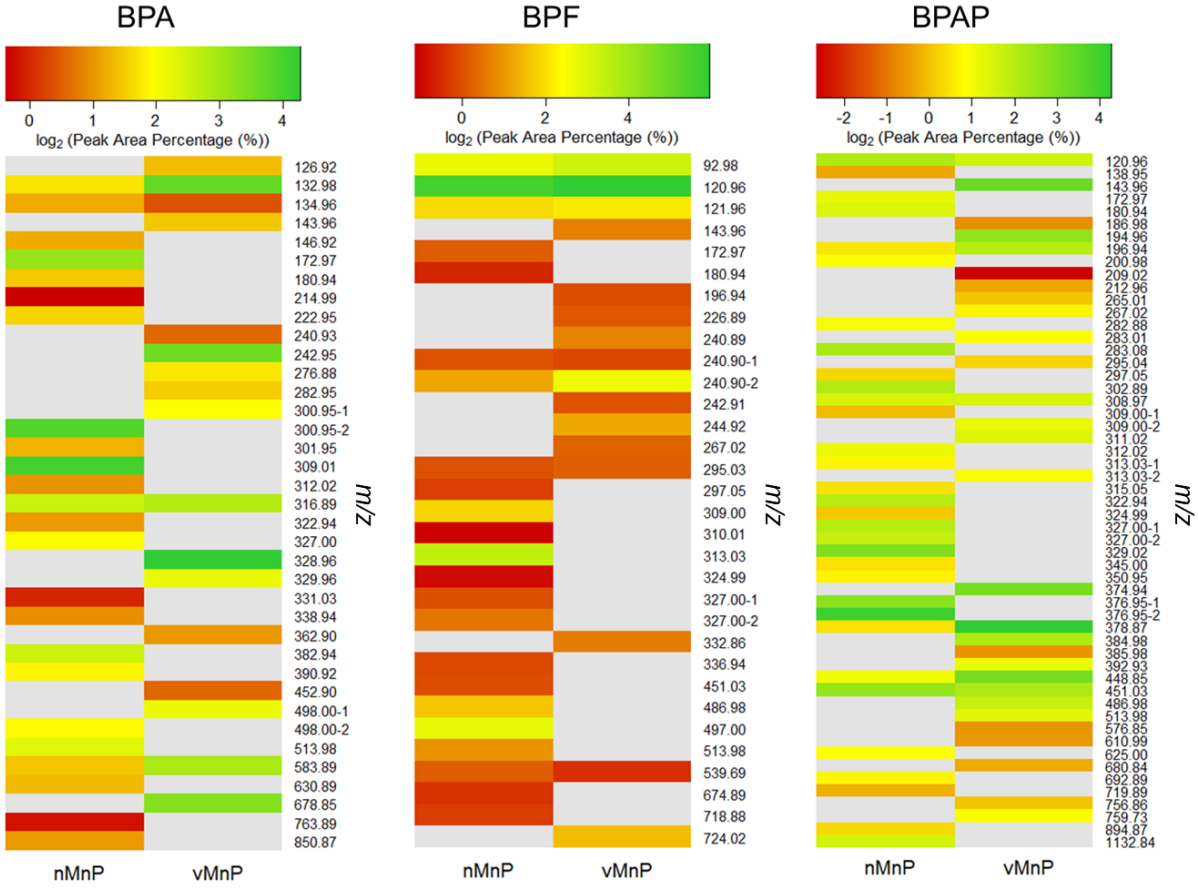


**Figure 3.3** Comparison of Product Profiles Among vMnP and nMnP Treatments for BPA, BPF, and BPAP. Products were separated and named by their UPLC retention time and mass-to-charge ratios, and plotted based on their relative abundance. Treatments by vMnP and nMnP generated significant different products. Grey color indicates that the ion was not detected in the sample.

In the case of BPA, 17 and 24 products were detected after vMnP and nMnP treatments respectively, most of which were not found in proposed MnP mediated BPA transformation. The packaged and unpackaged forms of MnP enzyme shared only 4 common products. Among the 17 species identified for vMnP treatment, 4 (Figure 3.S5, species A1-A4) were generated from

proposed MnP catalysis, making up about 43.6% of total MS response. For nMnP treatment, 24 species were identified, two of which were from the MnP catalyzed reaction (Figure 3.S5, species A1 and A3), and accounted for only 9.1% of total MS response. The ion 133, which is the first intermediate in the proposed pathway, was reported at an abundance of 13.1% of total MS response for vMnP as opposed to only 3.3% for nMnP. The next species in the pathway (Figure 3.S5, species A2) was only found in the sample from vMnP treatment. BPA trimers or oligomers (Figure 3.S5, species A4), which are formed at the end of the proposed pathway, exhibited an abundance of 10.1% of total MS response for vMnP, while those were not detected in the samples from rMnP treatment.

For BPF (Figure 3.3, middle panel), vMnP and nMnP treatments yielded more similar product profiles. Sixteen species were detected in the sample from vMnP treatment, five of which (Figure 3.S6, species F1- F5) were from proposed MnP-mediated reactions and made up for about 81.0% of total MS response. For nMnP treatment, 23 species were identified, which shared 7 species with the vMnP treatment, four of which (Figure 3.S6, species F1, F2, F3, and F4) were found in proposed enzymatic pathways and were about 60.0% of total MS response. Product F2 (4-hydroxybenzaldehyde), which is the second product in MnP catalyzed BPF transformation pathways, was the most abundant species in both treatments, suggesting the subsequent reactions converting F2 may not be favored. Although species F1 and F2 were very abundant in both conditions, they still exhibited a higher percentage in the sample from vMnP treatment.

Finally, the product profiles of BPAP were more complex than those of BPA and BPF (Figure 3.3, right panel). Twenty-nine and thirty-two product species were identified for vMnP and nMnP treatments respectively, only 6 of which were shared between two enzymes. Five

species (Figure 3.S7, P1-P5) in the proposed enzymatic pathway were found from vMnP treatment, which accounted for about 33.8% of the total MS response, while only 3 were identified from nMnP treatment, making up for less than 8% of total MS response, which agree with the findings for BPA and BPF. Together, these results imply that treatments by vMnP and nMnP resulted in significantly different product profiles, and transformation of BPs by vMnP fitted with proposed MnP-mediated pathways better than the transformation by nMnP.

### 3.3.5 Reduction in BPs' Toxicity

Exposure to BPA has been associated with a variety of toxic responses including strong reproductive effects across a variety of organisms through mechanisms that are sometimes distinct from its weak affinity for the estrogen receptor (ER).[33-35] BPA's reproductive effects can be considered a hallmark of its toxicity as BPA exposure leads to a decrease in fertility that correlates with a decreased viability of germ cells in a great number of animal species examined to date, including humans and well-established laboratory model organisms such as mouse, rat, zebrafish, drosophila, and *C. elegans* worms.[22-27, 36] The mechanisms underlying BPA's reproductive effects are also well conserved as BPA exposure was shown to cause an increase in germ cell death by apoptosis and an increase in chromosome errors and lethality in mouse and *C. elegans* early embryos.[22, 24, 27] In *C. elegans*, these findings were extended to the BPA analogue BPS suggesting that the similarity in chemical structure imparts comparable effects on germ cells.[17] The remarkable conservation of reproductive toxicity outcomes caused by BPA exposure was leveraged here to examine whether MnP-mediated degradation of BPA and its analogues decreases their associated toxicity by monitoring the model organism *C. elegans*.

Following a single-blind protocol, we first examined the induction of germline apoptosis in the midpoint of the *C. elegans* gonad by acridine orange staining. Following exposure to BPA and BPF at the reference concentration of 100 µM for 24 hours spanning the onset of reproduction (L4 to adult), we observed a significant 40% to 60% increase in the number of apoptotic nuclei when compared to the 0.1% ethanol vehicle control ($P \leq 0.05$, Student's t-test) (Figure 3.4). A similar significant increase was observed in the enzyme-free/mock treatment group. In contrast, vMnP treatment dramatically reduced BPA, BPF, and BPAP -mediated germline apoptosis effect to levels indistinguishable from controls. The results were more variable for the nMnP as BPA and BPF degradation did not reduce their impacts on germline apoptosis while it did for the BPAP group.

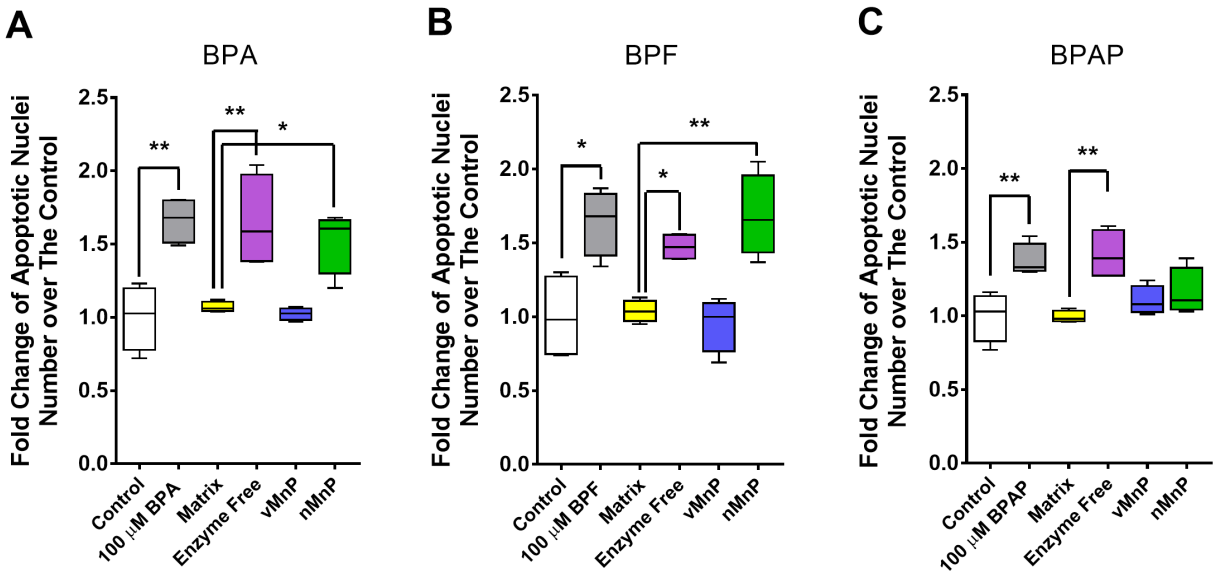


**Figure 3.4** Germline Apoptosis of Worms Exposed to Bisphenols and Their Biodegradation Products. As compared to vehicle control (0.1% ethanol), 24 hours exposure to 100µM of BPA (A), BPF (B), or BPAP (C) significantly increased apoptotic germline nuclei numbers by 66%, 64% and 38% respectively. The increase in germline apoptosis was also observed in the mock bisphenols groups with no treatment (Enzyme Free), as well as the nMnP treated BPA and BPF groups. In contrast, biodegradation mediated by vMnP completely removed the ability of BPA, BPF, and BPAP to induce germline apoptosis compared to the Matrix control (no chemical). Student's t-test performed for the comparison between the control and each 100µM bisphenol

group. One way-ANOVA with post-hoc Tukey HSD test performed for the comparison among all bisphenols treatment groups. *: $P<0.05$ and **: $P<0.01$. N=4.

Next, we assessed the impact of the various treatments on BPA, BPF, and BPAP-induced embryonic lethality (Figure 3.5). Compared to control, both BPA and BPAP exposure significantly increased the embryonic lethality by 48% and 38% respectively ($P\leq0.05$, student's t-test) while BPF exposure induced a 19% increase but failed to reach a statistical significance. Among all treatment groups -enzyme free/mock, nMnP, and vMnP- only the latter led to a reduction in embryonic lethality to a level comparable to controls. The stronger reduction in germline apoptosis compared to embryonic lethality can be explained by the fact that the solvent used 0.1% ethanol alone causes some degree of embryonic lethality and therefore increased the baseline of the lethality assay (Figure 3.S8). However, the embryonic results are particularly significant considering that no effect of any of the BPs was detected on later stages of the nematode's development as measured by larval survival assay (Figure 3.S9).

The dramatic decrease in the BPs' reproductive toxicity after vMnP treatment could be due to a reduction in their estrogenic activity. To test this possibility, we assessed the ability of nMnP and vMnP to decrease the association of BPA, BPF, and BPAP with the estrogen receptors α and β following treatment using a fluorescence displacement assay. After 24 hours, both nMnP- and vMnP-mediated transformation products showed a decreased ability to bind the ERs for all tested BPs (Figure 3.S10). Interestingly, vMnP exhibited a better performance towards reducing BPAP ER binding while nMnP displayed a preference towards BPA and BPF. However, taken together, these results highlight the potent detoxification of BPA, BPF, and BPAP by vMnP.

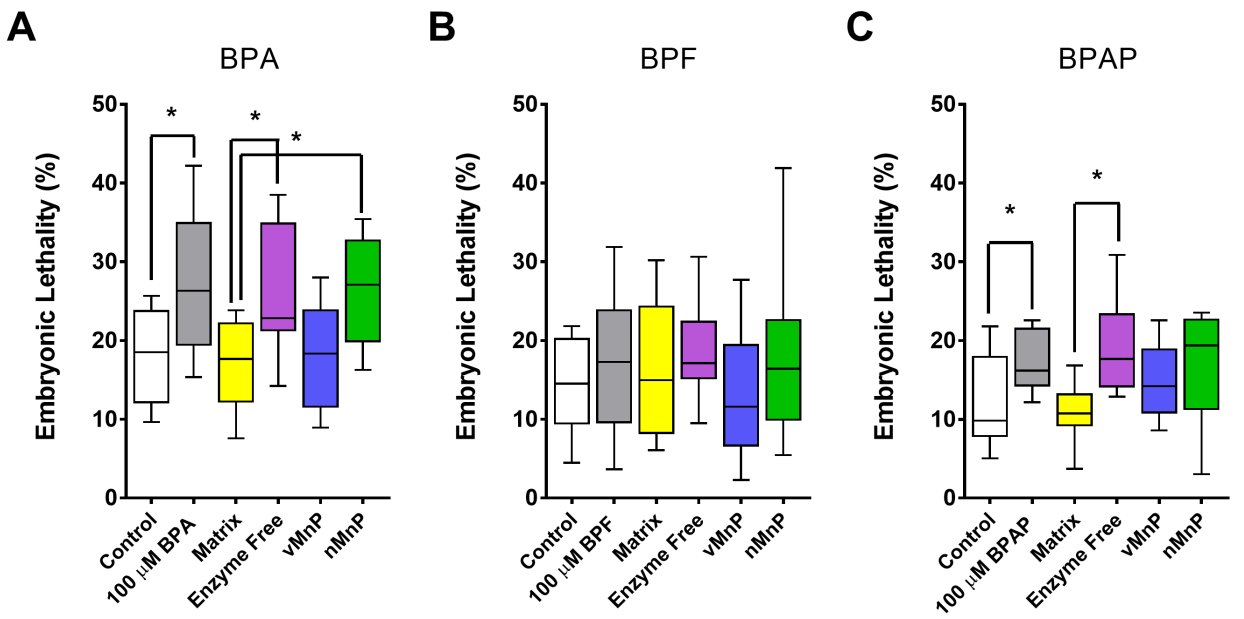


**Figure 3.5** Embryonic Lethality of Bisphenols and Their Biodegradation Products. Embryonic lethality is calculated as the percentage of unhatched eggs in all the eggs laid by each worm. Compared with the vehicle control (0.1% ethanol), exposure to 100 μM BPA (A) or BPAP (C) significantly increases the embryonic lethality by 48% and 38% respectively, while 100 μM BPF (B) showed a 22% increase but failed to reach statistical significance. After the biodegradation reaction, vMnP, but not nMnP, bisphenols treatment led to a reduction in embryonic lethality to a level comparable to the buffer control group (Matrix). Student's t-test performed for the comparison between the control and each 100μM bisphenol group. One way-ANOVA with post-hoc Tukey HSD test performed for the comparison among all bisphenols treatment groups. *: $P<0.05$. N=10-13.

### 3.4. Discussion

Application of white-rot fungi for removing organic micro-contaminants in water is becoming increasingly feasible.[3] As one of the major components in the extracellular enzymatic machinery of white-rot fungi, MnP is capable of degrading a wide variety of contaminants and has great potential in water treatment. By encapsulating MnP into vault nanoparticles, we observed significant improvement of BPA, BPF, and BPAP removal and remarkable decrease in reproductive toxicity of degradation products.

Unlike conventional encapsulation approaches that cause significant substrate diffusion resistance and enzyme inactivation, vault packaging had little effect on the enzymatic activity and caused negligible diffusion problems. Putting MnP into vaults led to different changes of $K_m$ for the four tested substrates. ABTS contains two sulfonate groups, thus is easily deprotonated in solution and exhibits negative charge. In contrast, $H_2O_2$ and guaiacol are neutral in the acidic assay buffer, and $Mn^{2+}$ is positively charged. Since vault particle exhibited a negative zeta-potential, we can infer that the electrostatic interaction between substrates and vaults resulted in the shift of $K_m$. Negatively charged substrates like ABTS are repelled by the particle, so that their concentrations in vaults are lower than them in the solution, which leads an increase of $K_m$. Likewise, positively charged substrate $Mn^{2+}$ is attracted and concentrated in vaults, thus it shows decreased $K_m$ for vMnP. More importantly, the similar $K_m$ between vMnP and rMnP for neutral substrates suggests vaults' shell is permeable and mass transfer resistance of soluble substrates across the shell is negligible. Thus, for soluble BPs, which are neutral in MnP reaction buffer, vault encapsulation is unlikely to induce substrate diffusional problems or $K_m$ increases. $k_{cat}$ values were consistent between vMnP and rMnP. Unlike the commonly used covalent binding or other strong interactions in enzyme encapsulation, which induce enzyme conformational changes and leads enzyme deactivation,[1] the antigen/antibody-like interaction affinity between the INT domain and the vaults' shell is strong enough to keep INT-fused MnP in the vault but may not affect the folding or conformation of fused MnP enzyme, thus rMnP can maintain its activity and functionality when encapsulated inside vaults.

The removal efficiencies of four tested BPs were ranked as BPA $\approx$ BPF > BPAP >> BPS, and vMnP showed higher removal rates than nMnP for all compounds except for BPS. The absence of BPS degradation was somewhat unexpected since it has two phenolic hydroxyl

groups that are favorite targets for MnP. However, similar results were also reported in a study testing natural attenuation of BPS in seawater,[37] which showed significant biodegradation of BPA and BPF, but not of BPS. One possible explanation is that the sulfonyl group that connecting two phenol functional groups makes BPS more electronegative (Figure 3.S1), thus BPS tends to be electron acceptor rather than donor. It is supported by a study comparing biodegradation of various BPs under aerobic and anaerobic conditions, which showed that BPS was highly tolerant against aerobic biodegradation but was more susceptible to anaerobic biodegradation.[38]

Comparing vMnP to nMnP in removing BPA, BPF, and BPAP, vMnP exhibited significantly higher transformation rates and extended functional longevity. To reduce the cost of enzyme usage and provide a cost-effective enzymatic treatment approach, we employed 10-100 times lower enzyme dosage than other studies,[2, 19] thus limited removal was observed using nMnP. It only lasted 0.5-1 hour in reactions, which was notably shorter than its storage life. The rapid enzyme inactivation can be attributed to the attack from $H_2O_2$,[1, 29] heme disruption caused by phenolic radicals,[39] or heat inactivation.[8] By encapsulating in vaults, enzymatic longevity in reactions was substantially improved (at least five folds during BPA degradation), which attests that vault encapsulation not only stabilizes enzymes during storage,[8] but also protects them from $H_2O_2$ and radical attack. The mechanism is not clear, but one possible way is to prevent heme release by hindering enzymatic conformation change upon attack.[4]

The distinct production of transformation products of each BPs between vMnP and nMnP treatments is also attributed to their different stability in reactions. With enhanced functional longevity, vMnP-mediated BPs transformation accorded more closely with proposed MnP catalytic mechanism (Figure 3.S5, 3.S6, and 3.S7), while the less stable nMnP resulted in

different products, the majority of which were not mapped to proposed MnP-mediated pathways. It is possible that BPs transformation intermediates that were formed by MnP activities were chemically transformed by oxidizing agents in the system, such as $H_2O_2$, which also contributed to the final product pool. For nMnP, the enzyme only survived long enough to convert BPA, BPF, and BPAP to the initial intermediates, as it was inactivated rapidly in the reactions. Afterwards, these initial intermediates were transformed mostly *via* chemical reactions, forming the majority of the detected products, which are not in the general enzymatic transformation pathways (Figure 3.S5, 3.S6, and 3.S7). For instance, in nMnP mediated BPA transformation, the species with a m/z of 181 is probably a product from chemical oxidation of A1 (Figure 3.S5) at the phenoxy group.[40] In contrast, vMnP lasted much longer in the reactions, which allowed the continued transformation to downstream products, such as BPA trimers or oligomers, which are relatively inert to chemical reactions and less toxic as discussed in detail below. Additionally, vMnP catalyzed reactions also consumed $H_2O_2$, thus further reduced the chance of direct chemical oxidation.

Finally, vMnP treatment significantly reduced the toxicity of the BPs tested, unlike nMnP treatment. For this purpose, we used the nematode *C. elegans* because of its tractability, short reproductive period, its conservation of reproductive pathways and of reprotoxicity response to BPA.[17, 22] Interestingly, we found that the ability of BPA and BPF to increase the germline apoptosis was eliminated by vMnP treatment but not by nMnP. As compared to nMnP, vMnP was more efficient in reducing the fertility impact of BPA and BPAP on nematodes. These results corroborate that vMnP not only efficiently removes the parent BPs from solution but also leads to the production of reaction intermediates and final products that are altogether less reprotoxic than the parent compounds. Divergence between vMnP and nMnP in decreasing

estrogenic activity of BPs was also noted. We attribute these differences to the distinct enzymatic kinetics with differing final product profiles. The partial overlap between the reprotoxicity assays and the ER binding assay is supported by the literature on BPA which shows that BPA-induced reproductive effects only partially correlate with its described weak estrogenic affinity.[33-35] Altogether, these experiments therefore highlight the utility and sensitivity of the reproductive endpoints in *C. elegans*, which can therefore serve to assess the efficacy of various water treatment strategies.

Previous studies on advanced oxidation of BPA showed that the product toxicity is highest at earlier time points, which was attributed to the accumulation of initial oxidation intermediates.[20, 21] It is believed that these initial intermediates are more toxic, while higher-molecular weight intermediates such as BPA dimers, trimmers, or oligomers, are relatively less toxic. In this study, although very low amounts of initial intermediates in the enzymatic pathway were detected for nMnP, it is possible that these compounds were chemically converted to structurally similar compounds, which still possess reproductive toxicity. For the vMnP system, significant amount of BP oligomers were detected, suggesting the conversion of initial intermediates to less toxic polymeric products *via* the enzymatic pathway. Thus, our results imply that this difference in product profiles might underlie the remarkable amelioration of BPs' toxicity following vMnP treatment.

### 3.5. Conclusions

This study evaluated the use of vault nanoparticles encapsulated MnP enzymes as an effective water treatment approach, and assessed the health risk of treatment products using a combination of *in vivo* and *in vitro* assays. It was demonstrated that vault encapsulation enhances

enzymatic functional longevity in reactions, and lowers enzyme dosage requirement for effective removal of bisphenolic water contaminants. The reduction in BPA, BPF, and BPAP's reproductive toxicity in the nematode *C. elegans* following vMnP treatment aligns with their efficient removal after 24 hours and suggests that the process does not generate significant amounts of degradation products that also carry reproductive activity. Therefore, enzyme stabilization in vault nanoparticles combined with rigorous assessment of product toxicity opens up an exciting perspective toward the application of safe and inexpensive enzymatic systems for the treatment of bisphenols and other endocrine-disrupting compounds in water.

## 3.6 Supporting Information

### Characterization of Vault Encapsulated MnP Enzymes

The formation of rMnP and vault complex was confirmed by Coomassie staining and Western blot analysis (Figure S2A). While by Coomassie staining vaults showed a clear band around 100 kD, which is the size of MVP peptides forming vaults' shell, only rMnP was detectable by Western blot. Probably due to its large size or the effect of MnP on INT binding affinity, the copy numbers of rMnP per vault were generally lower than those of other INT fused proteins we have tested. Further examination with negative stain transmission electron microscopy revealed vMnP had identical morphology (Figure S2B) to the previously reported empty or INT bound vault nanoparticles.[12] The zeta potentials between empty vaults and vaults packaged with rMnP were not significantly different (-20.50±1.29 mV for empty vaults vs. -18.65±2.45 mV for packaged vaults, Figure S2D), indicating the incorporation of rMnP did not alter vaults' electrokinetic properties. The hydrodynamic diameters of empty and packaged vaults both centered at 50 nm (Figure S2C), but more distribution at larger diameters was observed for vaults containing rMnP, suggesting the packaging of rMnP slightly up-shifted vault particles' hydrodynamic sizes. Additionally, the narrow distribution (45-65 nm) of both vaults also suggests that vault particles are uniformly dispersed.

### Enzyme Kinetics Studies

Manganese divalent ion substrate assays were performed in 200 μL mixture containing pH 4.0 50 mM malonate buffer, MnP (5 μL of either 1.37 μM of vMnP, or 1.08 μM of rMnP or 0.24 μM of nMnP), $MnCl_2$ (50 – 1000 μM), and 100 μM $H_2O_2$. Assays for $H_2O_2$ substrate were performed in the similar system but containing 1000 μM $MnCl_2$ and 5 – 100 μM $H_2O_2$. The

formation of $Mn^{3+}$-malonate was recorded by an increase in absorbance at 270 nm ($\varepsilon_{207nm}$ = 11.59 $mM^{-1}$ $cm^{-1}$). Reaction rates for $Mn^{2+}$ and $H_2O_2$ were calculated according to stoichiometry of 1 mol of $Mn^{3+}$-malonate produced per 1 mole of $Mn^{2+}$ and 0.5 mol of $H_2O_2$ consumed, respectively. ABTS kinetics assays were performed in 400 µL solution containing pH 4.0 50 mM malonate buffer, MnP (3 µL of either 1.60 µM vMnP or 0.47 µM nMnP, or 4 µL of 1.04 µM rMnP), 2 mM $MnCl_2$, 100 µM $H_2O_2$, and 2.5 – 500 µM ABTS. ABTS reaction rates were determined by measuring absorbance change rate at 420 nm, where is the absorption peak of its oxidation product ($\varepsilon_{420nm}$ = 36.0 $mM^{-1}$ $cm^{-1}$). For substrate guaiacol, the assays were carried in 50 mM malonate buffer containing MnP enzyme (12 µL of either 1.60 µM vMnP or 0.47 µM nMnP, or 16 µL of 1.04 µM rMnP), 2 mM $MnCl_2$, 100 µM $H_2O_2$ and guaiacol (5 – 125 µM) with a final volume of 400 µL. Guaiacol oxidation product was monitored by an increase in absorbance at 465 nm ($\varepsilon_{465nm}$ = 12.1 $mM^{-1}$ $cm^{-1}$) to calculate guaiacol reaction rates.

**Product Profile Characterizations**

The analysis was performed with an ACQUITY UPLC system (Waters, Milford, MA) connected to a Waters LCT Premier mass spectrometer. UPLC separation was carried out with an ACQUITY UPLC BEH C18 column (2.1 mm x 50 mm, 1.7 µm particle size). The mobile phase was operated at 0.3 mL/min, compromising methanol and water. UPLC elution gradient started with 20% methanol (v/v) and increased to 95% (v/v) methanol at 5 minutes and maintained for 1 minute. Methanol was then returned to 20% at 6.1 minutes and held for 3.9 minutes to equilibrate the column before the next injection. The mass spectrometer was operated in negative electrospray ionization (ESI) mode in the *m/z* 70-2000 mass range with capillary voltage 2.0 kV, desolvation gas 600 L $h^{-1}$ and 350 °C, cone gas 20 L $h^{-1}$ and sample cone voltage

70 V. Qualitative and quantitative analyses of UPLC/MS data were carried out using MZmine 2. Detailed data processing methods and parameters are listed in Table S1.

**HPLC Analysis**

The residual bisphenol concentrations were measured using a Hewlett Packard high performance liquid chromatograph (HP 1050 HPLC system) equipped with an Agilent C18 column (4.6 x 250 mm, 5 μm particle size). The mobile phase was run at 0.5 mL/min, consisting of 70% methanol, 30% $H_2O$ and 0.1% acetic acid (v/v) for BPA and BPF, and 80% methanol, 20% $H_2O$ and 0.1% acetic acid (v/v) for BPAP. BPA concentrations were determined by a UV detector at 277 nm, and BPF and BPAP concentrations were determined at 279 nm.

**SPE Procedure**

The remaining 10 mL solution was subjected to solid-phase extraction (SPE) performed using 1 cc HLB cartridges (30 mg sorbent, 30 μm particle size) from Waters (Milford, MA), which were pre-conditioned with 2 mL of methanol and 2 mL of ethanol followed by 2 mL of water. The solution was passed through the conditioned cartridge at a flow rate of 1 drop/second. Reaction vials were repeatedly washed (3 times) with 5 mL of water, which was also passed through the same SPE cartridges. Subsequently, cartridges were washed with 5 mL of water, followed by air dry for 10-15 minutes at about 15 bar, and then eluted with 1 mL of ethanol, which was evaporated to dryness under ultra-high purity $N_2$ at room temperature. The residue was dissolved in 200 μL of ethanol, and transferred to a 300 μL glass vial and again dried under $N_2$ at room temperature. The final residue was reconstituted in 10 μL of ethanol, for product characterization and *in vitro* and *in vivo* toxicity tests.

**Table 3.S1** Recovery of Bisphenol Parent Compounds in Concentrated SPE Eluates.

| Compound | Recovery (%) |
|---|---|
| BPA | 105±7.5 |
| BPF | 97±3.4 |
| BPAP | 89±3.7 |

**Table 3.S2** Parameters for MZmine.

| Step | Parameter | Value |
|---|---|---|
| Mass Detection | MS level | 1 |
| | Polarity | - |
| | Mass detector | Centroid |
| | Noise level | 1.00E+02 |
| Chromatogram Builder | Retention time | 0.00-6.00 min |
| | MS level | 1 |
| | Min time span (min) | 0.1 |
| | Min height | 2.00E+02 |
| | m/z tolerance | 0.005 m/z or 5.0 ppm |
| Chromatogram deconvolution | Algorithm | Local minimum search |
| | Chromatographic threshold | 70.00% |
| | Search minimum in RT range (min) | 0.3 |
| | Minimum relative height | 1.00% |
| | Minimum absolute height | 2.00E+02 |
| | Min ratio of peak top/edge | 1.5 |
| | Peak duration range (min) | 0.00-6.00 |
| Retention time normalizer | m/z tolerance | 0.005 m/z or 5.0 ppm |
| | Retention time tolerance | 0.1 absolute (min) |
| | Minimum standard intensity | 5.00E+02 |
| Alignment | m/z tolerance | 0.005 m/z or 5.0 ppm |
| | Weight for m/z | 10 |
| | Retention time tolerance | 0.1 absolute (min) |
| | Weight for RT | 10 |

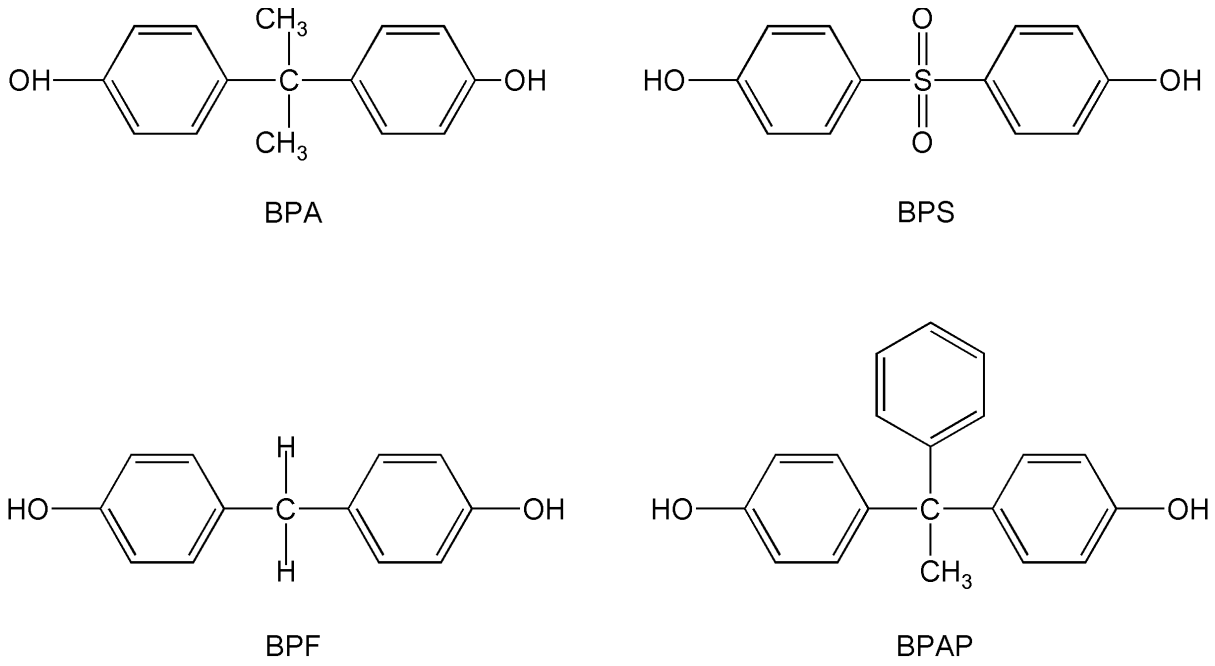


**Figure 3.S1** Chemical Structures of BPA, BPS, BPF, and BPAP.

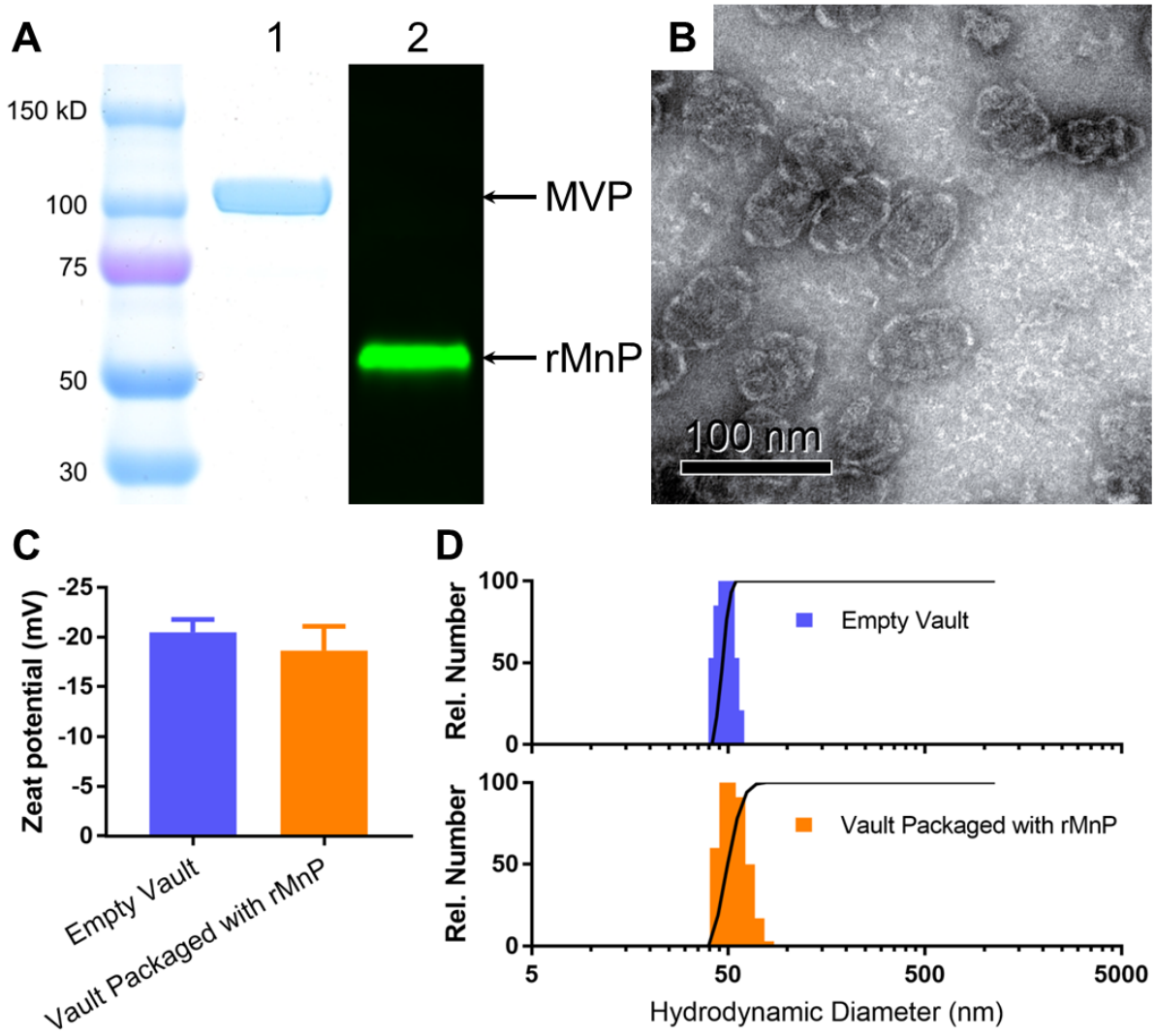


**Figure 3.S2** Characterization of Vault Nanoparticles Packaged with MnP. (A) Vaults containing rMnP were fractionated on a 4-15% SDS-PAGE and analyzed by Coomassie staining (lane 1) and Western blotting using anti-INT antibody (lane 2). MVP and rMnP bands are indicated by arrows. (B) Negative-stained TEM image of vault particles packaged with rMnP. (C) Comparison of Zeta potentials of empty vaults and vaults containing rMnP. Error bars represent one standard error of the mean (n=10). (D) Number –based distribution of hydrodynamic diameters of empty vaults and vault particles containing rMnP.

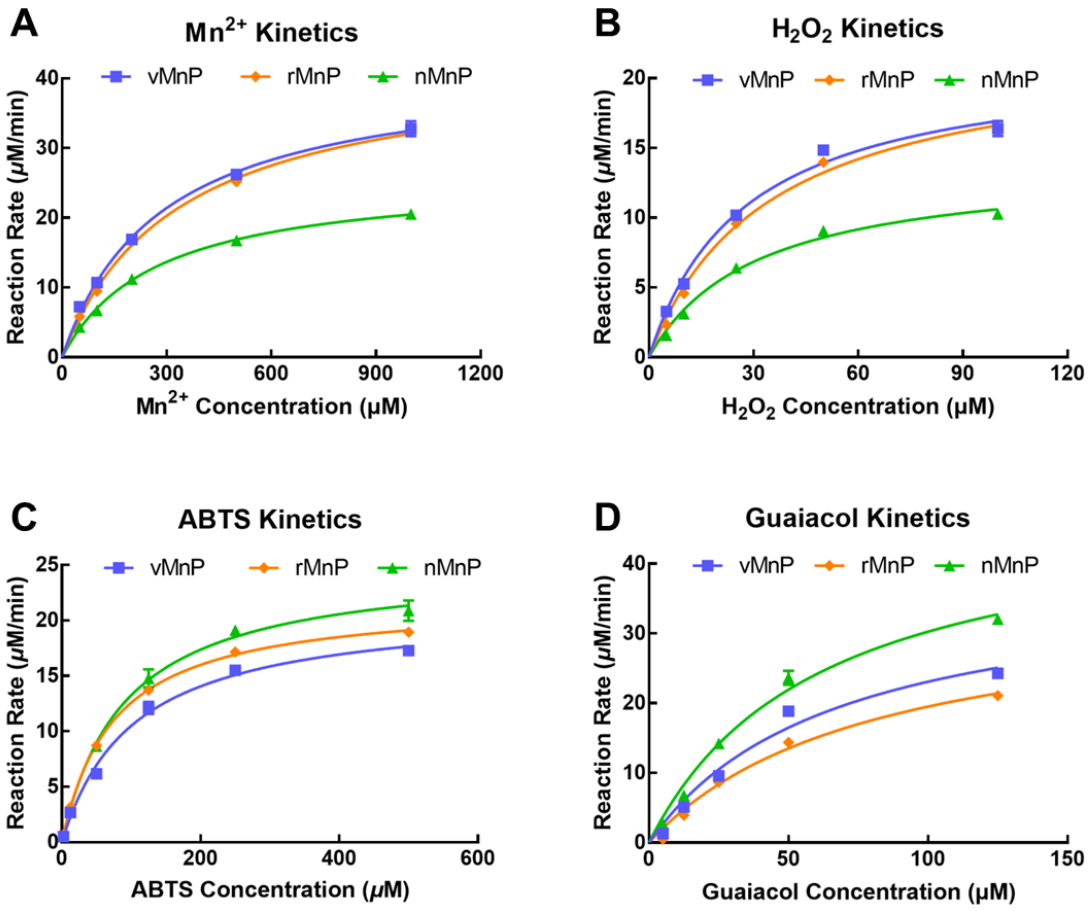


**Figure 3.S3** Enzyme Kinetics of vMnP, rMnP, and nMnP using $Mn^{2+}$ (A), H2O2 (B), ABTS (C), and Guaiacol (D) as Substrates. Error bars represent one standard error of the mean (n=3).

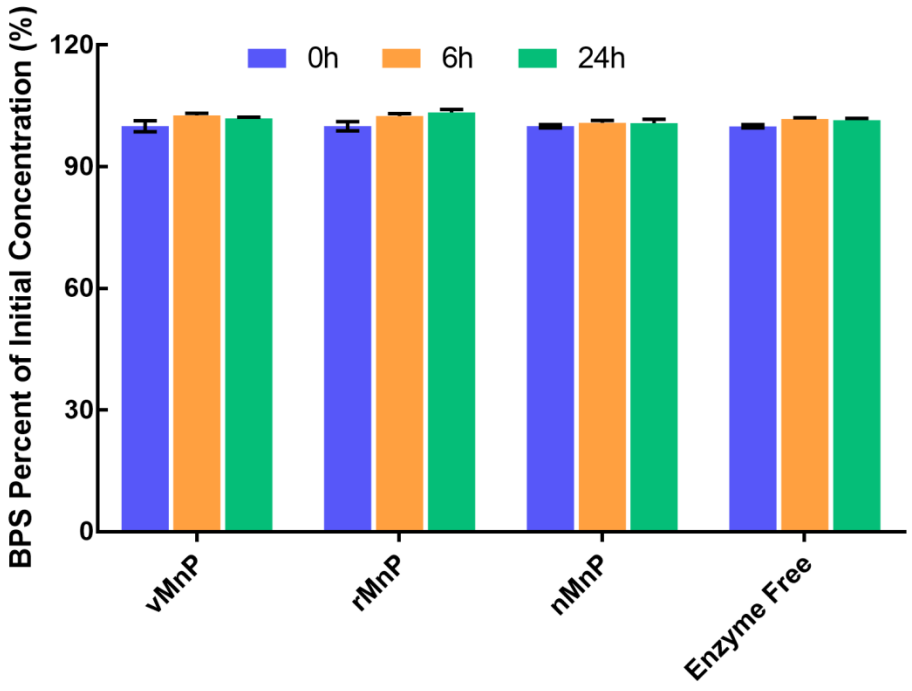


**Figure 3.S4** No Significant BPS Degradation in 24 Hours. Error bars represent one standard error of the mean (n=3).

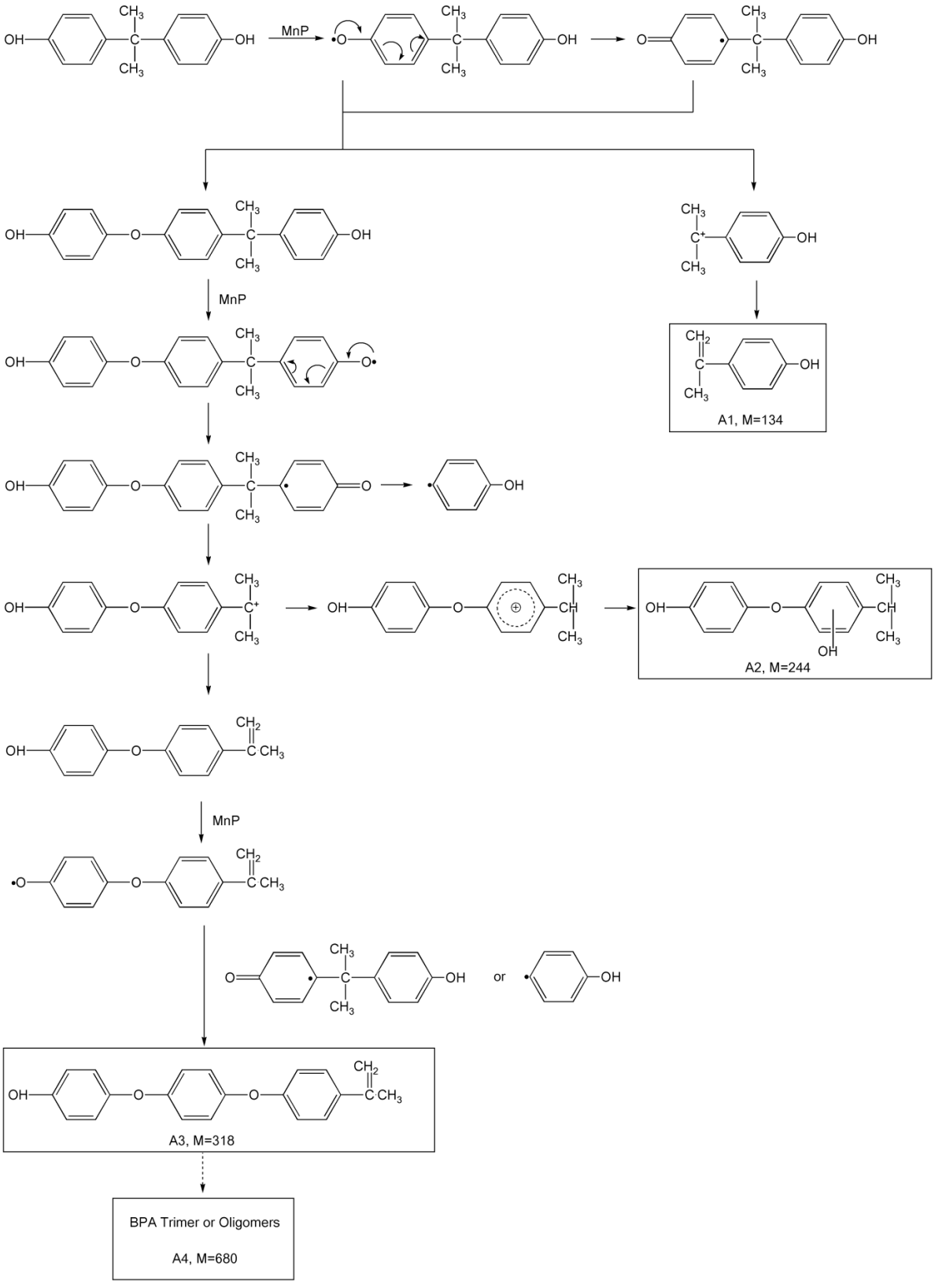


**Figure 3.S5** Proposed MnP-catalyzed BPA Transformation Pathway.

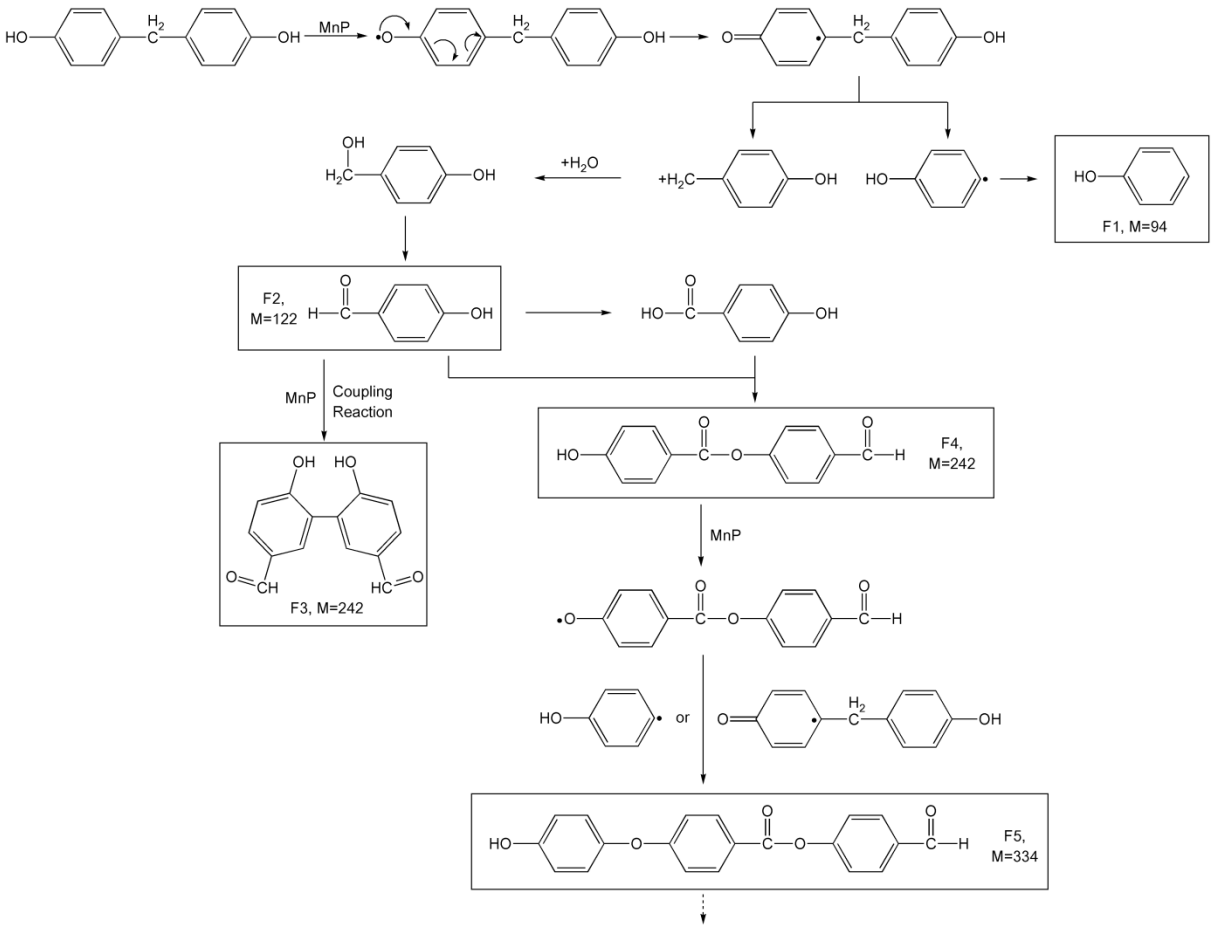


**Figure 3.S6** Proposed MnP-catalyzed BPF Transformation Pathway.

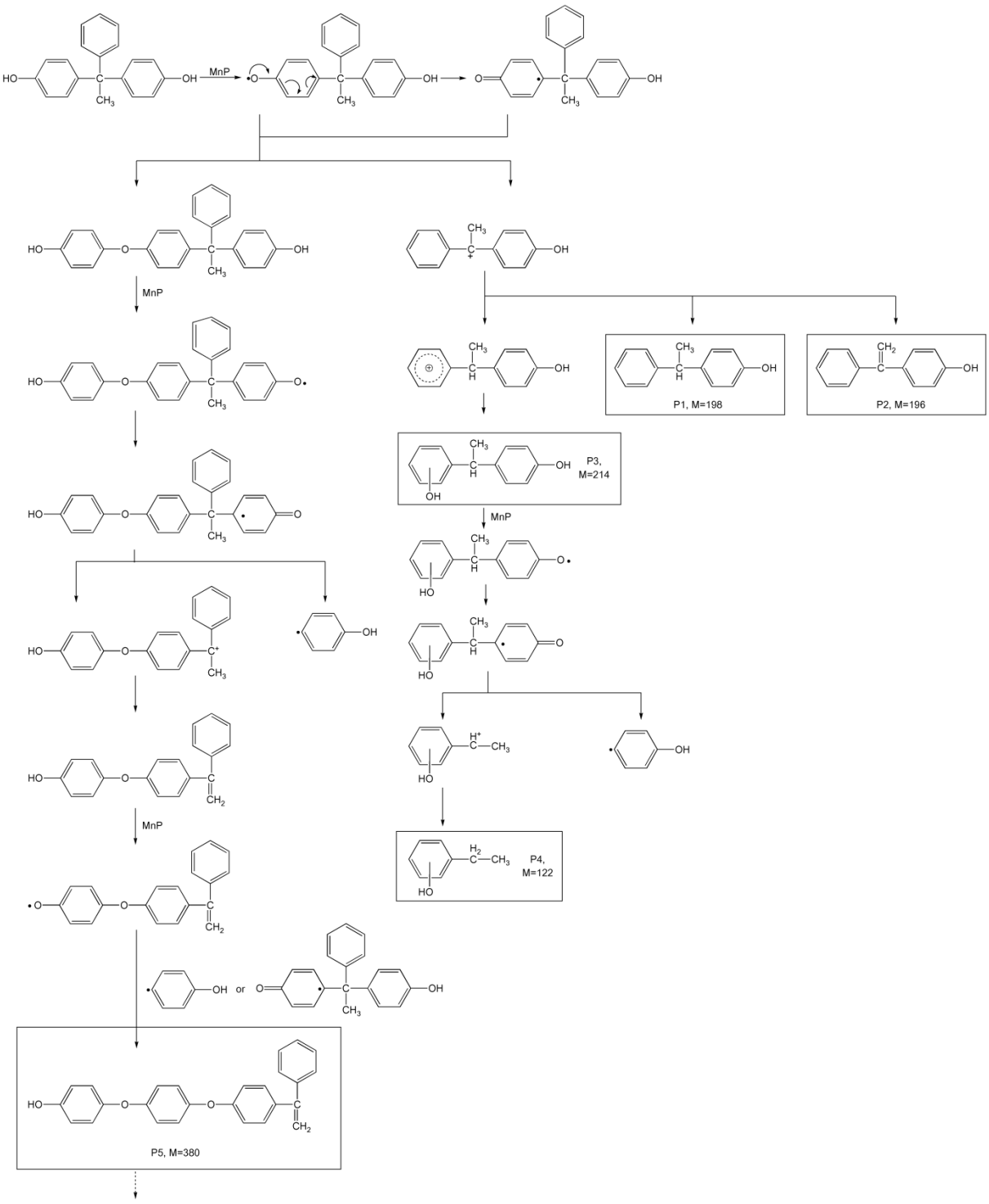


**Figure 3.S7** Proposed MnP-catalyzed BPAP Transformation Pathway.

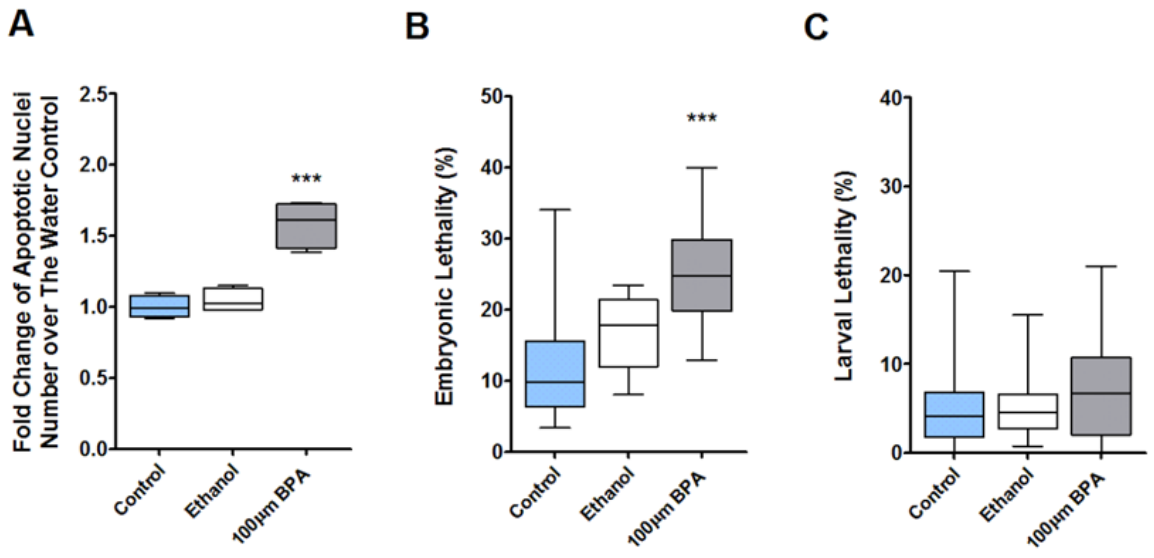


**Figure 3.S8** Ethanol Vehicle Does Not Affect *C. elegans* Reproductive Features. Compared with the culture medium without ethanol (control), exposure to 0.1% final concentration of ethanol in medium does not significantly increase germline apoptosis (A), embryonic lethality (B), or larval lethality (C) of exposed nematodes ($P>0.05$). 100 μM BPA was used here as a positive control. One way-ANOVA with post-hoc Tukey HSD test performed for the comparison among all treatment groups. ***: $P<0.001$. N=4 for apoptosis assay and N=12-17 for embryonic lethality and larval lethality examination.

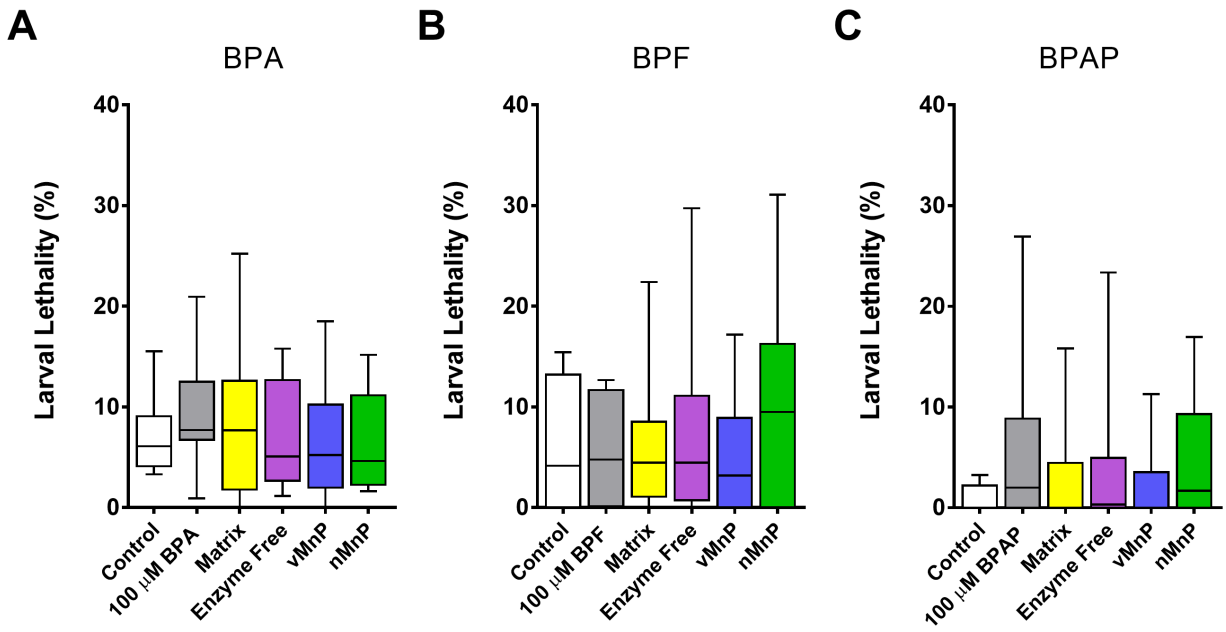


**Figure 3.S9** Larval Lethality of BPs and Their Degradation Products. The rate of larval lethality represents the percentage of larvae not surviving to the adulthood. Compared to the vehicle control (0.1% ethanol), neither exposure to untreated BP compounds nor their biodegradation products significantly increases larval lethality of nematodes. Student's t-test performed for the comparison between the control and each 100 μM bisphenol group. One way-ANOVA with post-hoc Tukey HSD test performed for the comparison among all BPs treatment groups. N=10-13.

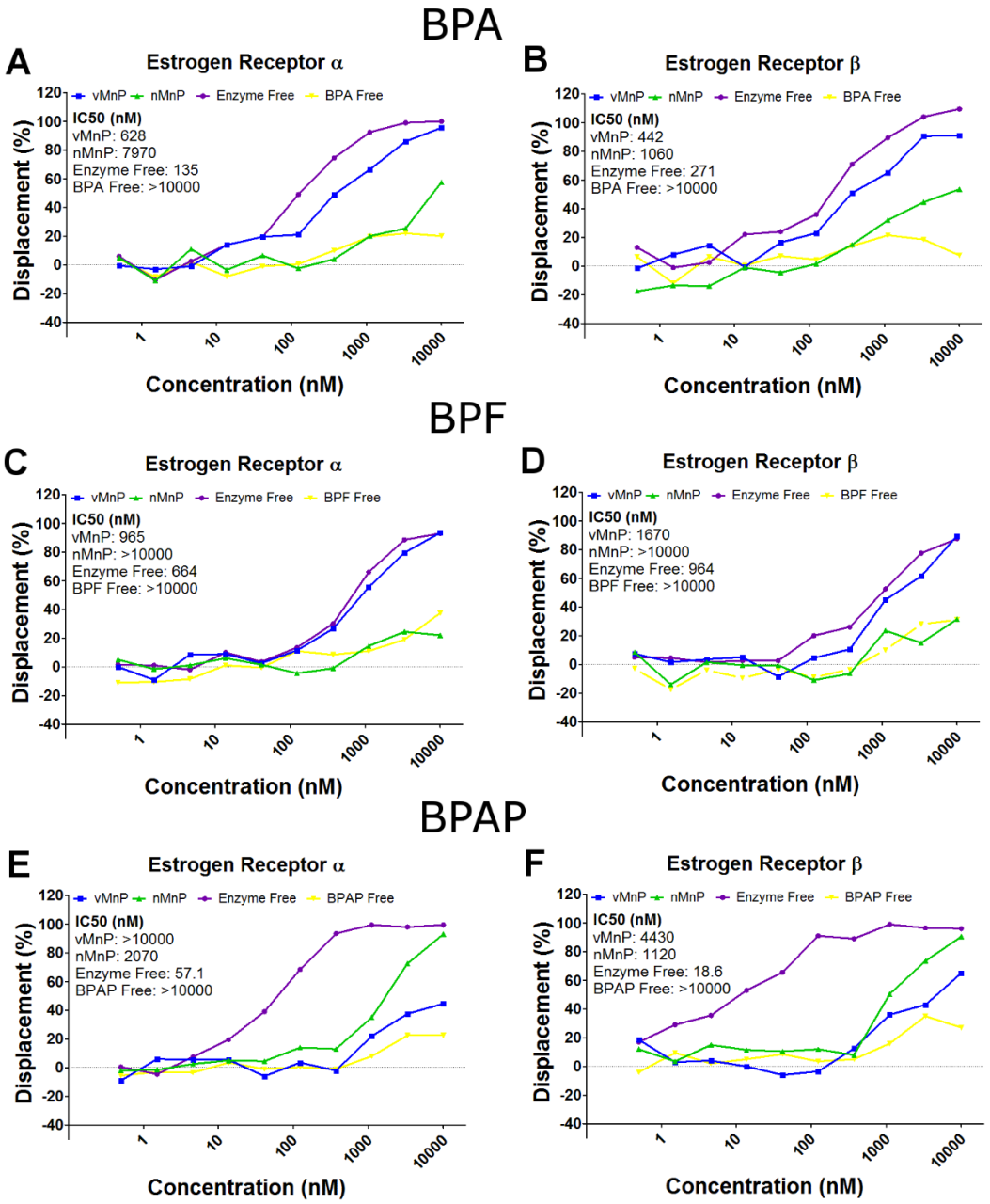


**Figure 3.S10** vMnP and nMnP Show Divergence in Decreasing BPs Estrogenic Activity. Compared to buffer control (Bisphenol Free), untreated BPA, BPF, and BPAP (Enzyme free) efficiently associate with both estrogen receptors α and β. The nMnP-mediated biodegradation exhibits a greater capacity than vMnP to reduce the ER binding affinity of BPA samples (A, B) and BPF (C, D). By contrast, vMnP possesses a greater efficiency at reducing the ER binding affinity of BPAP (E, F). Displacement (%) represents the percentage of fluorescent probes replaced on the estrogen receptor by the chemical at the tested concentration. The half maximal inhibitory concentration ($IC_{50}$) of each chemical was calculated based on their displacement (%) curves respectively.

### 3.7 References


1. Franssen, M. C. R.; Steunenberg, P.; L. Scott, E.; Zuilhof, H.; Sanders, J. P. M. Immobilised enzymes in biorenewables production. *Chemical Society Reviews* **2013,** *42*, 6491-6533.
2. Hirano, T.; Honda, Y.; Watanabe, T.; Kuwahara, M. Degradation of bisphenol a by the lignin-degrading enzyme, manganese peroxidase, produced by the white-rot basidiomycete, Pleurotus ostreatus. *Bioscience Biotechnology and Biochemistry* **2000,** *64* (9), 1958-1962.
3. Mir-Tutusaus, J. A.; Baccar, R.; Caminal, G.; Sarrà, M. Can white-rot fungi be a real wastewater treatment alternative for organic micropollutants removal? A review. *Water Research* **2018,** *138*, 137-151.
4. Wei, W.; Du, J. J.; Li, J.; Yan, M.; Zhu, Q.; Jin, X.; Zhu, X. Y.; Hu, Z. M.; Tang, Y.; Lu, Y. F. Construction of Robust Enzyme Nanocapsules for Effective Organophosphate Decontamination, Detoxification, and Protection. *Advanced Materials* **2013,** *25* (15), 2212-2218.
5. Cipolatti, E. P.; Valério, A.; Henriques, R. O.; Moritz, D. E.; Ninow, J. L.; Freire, D. M. G.; Manoel, E. A.; Fernandez-Lafuente, R.; Oliveira, D. d. Nanomaterials for biocatalyst immobilization – state of the art and future trends. *RSC Advances* **2016,** *6*, 104675-104692.
6. Meryam Sardar, R. A. Enzyme Immobilization: An Overview on Nanoparticles as Immobilization Matrix. *Biochemistry & Analytical Biochemistry* **2015,** *4*, 1.
7. Polka, J. K.; Hays, S. G.; Silver, P. A. Building Spatial Synthetic Biology with Compartments, Scaffolds, and Communities. *Cold Spring Harbor Perspectives in Biology* **2016,** *8* (8), a024018.

8. Wang, M.; Abad, D.; Kickhoefer, V. A.; Rome, L. H.; Mahendra, S. Vault nanoparticles packaged with enzymes as an efficient pollutant biodegradation technology. *ACS Nano* **2015,** *9* (11), 10931-10940.

9. Rome, L. H.; Kickhoefer, V. A. Development of the vault particle as a platform technology. *ACS Nano* **2013,** *7* (2), 889-902.

10. Han, M.; Kickhoefer, V. A.; Nemerow, G. R.; Rome, L. H. Targeted vault nanoparticles engineered with an endosomolytic peptide deliver biomolecules to the cytoplasm. *ACS Nano* **2011,** *5*, 6128-6137.

11. Stephen, A. G.; Raval-Fernandes, S.; Huynh, T.; Torres, M.; Kickhoefer, V. A.; Rome, L. H. Assembly of vault-like particles in insect cells expressing only the major vault protein. *Journal of Biological Chemistry* **2001,** *276* (26), 23217-23220.

12. Kickhoefer, V. A.; Garcia, Y.; Mikyas, Y.; Johansson, E.; Zhou, J. C.; Raval-Fernandes, S.; Minoofar, P.; Zink, J. I.; Dunn, B.; Stewart, P. L.; Rome, L. H. Engineering of vault nanocapsules with enzymatic and fluorescent properties. *Proceedings of the National Academy of Sciences of the United States of America* **2005,** *102* (12), 4348-4352.

13. Liao, C. Y.; Liu, F.; Moon, H. B.; Yamashita, N.; Yun, S. H.; Kannan, K. Bisphenol analogues in sediments from industrialized areas in the United States, Japan, and Korea: spatial and temporal distributions. *Environmental Science & Technology* **2012,** *46* (21), 11558-11565.

14. Chen, M. Y.; Ike, M.; Fujita, M. Acute toxicity, mutagenicity, and estrogenicity of bisphenol-A and other bisphenols. *Environmental Toxicology* **2002,** *17* (1), 80-86.

15. Yamazaki, E.; Yamashita, N.; Taniyasu, S.; Lam, J.; Lam, P. K. S.; Moon, H. B.; Jeong, Y.; Kannan, P.; Achyuthan, H.; Munuswamy, N.; Kannan, K. Bisphenol A and other

bisphenol analogues including BPS and BPF in surface water samples from Japan, China, Korea and India. *Ecotoxicology and Environmental Safety* **2015,** *122*, 565-572.

16. Lee, S.; Liao, C.; Song, G. J.; Ra, K.; Kannan, K.; Moon, H. B. Emission of bisphenol analogues including bisphenol A and bisphenol F from wastewater treatment plants in Korea. *Chemosphere* **2015,** *119*, 1000-1006.
17. Chen, Y. C.; Shu, L.; Qiu, Z. Q.; Lee, D. Y.; Settle, S. J.; Hee, S. Q.; Telesca, D.; Yang, X.; Allard, P. Exposure to the BPA-substitute bisphenol S causes unique alterations of germline function. *Plos Genetics* **2016,** *12* (7), e1006223.
18. Audebert, M.; Dolo, L.; Perdu, E.; Cravedi, J. P.; Zalko, D. Use of the γH2AX assay for assessing the genotoxicity of bisphenol A and bisphenol F in human cell lines. *Archives of Toxicology* **2011,** *85* (11), 1463-1473.
19. Huang, Q. G.; Weber, W. J. Transformation and removal of bisphenol A from aqueous phase *via* peroxidase-mediated oxidative coupling reactions: efficacy, products, and pathways. *Environmental Science & Technology* **2005,** *39* (16), 6029-6036.
20. Lu, N.; Lu, Y.; Liu, F. Y.; Zhao, K.; Yuan, X.; Zhao, Y. H.; Li, Y.; Qin, H. W.; Zhu, J. $H_3PW_{12}O_{40}/TiO_2$ catalyst-induced photodegradation of bisphenol A (BPA): kinetics, toxicity and degradation pathways. *Chemosphere* **2013,** *91* (9), 1266-1272.
21. Olmez-Hanci, T.; Arslan-Alaton, I.; Genc, B. Bisphenol A treatment by the hot persulfate process: oxidation products and acute toxicity. *Journal of Hazardous Materials* **2013,** *263*, 283-290.
22. Allard, P.; Colaiacovo, M. P. Bisphenol A impairs the double-strand break repair machinery in the germline and causes chromosome abnormalities. *Proceedings of the National Academy of Sciences of the United States of America* **2010,** *107* (47), 20405-10.

23. Chen, J.; Saili, K. S.; Liu, Y.; Li, L.; Zhao, Y.; Jia, Y.; Bai, C.; Tanguay, R. L.; Dong, Q.; Huang, C. Developmental bisphenol A exposure impairs sperm function and reproduction in zebrafish. *Chemosphere* **2017,** *169*, 262-270.

24. Hunt, P. A.; Koehler, K. E.; Susiarjo, M.; Hodges, C. A.; Ilagan, A.; Voigt, R. C.; Thomas, S.; Thomas, B. F.; Hassold, T. J. Bisphenol A exposure causes meiotic aneuploidy in the female mouse. *Current biology* **2003,** *13* (7), 546-53.

25. Kato, H.; Furuhashi, T.; Tanaka, M.; Katsu, Y.; Watanabe, H.; Ohta, Y.; Iguchi, T. Effects of bisphenol A given neonatally on reproductive functions of male rats. *Reproductive Toxicology* **2006,** *22* (1), 20-9.

26. Li, D. K.; Zhou, Z.; Miao, M.; He, Y.; Wang, J.; Ferber, J.; Herrinton, L. J.; Gao, E.; Yuan, W. Urine bisphenol-A (BPA) level in relation to semen quality. *Fertility and Sterility* **2011,** *95* (2), 625-630.

27. Susiarjo, M.; Hassold, T. J.; Freeman, E.; Hunt, P. A. Bisphenol A exposure in utero disrupts early oogenesis in the mouse. *Plos Genetics* **2007,** *3* (1), e5.

28. Kar, U. K.; Srivastava, M. K.; Andersson, A.; Baratelli, F.; Huang, M.; Kickhoefer, V. A.; Dubinett, S. M.; Rome, L. H.; Sharma, S. Novel CCL21-vault nanocapsule intratumoral delivery inhibits lung cancer growth. *PLoS ONE* **2011,** *6* (5), e18758.

29. Wariishi, H.; Akileswaran, L.; Gold, M. H. Manganese peroxidase from the basidiomycete *Phanerochaete chrysosporium*: spectral characterization of the oxidized states and the catalytic cycle. *Biochemistry* **1988,** *27* (14), 5365-5370.

30. Allard, P.; Kleinstreuer, N. C.; Knudsen, T. B.; Colaiacovo, M. P. A *C. elegans* screening platform for the rapid assessment of chemical disruption of germline function. *Environmental Health Perspectives* **2013,** *121* (6), 717-24.

31. Gartner, A.; Boag, P. R.; Blackwell, T. K. Germline survival and apoptosis. In *WormBook*, The *C. elegans* Research Community, Ed.; 2008; pp 1-20.

32. Chen, X. Y.; Zaro, J. L.; Shen, W. C. Fusion protein linkers: property, design and functionality. *Advanced Drug Delivery Reviews* **2013,** *65* (10), 1357-1369.

33. Maffini, M. V.; Rubin, B. S.; Sonnenschein, C.; Soto, A. M. Endocrine disruptors and reproductive health: the case of bisphenol-A. *Molecular and Cellular Endocrinology* **2006,** *254-255*, 179-86.

34. Rubin, B. S. Bisphenol A: an endocrine disruptor with widespread exposure and multiple effects. *The Journal of Steroid Biochemistry and Molecular Biology* **2011,** *127* (1-2), 27-34.

35. Vandenberg, L. N.; Hauser, R.; Marcus, M.; Olea, N.; Welshons, W. V. Human exposure to bisphenol A (BPA). *Reproductive Toxicology* **2007,** *24* (2), 139-77.

36. Atli, E. The effects of three selected endocrine disrupting chemicals on the fecundity of fruit fly, *Drosophila melanogaster*. *Bulletin of Environmental Contamination and Toxicology* **2013,** *91* (4), 433-7.

37. Danzl, E.; Sei, K.; Soda, S.; Ike, M.; Fujita, M. Biodegradation of bisphenol A, bisphenol F and bisphenol S in seawater. *International Journal of Environmental Research and Public Health* **2009,** *6* (4), 1472-1484.

38. Ike, M.; Chen, M. Y.; Danzl, E.; Sei, K.; Fujita, M. Biodegradation of a variety of bisphenols under aerobic and anaerobic conditions. *Water Science and Technology* **2006,** *53* (6), 153-9.

39. Mao, L.; Luo, S. Q.; Huang, Q. G.; Lu, J. H. Horseradish peroxidase inactivation: heme destruction and influence of polyethylene glycol. *Scientific Reports* **2013,** *3*, 3126.

40. Zazo, J. A.; Casas, J. A.; Mohedano, A. F.; Gilarranz, M. A.; Rodriguez, J. J. Chemical pathway and kinetics of phenol oxidation by Fenton's reagent. *Environmental Science & Technology* **2005,** *39* (23), 9295-9302.

## Chapter 4 Synthesis and Assembly of Human Vault Particles in Yeast

### 4.1 Introduction

The largest cytoplasmic ribonucleoprotein particles, vaults, have been isolated from numerous eukaryotic species, whose structure is highly conserved and has a unique barrel-like morphology.[1] The major vault protein (MVP) is the most abundant component of native vaults, and accounts for about 75% of the total protein mass in the particle.[2] Seventy-eight copies of MVP are assembled into the barrel-like shell of the particle co-translationally on the polyribosome.[3, 4] Multiple copies of two additional protein components, vault poly(ADP-ribose) polymerase (VPARP) and telomerase-associated protein-1 (TEP1), and one or more copies of the non-coding vault RNA are found in native vault particles.[5-7] Cryo-EM reconstruction of rat liver vaults treated with ribonuclease and vaults purified from VPARP and TEP1 knockout mice localized these three components to the inside of the vault lumen.[8, 9] Although the biological function of native vault particles and their components is still mysterious, vaults have been implicated in a broad range of cellular functions including innate immunity, multi-drug resistance, cell signaling, nuclear-cytoplasmic transport, mRNA localization, and nuclear pore assembly.[10, 11]

Expression of the cDNA encoding the MVP protein in insect cells using the baculovirus system is capable of directing the assembly of vault-like particles on polyribosomes.[4, 12] The empty recombinant vault particles have dimensions of 41 x 41 x 72.5 nm, and are virtually indistinguishable from native vaults when viewed under a transmission electron microscope (TEM).[1, 12] Differential cryo-EM mapping of engineered recombinant vaults with N-terminal or C-terminal tags showed that the C-termini of MVP were present at two ends of the particle facing outward, while the N-termini were buried at the particle waist.[8] A strategy for packaging

exogenous proteins into recombinant vault particles was developed by fusing these proteins to an MVP interaction domain termed INT. The INT domain, is a 162-amino acid region found at the C-terminus of VPARP.[7] This domain has a strong affinity for interaction with a segment of MVP that is localized in the vault interior, and acts as a packaging signal directing fusion protein into the vault lumen.[13] Recombinant vaults are non-toxic, non-immunogenic, and biodegradable, which makes the particle an ideal carrier for macromolecules.[11] Taking advantage of these properties, recombinant vaults have been engineered to enhance their functionality with various added domains to impart new activities like: cell targeting,[14] cytoplasmic targeting,[15] fluorescence,[13] and amphiphilicity,[16] which are being explored in therapeutic applications.[17] We recently reported that encapsulation of enzymes in recombinant vault particles can also improve their longevity and catalytic activities.[18] Manganese peroxidase (MnP), which is a widely used lignin-degrading enzyme in treating environmental contaminants, such as phenolics,[19] aromatic hydrocarbons,[20] and azo dyes,[21] was packaged into vaults using the INT strategy. The packaged MnP showed better thermal stability than free MnPs and biotransformed phenol at a higher rate, signifying that vault encapsulation can serve as an approach for stabilizing biodegradative enzymes and delivering enzymatic bioremediation. Comparing to other enzyme encapsulation materials, recombinant human vault particles are derived from human vaults, and are biocompatible and biodegradable, implying they are unlikely to pose risks to human health or the environment.

Current production of recombinant vault nanoparticles is only conducted in *Spodoptera frugiperda* (Sf9) insect cells because they are one of the few eukaryotes lacking endogenous vaults.[12] However, this approach is complex and costly for industrial scale applications. To develop an economically competitive technique for recombinant vaults production, organisms

that lack endogenous vaults are desired as they simplify the purification. Among all alternative organisms, yeast is a promising one for large-scale expression and preparation for human applications. Yeast have been successfully used for several decades for the production of heterologous proteins of various origins,[22] and for the synthesis of protein nanostructures, such as virus-like particles (VLP),[23] which share some morphological similarities in size and structure with vaults. However, they have significantly distinct assembly manners. VLPs are assembled from capsid proteins *via* unassisted self-assembly, or scaffolding protein-assisted assembly, or viral nucleic acid-assisted assembly.[24] Vaults, on the other hand, are polyribosome orchestrated structures and require dozens of well-organized ribosomes on a single MVP mRN.[4] Although recombinant vaults are composed of a single protein species like non-enveloped single capsid VLP, it cannot be reassembled from disassembled MVP proteins *in vitro*. Due to the unique assembly manner, two challenges stand out with yeast vault synthesis. First, polyribosome topology and structure may vary among species,[25-27] thus it is unknown whether yeast polyribosome can assist vault assembly. The other challenge is that yeast cells at different stages have distinct polyribosome profiles,[28] which may lead to assembly of vaults with altered structures.

The objectives of the present work were to determine if vault particles can be produced and assembled in yeast cells, and to characterize their morphology and ability to package INT domain fused proteins. Finally, the encapsulation of enzymes in yeast vaults was tested for improvements in enzymatic stability and biodegradation of phenolic compounds.

## 4.2 Material and Methods

### 4.2.1 Plasmid Subcloning, Yeast Transformation, and Protein Expression

The human MVP cDNA (GenBank accession No. X79882.2) was codon optimized with an initiation codon (5'-ACCATGGCA-3') fitting Kozak's rule[29, 30] and subcloned downstream of the GAP promoter ($P_{GAP}$) in the yeast vector pGAPZA (Invitrogen) into the EcoRI and KpnI sites to generate the yeast expression vector yMVP-pGAPZA. Afterwards, the plasmid was linearized with BspHI, and transformed into *P. pastoris* protease deficient strain SMD1168 using the GenePulser electroporator (Bio-Rad Labs) as described previously.[31] Electroporation was performed at 1.5 kV, 200 Ω, and 25 μF by a single pulse. The transformation mixture was plated on YPDS agar (yeast extract 10 g/L, peptone 20 g/L, dextrose 20 g/L, sorbitol 182.2 g/L, and agar 20 g/L) containing 100 $\mu$g/mL of the antibiotic Zeocin. Zeocin resistant transformants were selected and re-streaked on new YPD plates (yeast extract 10 g/L, peptone 20 g/L, dextrose 20 g/L, and 20 g/L agar) containing Zeocin to select single colonies. Eleven positive colonies were inoculated into 3 mL of YPD medium (yeast extract 10 g/L, peptone 20 g/L, and dextrose 20 g/L) with 100 $\mu$g/mL Zeocin and cultured at 30°C and 200 rpm. After overnight incubation, cells were collected, lysed, and subjected to SDS-PAGE, followed by Coomassie staining to confirm expression of MVP. The colony that had highest MVP yield was selected and employed in all further experiments. To assess the time course of MVP expression, the selected colony was inoculated into 3 mL of YPD medium with 100 μg/mL Zeocin and cultured at 30°C and 200 rpm overnight, which was then used to inoculate 500 mL YPD to an $OD_{600}$ of 0.03. The cultures were maintained at 30°C, 200 rpm for 30 hours. Cells were harvested in a pre-weighted 50 mL tube by centrifuging at 3000 x g for 5 minutes at 4°C, and washed with 10 mL deionized water. Wet cell pellets were weighed and stored at -80°C.

### 4.2.2 Preparation of Vault Particles from Yeast Cells

Each gram of yMVP wet cell pellet was resuspended in 3 mL of breaking buffer (50 mM sodium phosphate, pH 7.4, 1 mM EDTA, and 5% glycerol) containing 1 mM dithiothreitol (DTT), 1 mM phenylmethylsulfonyl fluoride (PMSF), and 50 µL of protease inhibitor (PI) cocktail (Sigma-Aldrich P8849). Cells lysis was performed by vortexing with 4 mL of glass beads (0.5 mm diameter), and the crude lysate was collected and centrifuged at 20,000 x g for 20 min at 4 °C. Subsequently, clarified supernatant (S20) was centrifuged at 100,000 x g for 1 h at 4°C to collect vault particles and other macro-complexes in the pellet (P100). The supernatant (S100) was also saved for analysis. Vault particles in the P100 were then purified *via* discontinuous density gradient centrifugation following the standard vault purification protocol as previously described.[12]

### 4.2.3 Quantification of yMVP

Concentrations of yMVP protein in S20 and S100 were quantified by an enzyme-linked immunoabsorbent assay (ELISA) using purified insect cell produced human MVP (hMVP) as the standard. Masses of yMVP in P100 were calculated by subtracting yMVP in S100 from it in S20. One-hundred microliter of serially diluted yMVP samples and hMVP standards were added to 96-well ELISA plates in triplicates and incubated at 4°C overnight. After removing unbound material, plates were blocked with 100 µL of 5% (v/v) normal goat serum (NGS) in PBS containing 0.05% (v/v) Tween 20 (PBST) at room temperature for 1 hour, and washed three times with 200 µL/well of PBST before addition of 100 µL/well of anti-MVP polyclonal antibody in PBST containing 5% (v/v) NGS. Plates were incubated with the primary antibody at room temperature for 1 hour, and washed three times with 200 µL/well of PBST. One hundred microliters of 1:2000 diluted HRP-conjugated goat anti-rabbit IgG antibody (Bio-Rad) in PBST

with 5% (v/v) NGS was then added to each well. After 1-hour incubation at room temperature, followed by three washes with 200 μL/well of PBST, 100 μL of TMB+ substrate-chromogen solution (Agilent Dako) was added to each well. Reactions were maintained for 10-30 minutes, and stopped by adding 100 μL of 1 N $H_2SO_4$ per well. OD at 450 nm was recorded and used for calculating yMVP concentrations.

### 4.2.4 Real-time qRT-PCR Analysis

The yMVP mRNA transcript levels were determined by real-time quantitative reverse transcription PCR (real-time qRT-PCR). Total nucleic acid was extracted from cells harvested at the exponential phase (OD~2), early transitional stage (OD~14), middle transitional stage (3 hours after OD reached 14), and late transitional stage (5 hours after OD reached 14), followed by genomic DNA removal using a RapidOut DNA Removal Kit (Thermo Scientific). First-strand cDNA was synthesized using an EasyScript cDNA Synthesis Kit (Lamda Biotech) with Oligo-dT primer, and used as the template in real-time qRT-PCR measurements. Reactions were set up following recommended conditions by the Luminaris Color HiGreen qPCR Master Mix manual (Thermo Scientific). *P. pastoris* expressing mCherry-INT under the control of $P_{GAP}$ was included as a control. Quantification was performed using threshold cycle ($2^{-\Delta\Delta CT}$) method with *P. pastoris* indigenous glyceraldehyde 3-phosphate dehydrogenase (GAPDH) mRNA, which is also under the control of $P_{GAP}$, as the internal reference to minimalize the effect of culture condition and phase on gene transcription, and the culture collected at exponential phase as the calibrator sample.[32] Primers used in real-time qRT-PCR are summarized in Table 4.S1.

### 4.2.5 Packaging of INT-fused Protein into Yeast Vaults

A fluorescent protein, mCherry, was chosen to test the packaging ability of yeast vaults. Cells expressing mCherry fused to INT (mCherry-INT) were lysed with yMVP cell pellets as described above. Crude lysates were incubated on ice for 30 minutes before the first centrifugation. Yeast vaults packaged with mCherry-INT were isolated following the vault purification procedure described above. The fluorescence intensity was measured at 615 nm with excitation at 560 nm.

### 4.2.6 Characterization of Yeast Vaults

Purified vaults were examined by negative staining TEM to evaluate their size, morphology and dispersion. Samples were absorbed on carbon-coated copper EM grids by floating the grids on 20 µL vault solution for 5 min at room temperature. The grids were then blotted on a filter paper and stained by floating on 1 mL of 1% uranyl acetate (UA) aqueous solution for 5 min. Extra UA solution was blotted on a filter paper, and the grid was air dried prior to viewing in a TEM (JEOL 1200EX). Phase analysis light scattering (PALS) was used to determine the zeta potential of purified vault particles.

### 4.2.7 Evaluation of Yeast Vaults Packaged MnP

INT fused MnP (rMnP) was produced and secreted by insect Sf9 cells as previously described.[18] The Sf9 culture infected with rMnP baculoviruses was collected at 72 hours, and spun at 3000 x g for 5 minutes at 4°C to remove cells and cell debris. Baculoviruses and small cell debris were removed from the supernatant by centrifugation at100,000 x g for 1 hour. To obtain rMnP crude extract, the supernatant was concentrated using 30 kDa Amicon Ultra centrifugal filters (Millipore Sigma), and desalted using a PD-10 column (GE Healthcare Bio-

Sciences). rMnP was eluted in Buffer A, and passed through a 0.2 μm filter. To make yeast vaults packaged with rMnP (hereafter rMnP-yMVP), purified yeast vaults were added to the virus free rMnP culture supernatant, and mixed at 4 °C for 1 hour. rMnP-yMVP was separated from unpackaged rMnP by 1 hour centrifugation at 100,000 x g. Supernatant was decanted, and the rMnP-yMVP pellet was resuspended in buffer A. rMnP and rMnP-yMVP were stored at -20°C and 4°C before use, respectively. Fungus produced native MnP (nMnP) was purified from the fungus *Phanerochaete chrysosporium* as described previously.[18]

To compare the thermal stability of MnP enzymes, triplicates of rMnP-yMVP, rMnP, and nMnP were incubated at 25°C. MnP enzymatic activities were measured at 0, 1, 2, 4, 6, and 8 hours using 2,2'-azino-bis(3-ethylbenzothiazoline-6-sulphonic acid) (ABTS) oxidation assay, which was performed in pH 4.0 50 mM malonate buffer containing 0.5 mM ABTS, 2 mM $MnCl_2$, MnP samples, and 0.3 mM $H_2O_2$. The formation of oxidized ABTS was monitored by recording the absorbance change at 420 nm, where is the absorption peak of ABTS oxidation product ($\varepsilon_{420nm}$ = 36,000 L $mol^{-1}$ $cm^{-1}$). ABTS oxidation rates were calculated according to stoichiometry of 1 mol of oxidized ABTS produced per 1 mol of ABTS consumed. One unit of MnP is defined as the amount of enzyme required to react 1 μmol/min of substrate. Residual activities at different time points were normalized to their initial activity and plotted against time.

Bisphenol A (BPA) biodegradation tests were conducted in pH 4.5 50 mM malonate buffer containing 150 μM BPA, 1.5 mM $MnCl_2$, 0.3 mM $H_2O_2$, and 29 U/L MnP (rMnP-yMVP, rMnP, or nMnP) at 25°C in a shaking incubator (200 rpm). Activities of MnPs were measured in pH 4.5 50 mM malonate buffer with 0.1 mM ABTS, 2 mM $MnCl_2$, and 0.4 mM $H_2O_2$. Enzyme free condition, which contained all components except MnP, was included as a negative control. Triplicate samples were quenched at 0, 6.5, and 24 hours by adding two volumes of methanol,

followed by passage through 0.2 μm filters. Residual BPA concentrations were measured using a Hewlett Packard high-performance liquid chromatograph (HP 1050 HPLC system). HPLC separation was carried out with an Agilent C18 column (4.6 x 250 mm, 5 μm particle size). The mobile phase was operated at 0.5 mL/min, comprising 70% methanol, 30% water, and 0.1% acetic acid. UV detector was monitored at 277 nm.

## 4.3 Results and Discussion

### 4.3.1 Expression of yMVP

Although vault particles have been isolated from numerous eukaryotic organisms, yeast, worms, insects, and plants all lack endogenous vaults. In fact, no MVP homologue has been detected in the genome of these organisms. Thus, as expected, the native yeast *P. pastoris* cells did not contain MVP protein (Figure 4.1A, lane 3). The human MVP coding sequence was expressed under the control of the constitutive $P_{GAP}$ in yeast. Unlike the other commonly used AOX promoter, which is only induced by methanol and strongly repressed by other carbon sources, such as glucose, ethanol, and glycerol, $P_{GAP}$ is continuously expressed, although the expression is affected by the carbon source used.[33] Glucose, the main carbon source used in YPD medium, was proven to provide good expression of $P_{GAP}$.

The expression of MVP coding sequence under control of $P_{GAP}$ in *P. pastoris* led to efficient production of yMVP protein. *P. pastoris* (yMVP-pGAPZA) and untransformed cells were grown in YPD for 30 hours at which time the culture reached stationary phase. Cells were then collected, lysed, centrifuged, and the supernatant, S20, was analyzed for expression. As shown in Figure 4.1A, a protein at the expected size (~100kDa) was detected in the S20 of yMVP-pGAPZA *P. pastoris* clone (Figure 4.1A, lane 1), but not in extracts of untransformed

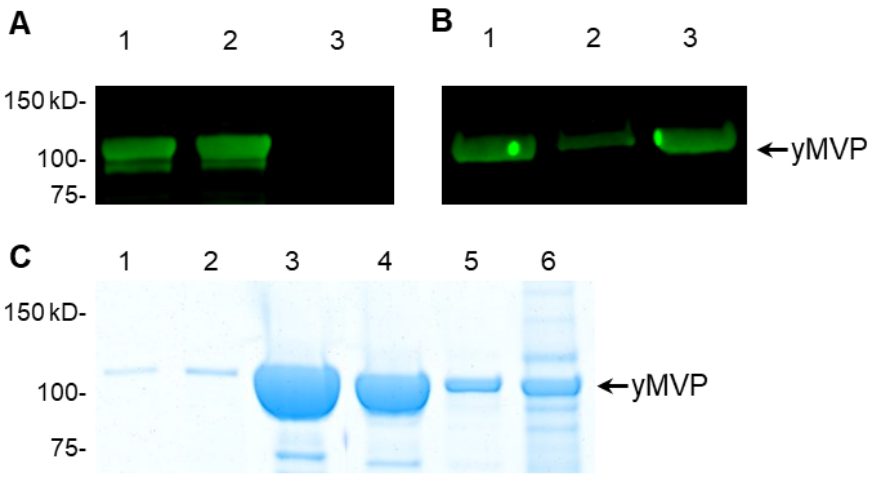


**Figure 4.1** Expression of yMVP in Yeast *P. pastoris* Culture. (A) S20 and crude lysate (lane 1 and 2) of transformed *P. pastoris* cells and S20 of native (lane 3) *P. pastoris* cells were resolved on a 4-15% SDS-PAGE and visualized by Western blotting with anti-MVP antibodies. No band is observed in the lysate from native *P. pastoris* cells, while the lysate from yMVP-pGAPZA transformed *P. pastoris* shows a band at expected size (100 kD). (B) Western blot analysis of yMVP in different fractions separated by centrifugation. Lane 1: S20. Lane 2: S100. Lane 3: P100. (C) Distribution of yMVP in sucrose gradient. Lanes 1-6 correspond to sucrose fractions 20, 30, 40, 45, 50, and 60%. Equal volume of resuspended pellets from each sucrose fraction was loaded on the gel.

yeast culture (Figure 4.1A, lane 3). Comparing yMVP in crude lysate (Figure 4.1A, lane 2) and S20, no significant difference was observed. These results suggest that yMVP was expressed under control of $P_{GAP}$ in *P. pastoris* and stayed in the soluble fraction. Afterwards, the S20 was centrifuged at 100,000 x g to pellet large complexes, followed by fractionation on a step sucrose gradient as previously described.[12] Following fractionation at 100,000 x g, around 15% of yMVP remained in the S100 (lane 2 in Figure 4.1B), while the majority (about 85%) of yMVP was in the P100 (lane 3 in Figure 4.1B), paralleling expression patterns seen in insects and native mammalian cells. The yMVP in P100 were assumed to be the assembled vault particles, while yMVP in the S100 probably resulted from incompletely assembled vaults or degradation products.[4] Analysis of sucrose gradient fractions (Figure 4.1C) showed that the distribution of yMVP was consistent with the pattern observed for recombinant vaults from insect cells and

native vaults from various tissue culture cell lines.[4] The yMVP was detected throughout all sucrose layers, but was found to be most abundant in the 40% and 45% fractions, where the assembled intact vaults are usually found [4].

### 4.3.2 Formation of Vault Particles

Intact vault particles with uniform size and shape were found in purified yMVP samples. The 40% and 45% sucrose fractions were examined by TEM and found to contain abundant vault particles and some contaminating ribosomes. The particles were further purified by anion-exchange chromatography prior to viewing by TEM. The morphology of the TEM images demonstrated that yeast cells were able to synthesize and assemble yMVP into intact vault particles. Figure 4.2A shows the typical negatively stained yeast vault particles observed at two magnifications. The isolated vaults were morphologically indistinguishable from vaults produced by insects (Figure 4.2B) or endogenous vaults found in various organisms under TEM.[12, 34] Each particle had two caps and a barrel-like body (Figure 4.2C). The waist area, where the two vault halves come together was narrower than the rest of the barrel body. These particles were about 64 nm (±3 nm, n=30) in length and 36 nm in width (±2.5 nm, n=30), which are smaller than the 42 nm x 75 nm structure resolved by Cryo-EM[35] and the 40 nm x 67 nm structure resolved by X-ray diffraction [3]. The decrease in vault size in TEM images was also observed for insect vaults, which is probably due to the shrinking of particles during air-drying or a compression resulting from deposited uranyl acetate.[4]

### 4.3.3 Comparison between Yeast Vaults and Insect Vaults

To date, vaults have only been heterologously expressed in two eukaryotic hosts: yeast

and insect cells. Thus, we next compared the basic physical and chemical properties between vaults produced in these two systems to understand whether the expression host affects the structure and properties of vaults. As shown in Figure 4.2 A and B, the morphology and shape of vaults produced in both systems were very close to each other, with two caps and a barrel-like body in the middle. Both vault particles are negatively charged and had similar zeta potentials around -19 mV. The yield of recombinant vaults in *P. pastoris* ranged between 7 mg/L and 11 mg/L, which was closed to the 10 mg/L yields from laboratory scale Sf9 cultures.

As vault particles are uniquely assembled on ordered polyribosome templates, the high degree of morphological homology between yeast and insect cells produced human vaults underlines that polyribosome typology may conserve between eukaryotic species,[4] implying the synthesis and assembly of human vaults can be achieved in all eukaryotes.

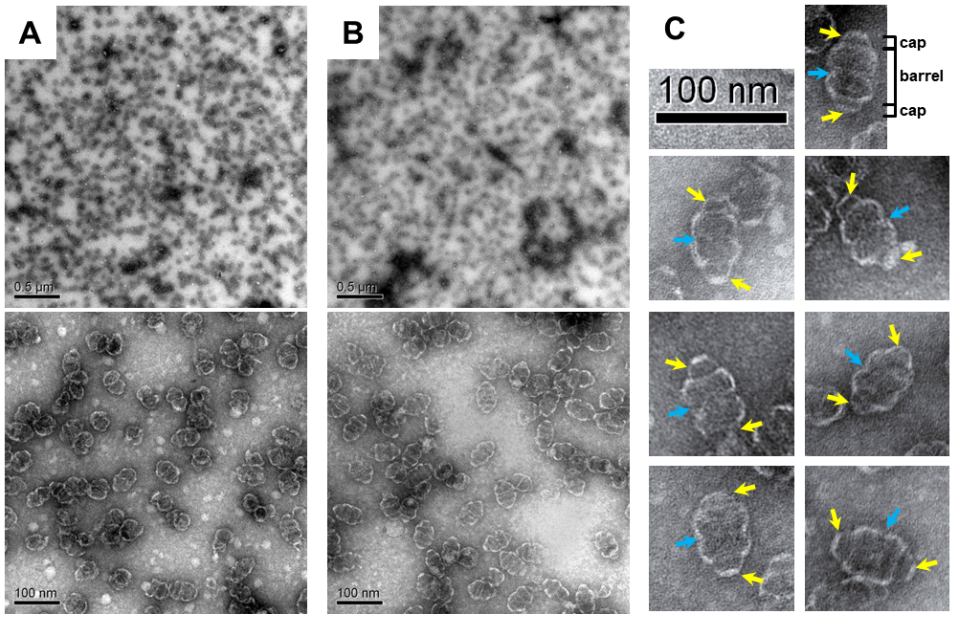


**Figure 4.2** Recombinant Vault particles Assembled in Yeast *P. pastoris* Expressing yMVP. (A) Recombinant vault particles purified from *P. pastoris* culture. (B) Recombinant vault particles purified from insect Sf9 cells. (C) Zoom-in view of individual yeast vault particles. Yellow arrows indicate the caps, and blue arrows indicate the waists of the particles.

### 4.3.4 Accumulation of Total yMVP Protein and Assembled Vault Particles

As $P_{GAP}$ allows for constitutive expression of yMVP in *P. pastoris*, we next accessed the accumulation of yMVP protein and assembled yeast vaults in cells over time. S20 of cell crude lysate was ultracentrifuged and separated into two fractions: S100 and P100 (Figure 4.3A). Yeast MVP in S100 is likely from degraded or incomplete vault particles,[4] while yMVP in P100 is believed to be assembled vaults. Optical density at 600 nm ($OD_{600}$) was also recorded to determine cell growth phase. As shown in Figure 4.3B, the *P. pastoris* (yMVP-pGAPZA) culture growth was divided into three phases, including exponential phase (before 19.5h), transitional stage (from 19.5h to 26.5h), and stationary phase (after 26.5h). Concentrations of total yMVP protein and assembled vaults changed significantly overtime, but not following similar OD pattern. Figure 4.3B shows that yMVP and assembled vault particles slowly accumulated in exponential phase, and reached 1.1 and 0.8 mg/g cells at 19.5h, respectively. After entering the transitional stage, an increased accumulation rate of yMVP in S20 and P100 fractions was observed. In the seven-hour-long transitional stage, the yield of total yMVP protein and assembled vaults tripled, and finally reached 3.3 and 3.0 mg/g cells, respectively. The same results were also observed in two separated repeats (Figure 4.S1 and 4.S2).

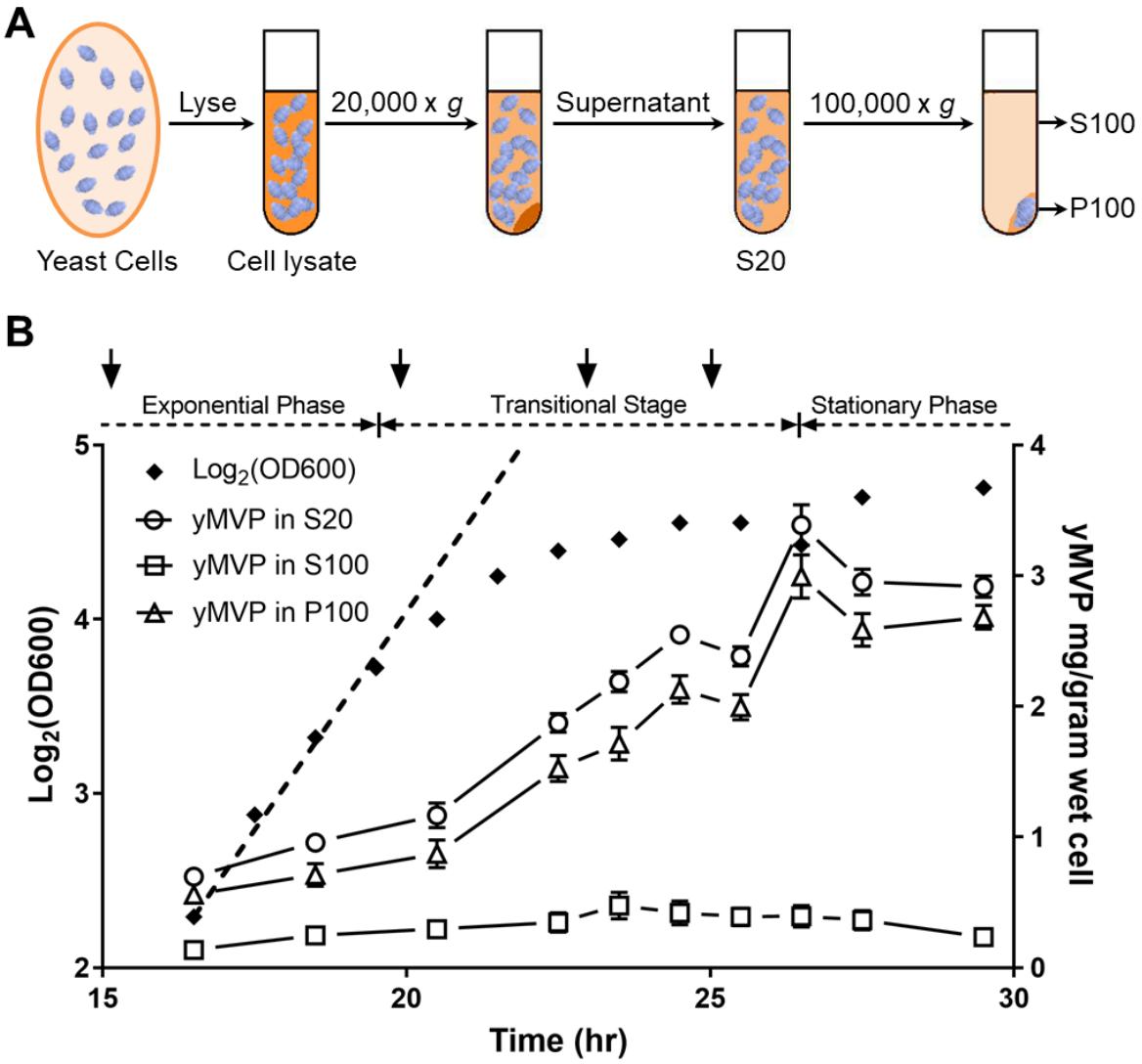


**Figure 4.3** Accumulation of Cell Biomass and yMVP in *P. pastoris* Culture. (A) Schematic of yMVP isolation using differential centrifugation. (B) Yeast growth curve and expression of yMVP overtime. Samples were collected hourly from 16.5 to 27.5 h plus at 29.5 h for recording $OD_{600}$. Culture growth was divided into three phases, including exponential phase, transitional stage, and stationary phase. The dash line represents the $OD_{600}$ trend assuming the culture keeps growing exponentially. Samples were collected at 16.5, 18.5, 20.5, 22.5, 23.5, 24.5, 25.5, 26.5, 27.5 and 29.5h for analyzing S20 and S100. The amount of yMVP in S20 and S100 fractions was determined using Q-ELISA, and normalized to cell biomass. Concentrations of yMVP in P100 were calculated by subtracting yMVP in S100 from S20. Arrows indicate the sampling points for transcriptional level analysis. Error bars represent one standard deviation (n=6-12).

The yield of assembled yeast vaults was low in exponentially growing cells but continued to increase until the cultures reached late transitional stage. This was somewhat surprising as

vault synthesis and assembly were expected to cease after exponential phase. Vault particles have been shown to be synthesized and assembled on polyribosome structures in insect cells.[4] However, previous studies on yeast polyribosomes found that polyribosomes could only be isolated from cells in the log phase and the cultures grown into the stationary phase lacked polyribosomes.[28, 36] Although it is possible that vaults are assembled by a different mechanism in yeast, it is highly likely that the decay of polyribosomes that formed on yMVP mRNAs was hindered. Polyribosomes in eukaryotic cells form progressively on mRNAs, experiencing three main conformations including circle, line, and 3D helices.[37, 38] During the first few rounds of translation, ribosomes are gradually loaded on the mRNAs, inducing mRNA conformational change, and forming the initial circular and linear polyribosomes. As translation rounds increase, more ribosomes are loaded on the mRNA, and the circular and linear polyribosomes are transformed into densely packed 3D helices. The formation of highly ordered vault structures requires co-translation of multiple MVP peptides on a single MVP mRNA one following another without break for dozens of rounds. Therefore, the polyribosome structure associated with vault MVP mRNA is likely to be the highly condensed 3D helices, rather than the linear or circular conformation. Such compact and ordered 3D helical structures of polyribosomes can possibly hinder the degradation and prolong their life in yeast cells through the transitional stage.

Previous studies suggest that trapping of mRNA on polyribosomes can reduce the decay of mRNA.[39, 40] Thus, to confirm the presence of MVP mRNA associated polyribosomes in transitional stage cells, we analyzed the change of relative transcript levels of yMVP mRNA using *GAPDH* as the reference gene. As shown in Figure 4.4, yMVP mRNA relative level significantly increased over time and doubled at the end of transitional stage comparing to middle exponential phase (OD~2), while the relative mRNA level of mCherry-INT maintained

constant through exponential phase and transitional stage. Protein concentration change also agrees with the Real-time qRT-PCR results. Production of mCherry-INT mostly occurred in exponential phase, and only increased by 38% after culture reached translational stage (Figure 4.S3), whereas the yield of yMVP increased 300% in the translational stage (Figure 4.3B). Since expression of yMVP, mCherry-INT, and GAPDH were all under the control of $P_{GAP}$, it indicates that yMVP mRNA decayed slower than mCherry-INT and GAPDH mRNA, confirming the prolonged survival of MVP mRNA associated polyribosomes through transitional stage.

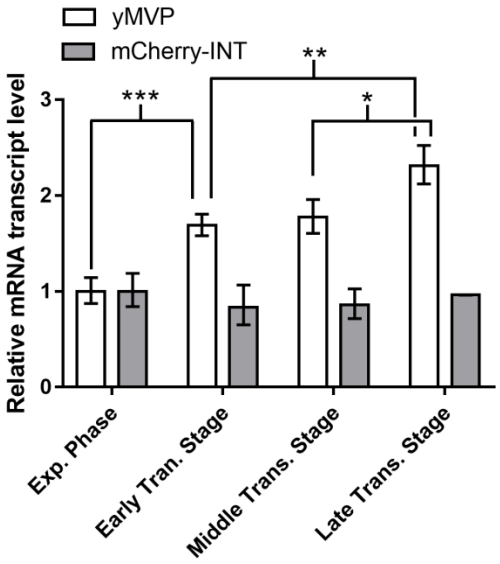


**Figure 4.4** Accumulation of yMVP mRNA Transcripts in *P. pastoris* (yMVP-pGAPZA) Cells. *P. pastoris* transformed with mCherry-INT-pGAPZA was used as a negative control. Total RNA was extracted from cells collected from middle exponential phase ($OD_{600}$~2), early transitional stage, middle transitional stage and late transitional stage as indicated in Figure 4.3 by arrows, and measured by real-time qRT-PCR. Relative mRNA transcript levels of yMVP or mCherry-INT were normalized to the value obtained with the exponential cells using *P. pastoris* GAPDH gene as the internal reference gene. An increase of yMVP mRNA transcript level was observed, while the level mCherry-INT mRNA was maintained constant from exponential phase to transitional stage. * = $p < 0.05$. ** = $p < 0.01$. *** = $p < 0.005$.

### 4.3.5 Sequestering of INT-fused Proteins into Yeast Vaults

The vault particle has been established as a superior delivery system. The particle acts

like a vehicle and is large enough to carry multiple copies of macromolecules or other complexes. To sequester exogenous components into the vault lumen, INT binding is the commonly used strategy. As a first step to demonstrate the feasibility of packaging vault cargo, we selected a monomeric protein with red fluorescent properties, mCherry. mCherry is used as a marker when tagged to molecules or cellular components. The protein is ~29 kDa with peak fluorescent excitation and emission at 587 nm and 610 nm, respectively. It matures quickly allowing it to be visualized soon after translation. We have used mCherry in previous insect cell line development to test vault packaging effectiveness.

As shown in Figure 4.5A and 4.5B, significant amounts of mCherry-INT were co-purified with vaults produced in *P. pastoris* and exhibited fluorescent properties, indicating yeast vaults are capable of packaging proteins fused to the INT domain[13, 41] and maintaining their bioactivity. Furthermore, TEM images show that packaged yeast vaults maintained their integrity and had morphologies similar to those of empty vaults (Figure 4.5C).

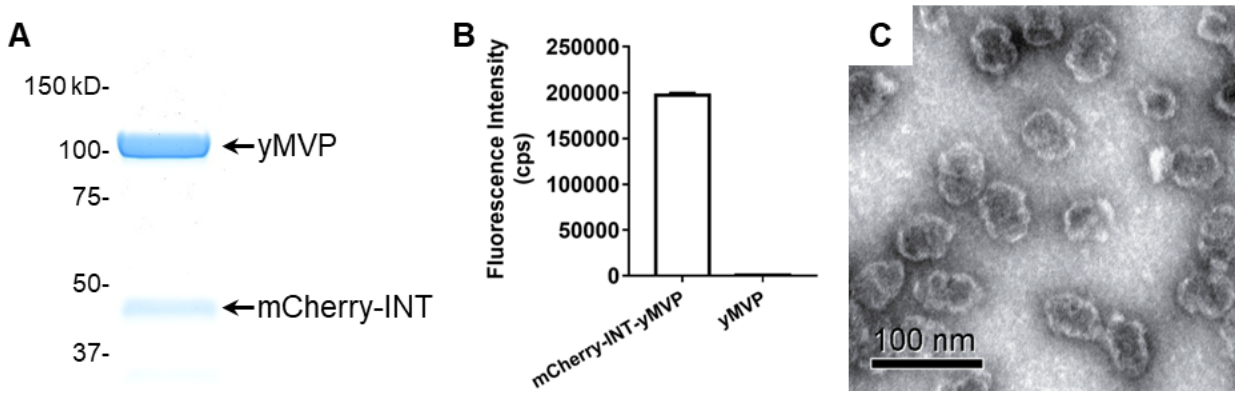


**Figure 4.5** Packaging of INT-fused proteins into Yeast Vaults. (A) Purified yeast vaults packaged with mCherry-INT were fractioned on 4-15% SDS-PAGE and analyzed using Coomassie staining. (B) Fluorescence intensity comparison between yeast vaults packaged with mCherry-INT and yeast vaults only. Samples were diluted to the same protein concentration (0.56 mg/mL) before measurements. (C) Yeast vaults packaged with mCherry-INT viewed under TEM.

### 4.3.6 Improved Stability and Catalytic Activities of MnP Packaged in Yeast Vaults

Thermal stability of MnP was significantly improved by packaging into yeast vaults. As shown in Figure 4.6A, the nMnP experienced a continuous activity loss throughout the testing period. After 8 hours incubation, nMnP only maintained 65% of its initial activity. For rMnP, it underwent a faster activity loss than nMnP. One hour incubation at 25°C led to 63% activity loss, and only 13% of initial activity was retained after 8 hours incubation, indicating rMnP was less resistant to thermal inactivation than the nMnP. However, following packaging of rMnP in to yeast vaults, its stability was significantly enhanced. The activity of rMnP-yMVP was maintained at 94% - 105% of its initial activity in the 8-hour testing period, suggesting the rMnP-yMVP did not undergo an activity loss or inactivation at 25°C in 8 hours. The temperature induced inactivation of enzymes has been attributed to the enzymatic conformational changes, involving tertiary structure disordering, such as breakage of disulfide bond and ionic interactions, and secondary structure disruption by breaking hydrogen bonds maintaining sub-structures.[42, 43] The enhancement of rMnP activity in yeast vaults is believed to be the result of constraint from vaults shells and surrounding rMnP enzyme molecules. The MVP peptides forming the vaults' shell act like cages, which can hinder the conformation changes of packaged rMnP. Additionally, each vault particle can package multiple copies of INT fusion protein clustered in a limited area adjacent to the waist of the vaults,[41] thus the surrounding rMnP molecules may also contribute to restraining structural changes in rMnP.

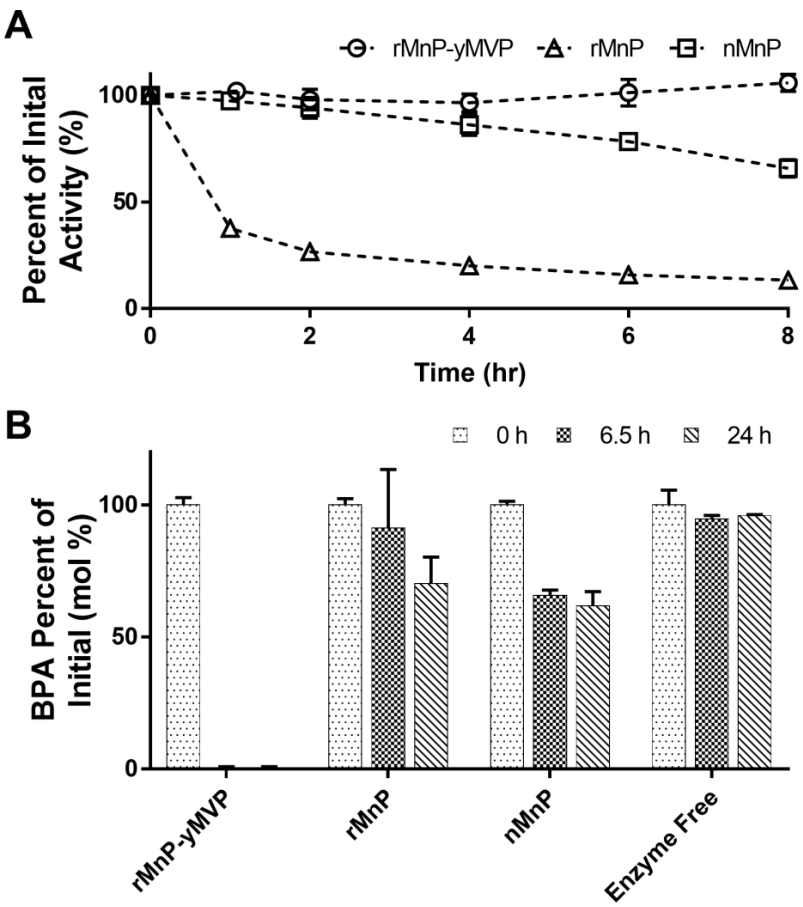


**Figure 4.6** Improved Stability and Biotransformation Performance of MnP Packaged in Yeast Vaults. (A) Thermal stability of different types of MnPs at 25°C. Yeast vaults packaged rMnP maintained its activity over the 8-hour testing period, while unpackaged MnPs experienced significant activity drops. (B) Biotransformation of BPA by different MnPs. All enzymes were dosed at 29 U/L initial activity, and samples were collected at 0, 6.5 and 24 h. In contrast to the slow and incomplete transformation by unpackaged rMnP or nMnP, treatment by rMnP packaged in yeast vaults resulted in nearly complete removal BPA in 6.5 h. Error bars represent one standard deviation of triplicate samples.

Yeast vaults packaged MnP also showed improved biocatalytic activity as compared to free MnPs. BPA, which is widely used in plastic and epoxy resin manufacturing, is one of the major endocrine disruptors found in the environment,[44] and was used as a model compound to test the efficiency of rMnP-yMVP. As the least stable MnP, rMnP only removed 30% BPA in 24 hours (Figure 4.6B). For nMnP, the removal rate increased to 39%, however, it was not statistically different from that of rMnP. In contrast, rMnP-yMVP, as the most stable form of

MnP, resulted in over 98% removal in 6.5 hours and the residual BPA concentration was below detection limit, which is much more efficient than unpackaged MnPs. Previous study using insect vaults packaged with rMnP also showed similar phenolic compound removal improvement,[18] which further suggests yeast vaults are comparable to insect vaults and *P. pastoris* is a viable alternative to insect cells for producing recombinant vaults. Interestingly, although nMnP showed better thermal stability than rMnP, and maintained 78% of its initial activity in 6 hours at 25°C, it did not show statistically higher BPA removal than rMnP, and did not induce significant BPA removal after 6.5 hours. It is possible that the stability of nMnP decreased in reactions due to the inactivation caused by $H_2O_2$, BPA radicals, or the lower pH.[45] But the yeast vaults packaged rMnP still maintained high stability and sustained activity in reactions.

### 4.4 Conclusions

Expression of MVP alone in yeast *P. pastoris* can lead to assembly of intact vault particles, which are morphologically similar to endogenous vaults isolated from various eukaryotes. Yeast has similar volumetric yield of vault particles to insect cells at laboratory scale, and recombinant yeast vaults maintain the ability to interact with INT-fused exogenous components, and improve the stability and catalytic activity of packaged enzymes, which make yeast *P. pastoris* a promising alternative to insect cells for producing recombinant vaults. In addition, the consistency of properties and morphological structure between yeast and insect cells produced vaults indicates that polyribosome templating is conserved among eukaryotic species and recombinant vaults can be synthesized with full integrity and functionality in all eukaryotic organisms that lack endogenous vault particles.

## 4.5 Supporting Information

### Experimental Methods

yMVP accumulation in *P. pastoris* (yMVP-pGAPZA): Two separated experiments were performed to study the accumulation of yMVP in *P. pastoris* (yMVP-pGAPZA) culture. In the first experiment, a 500 mL culture was maintained at 30°C, 200 rpm for 47h. $OD_{600}$ was recorded at 16, 18, 20, 22, 24, and 47h. Samples were taken at 20, 22, 24, and 47h for yMVP analysis. Partially purified yMVP was resolved on a 4-15% SDS-PAGE, followed by Coomassie staining. Each lane was loaded with yMVP obtained from the same wet weight of cells. In the second experiment, two separated cultures with the same initial $OD_{600}$ were maintained at 30°C, 200rpm. One culture was collected at late exponential phase, while the other culture was collected at stationary phase. Afterwards, yeast vaults was purified from cell pellets collected from the two cultures as described in Material and Methods, followed by anion-exchange chromatography. Protein concentrations of final purified vaults were quantified by bicinchoninic acid (BCA) assay.

mCherry-INT accumulation in *P. pastoris* (mCherry-INT-pGAPZA) and quantification: A 500 mL *P. pastoris* (mCherry-INT-pGAPZA) culture was maintained at 30°C, 200 rpm. OD600 was recorded at 16, 18, 20, 22, 24, and 26h. Cell pellet collected at each time point was lysed and centrifuged at 20,000 x g, and S20 fractions were used for mCherry-INT yield analysis. Relative levels of mCherry-INT protein in S20 was determined by quantifying intensities of mCherry-INT Western blot bands probed with anti-INT antibodies using ImageJ software, and normalizing to the first time point.

**Table 4.S1** Primers Used in real-time qRT-PCR.

| | Nucleotide Sequence (5'-3') |
|---|---|
| GAPDH Forward | ATGACCGCCACTCAAAAGACC |
| GAPDH Reverse | TTAGCAGCACCAGTGGAAGATG |
| yMVP Forward | GCTGTTGCTTCTGTTACTTTCG |
| yMVP Reverse | GCCATACCATCTGGACCTTTAG |
| mCherry-INT Forward | TTCAGTTGCCTGGAGCTTAC |
| mCherry-INT Reverse | TCTACCCTCGGCTCTTTCATA |

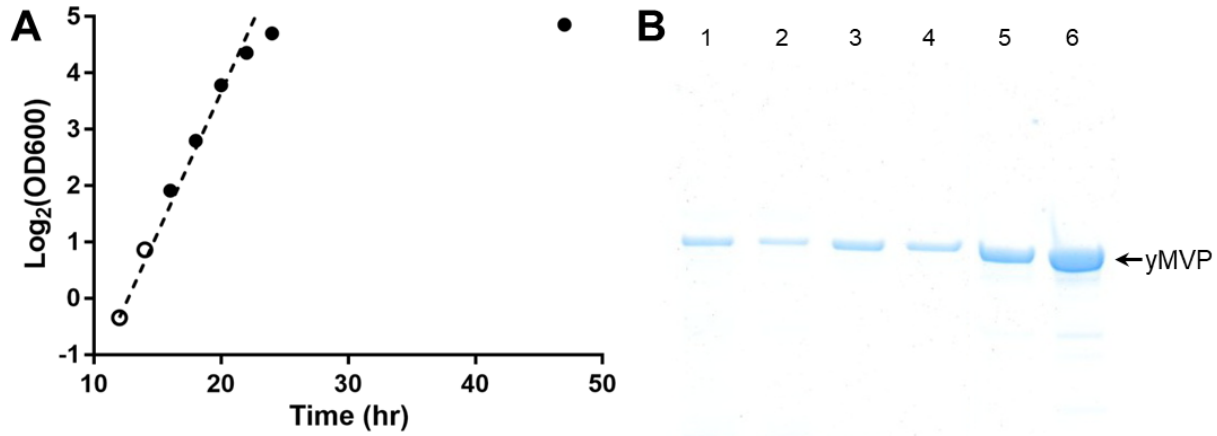


**Figure 4.S1** Accumulation of Cell Biomass and yMVP in *P. pastoris* Culture in a Separated Experiment. (A) Yeast growth curve. The dash line represents the $OD_{600}$ trend assuming the culture keeps growing exponentially. Open circles are sampling points for recording $OD_{600}$ only, and closed circles are sampling points for analyzing $DO_{600}$ and yMVP yield. (B) yMVP obtained from cells collected at different time were resolved on a 4-15% SDS-PAGE and visualized by Coomassie staining. Lane 1-6 correspond to yMVP purified from cells collected at 16, 18, 20, 22, 24, and 47h. No significant difference in yMVP yield was observed between samples collected at 16, 18, 20, and 22h, while samples collected at 22 and 24h showed increased amount of yMVP.

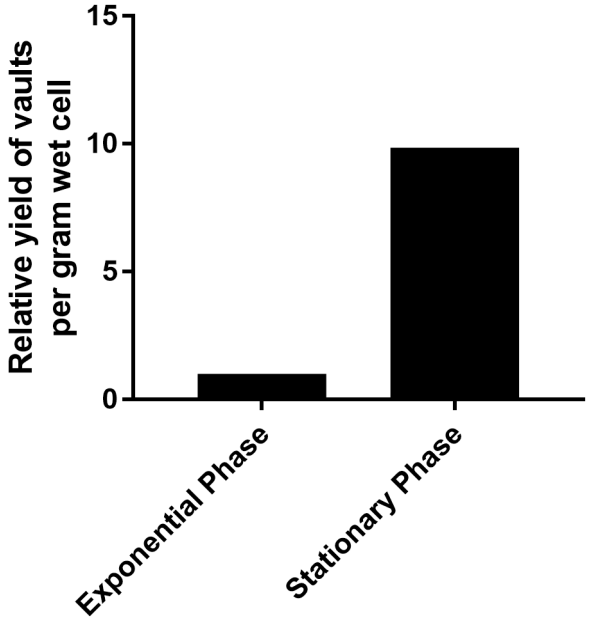


**Figure 4.S2** Comparison of Yeast Vaults Yield Between Cultures in Exponential Phase and Stationary Phase. Yeast vaults purified from cultures collected at different growth phases were quantified using BCA assay and normalized to wet cell mass. Comparing to the low yield at exponential phase, a nine-time higher vaults yield was obtained from culture at stationary phase.

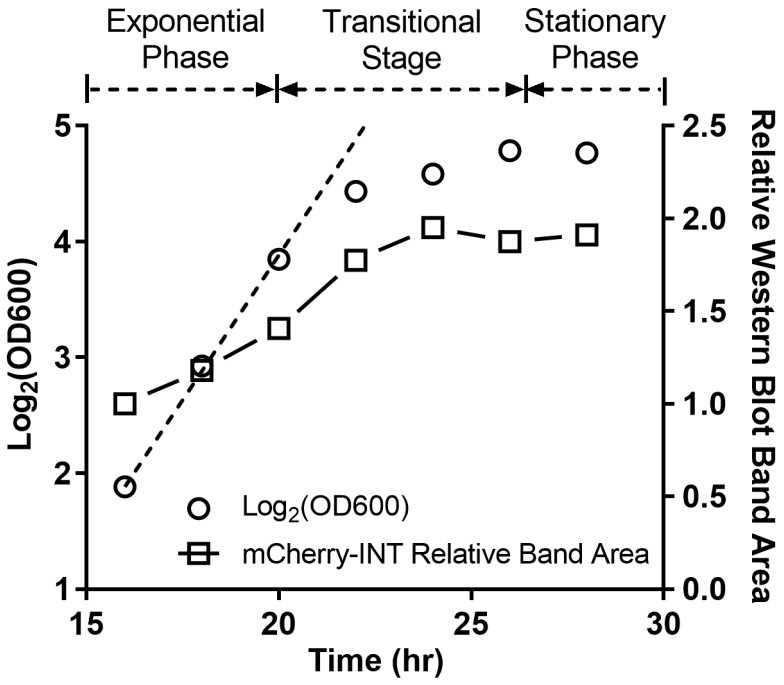


**Figure 4.S3** Accumulation of cell biomass and mCherry-INT in *P. pastoris* culture. Culture growth was divided into exponential phase, transitional stage, and stationary phase. The dash line represents the $OD_{600}$ trend assuming the culture keeps growing exponentially. The relative amount of mCherry-INT was determined by quantifying Western blot band intensities, and normalizing to the first time point.

## 4.6 References


1. Kedersha, N. L.; Rome, L. H. Isolation and characterization of a novel ribonucleoprotein particle: large structures contain a single species of small RNA. *Journal of Cell Biology* **1986,** *103* (3), 699-709.
2. Kedersha, N. L.; Heuser, J. E.; Chugani, D. C.; Rome, L. H. Vaults. III. Vault ribonucleoprotein particles open into flower-like structures with octagonal symmetry. *Journal of Cell Biology* **1991,** *112* (2), 225-235.
3. Tanaka, H.; Kato, K.; Yamashita, E.; Sumizawa, T.; Zhou, Y.; Yao, M.; Iwasaki, K.; Yoshimura, M.; Tsukihara, T. The structure of rat liver vault at 3.5 angstrom resolution. *Science* **2009,** *323*, 384-388.
4. Mrazek, J.; Toso, D.; Ryazantsev, S.; Zhang, X.; Zhou, Z. H.; Fernandez, B. C.; Kickhoefer, V. A.; Rome, L. H. Polyribosomes are molecular 3D nanoprinters that orchestrate the assembly of vault particles. *ACS Nano* **2014,** *8* (11), 11552-11559.
5. Kickhoefer, V. A.; Searles, R. P.; Kedersha, N. L.; Garber, M. E.; Johnson, D. L.; Rome, L. H. Vault ribonucleoprotein particles from rat and bullfrog contain a related small RNA that is transcribed by RNA polymerase III. *Journal of Biological Chemistry* **1993,** *268* (11), 7868-7873.
6. Kickhoefer, V. A.; Stephen, A. G.; Harrington, L.; Robinson, M. O.; Rome, L. H. Vaults and telomerase share a common subunit, TEP1. *Journal of Biological Chemistry* **1999,** *274* (46), 32712-32717.
7. Kickhoefer, V. A.; Siva, A. C.; Kedersha, N. L.; Inman, E. M.; Ruland, C.; Streuli, M.; Rome, L. H. The 193-kD vault protein, VPARP, is a novel poly(ADP-ribose) polymerase. *Journal of Cell Biology* **1999,** *146* (5), 917-928.

8. Mikyas, Y.; Makabi, M.; Raval-Fernandes, S.; Harrington, L.; Kickhoefer, V. A.; Rome, L. H.; Stewart, P. L. Cryoelectron microscopy imaging of recombinant and tissue derived vaults: localization of the MVP N termini and VPARP. *Journal of Molecular Biology* **2004,** *344* (1), 91-105.

9. Kickhoefer, V. A.; Liu, Y.; Kong, L. B.; Snow, B. E.; Stewart, P. L.; Harrington, L.; Rome, L. H. The telomerase/vault-associated protein TEP1 is required for vault RNA stability and its association with the vault particle. *Journal of Cell Biology* **2001,** *152* (1), 157-164.

10. Berger, W.; Steiner, E.; Grusch, M.; Elbling, L.; Micksche, M. Vaults and the major vault protein: novel roles in signal pathway regulation and immunity. *Cellular and Molecular Life Sciences* **2009,** *66* (1), 43-61.

11. Rome, L. H.; Kickhoefer, V. A. Development of the vault particle as a platform technology. *ACS Nano* **2013,** *7* (2), 889-902.

12. Stephen, A. G.; Raval-Fernandes, S.; Huynh, T.; Torres, M.; Kickhoefer, V. A.; Rome, L. H. Assembly of vault-like particles in insect cells expressing only the major vault protein. *Journal of Biological Chemistry* **2001,** *276* (26), 23217-23220.

13. Kickhoefer, V. A.; Garcia, Y.; Mikyas, Y.; Johansson, E.; Zhou, J. C.; Raval-Fernandes, S.; Minoofar, P.; Zink, J. I.; Dunn, B.; Stewart, P. L.; Rome, L. H. Engineering of vault nanocapsules with enzymatic and fluorescent properties. *Proceedings of the National Academy of Sciences of the United States of America* **2005,** *102*, 4348-4352.

14. Kickhoefer, V. A.; Han, M.; Raval-Fernandes, S.; Poderycki, M. J.; Moniz, R. J.; Vaccari, D.; Silvestry, M.; Stewart, P. L.; Kelly, K. A.; Rome, L. H. Targeting vault nanoparticles to specific cell surface receptors. *ACS Nano* **2009,** *3* (1), 27-36.

15. Han, M.; Kickhoefer, V. A.; Nemerow, G. R.; Rome, L. H. Targeted vault nanoparticles engineered with an endosomolytic peptide deliver biomolecules to the cytoplasm. *ACS Nano* **2011,** *5*, 6128-6137.

16. Buehler, D. C.; Toso, D. B.; Kickhoefer, V. A.; Zhou, Z. H.; Rome, L. H. Vaults engineered for hydrophobic drug delivery. *Small* **2011,** *7*, 1432-1439.

17. Kar, U. K.; Srivastava, M. K.; Andersson, A.; Baratelli, F.; Huang, M.; Kickhoefer, V. A.; Dubinett, S. M.; Rome, L. H.; Sharma, S. Novel CCL21-vault nanocapsule intratumoral delivery inhibits lung cancer growth. *PLoS ONE* **2011,** *6* (5), e18758.

18. Wang, M.; Abad, D.; Kickhoefer, V. A.; Rome, L. H.; Mahendra, S. Vault nanoparticles packaged with enzymes as an efficient pollutant biodegradation technology. *ACS Nano* **2015,** *9* (11), 10931-10940.

19. Hirano, T.; Honda, Y.; Watanabe, T.; Kuwahara, M. Degradation of bisphenol a by the lignin-degrading enzyme, manganese peroxidase, produced by the white-rot basidiomycete, Pleurotus ostreatus. *Bioscience Biotechnology and Biochemistry* **2000,** *64* (9), 1958-1962.

20. Eibes, G.; Cajthaml, T.; Moreira, M. T.; Feijoo, G.; Lema, J. M. Enzymatic degradation of anthracene, dibenzothiophene and pyrene by manganese peroxidase in media containing acetone. *Chemosphere* **2006,** *64* (3), 408-414.

21. Spadaro, J. T.; Renganathan, V. Peroxidase-catalyzed oxidation of azo dyes: mechanism of Disperse Yellow 3 degradation. *Archives of Biochemistry and Biophysics* **1994,** *312* (1), 301-307.

22. Cregg, J. M.; Cereghino, J. L.; Shi, J.; Higgins, D. R. Recombinant protein expression in *Pichia pastoris*. *Molecular Biotechnology* **2000,** *16*, 23-52.

23. Lua, L. H. L.; Connors, N. K.; Sainsbury, F.; Chuan, Y. P.; Wibowo, N.; Middelberg, A. P. J. Bioengineering Virus-Like Particles as Vaccines. *Biotechnology and Bioengineering* **2014,** *111* (3), 425-440.

24. Mateu, M. G. Assembly, stability and dynamics of virus capsids. *Archives of Biochemistry and Biophysics* **2013,** *531* (1-2), 65-79.

25. He, S. L.; Green, R. Chapter Ten - Polysome Analysis of Mammalian Cells. In *Methods in Enzymology*, Jon Lorsch, Ed.; Academic Press: 2013; Vol. 530, pp 183-192.

26. Pospísek, M.; Valásek, L. Chapter Nine - Polysome Profile Analysis – Yeast. In *Methods in Enzymology*, Jon Lorsch, Ed.; Academic Press: 2013; Vol. 530, pp 173-181.

27. Qin, D.; Fredrick, K. Chapter Eight - Analysis of Polysomes from Bacteria. In *Methods in Enzymology*, Jon Lorsch, Ed.; Academic Press: 2013; Vol. 530, pp 159-172.

28. Marcus, L.; Ris, H.; Halvorson, H.; Bretthauer, R.; Bock, R. Occurrence, isolation, and characterization of polyribosomes in yeast. *Journal of Cell Biology* **1967,** *34* (2), 505-512.

29. Kozak, M. An analysis of 5'-noncoding sequences from 699 vertebrate messenger RNAs. *Nucleic Acids Research* **1987,** *15* (20), 8125-8148.

30. Ahmad, M.; Hirz, M.; Pichler, H.; Schwab, H. Protein expression in *Pichia pastoris*: recent achievements and perspectives for heterologous protein production. *Applied Microbiology and Biotechnology* **2014,** *98* (12), 5301-5317.

31. Wang, J.-H.; Hung, W.; Tsai, S.-H. High efficiency transformation by electroporation of *Yarrowia lipolytica*. *The Journal of Microbiology* **2011,** *49*, 469-472.

32. Qin, X.; Qian, J.; Yao, G.; Zhuang, Y.; Zhang, S.; Chu, J. GAP Promoter Library for Fine-Tuning of Gene Expression in *Pichia pastoris*. *Applied and Environmental Microbiology* **2011,** *77*, 3600-3608.

33. Waterham, H. R.; Digan, M. E.; Koutz, P. J.; Lair, S. V.; Cregg, J. M. Isolation of the *Pichia pastoris* glyceraldehyde-3-phosphate dehydrogenase gene and regulation and use of its promoter. *Gene* **1997,** *186*, 37-44.

34. Kedersha, N. L.; Miquel, M. C.; Bittner, D.; Rome, L. H. Vaults. II. Ribonucleoprotein structures are highly conserved among higher and lower eukaryotes. *Journal of Cell Biology* **1990,** *110* (4), 895-901.

35. Kong, L. B.; Siva, A. C.; Rome, L. H.; Stewart, P. L. Structure of the vault, a ubiquitous celular component. *Structure* **1999,** *7* (4), 371-379.

36. Esposito, A. M.; Mateyak, M.; He, D.; Lewis, M.; Sasikumar, A. N.; Hutton, J.; Copeland, P. R.; Kinzy, T. G. Eukaryotic polyribosome profile analysis. *Journal of Visualized Experiments: JoVE* **2010,** (40), e1948.

37. Afonina, Z. A.; Myasnikov, A. G.; Shirokov, V. A.; Klaholz, B. P.; Spirin, A. S. Conformation transitions of eukaryotic polyribosomes during multi-round translation. *Nucleic Acids Research* **2015,** *43* (1), 618-28.

38. Kopeina, G. S.; Afonina, Z. A.; Gromova, K. V.; Shirokov, V. A.; Vasiliev, V. D.; Spirin, A. S. Step-wise formation of eukaryotic double-row polyribosomes and circular translation of polysomal mRNA. *Nucleic Acids Research* **2008,** *36* (8), 2476-2488.

39. Brandt, F.; Carlson, L.-A.; Hartl, F. U.; Baumeister, W.; Grünewald, K. The three-dimensional organization of polyribosomes in intact human cells. *Molecular Cell* **2010,** *39*, 560-569.

40. Sheth, U.; Parker, R. Decapping and decay of messenger RNA occur in cytoplasmic processing bodies. *Science* **2003,** *300* (5620), 805-808.

41. Lai, C. Y.; Wiethoff, C. M.; Kickhoefer, V. A.; Rome, L. H.; Nemerow, G. R. Vault nanoparticles containing an adenovirus-derived membrane lytic protein facilitate toxin and gene transfer. *ACS Nano* **2009,** *3* (3), 691-699.

42. Henley, J. P.; Sadana, A. Series-type enzyme deactivations: influence of intermediate activity on deactivation kinetics. *Enzyme and Microbial Technology* **1984,** *6* (1), 35-41.

43. Henley, J. P.; Sadana, A. Categorization of enzyme deactivations using a series-type mechanism. *Enzyme and Microbial Technology* **1985,** *7* (2), 50-60.

44. Chen, Y. C.; Shu, L.; Qiu, Z. Q.; Lee, D. Y.; Settle, S. J.; Hee, S. Q.; Telesca, D.; Yang, X.; Allard, P. Exposure to the BPA-substitute bisphenol S causes unique alterations of germline function. *Plos Genetics* **2016,** *12* (7), e1006223.

45. Aitken, M. D.; Irvine, R. L. Stability testing of ligninase and Mn-peroxidase from *Phanerochaete chrysosporium*. *Biotechnology and Bioengineering* **1989,** *34* (10), 1251-1260.

## Chapter 5 Vault Particles Templated Formation of Silica and Its Application in Enzyme Immobilization

### 5.1 Introduction

Mesoporous silica materials, because of their ultrahigh surface area, high stability, and tunable structures, have attracted interest from many areas, such as catalysis, energy conversion and storage, and drug delivery.[1-3] Since the first discovery of MCM-41 molecular sieves by Mobil Cooperation scientists,[4] numerous types of mesoporous silica materials have been synthesized, mainly through surfactant-templated procedures, which rely on the assembly of surfactant templates (S) and deposition of silica inorganic precursors (I) on their surfaces.[5, 6] Three major routes have been reported for surfactant-templated synthesis of mesoporous silica. The first route relies on direct ($S^+I^-$) or counter-ion mediated ($S^+X^-I^+$) electrostatic interaction, such as the original M41S family.[4, 7] Anionic surfactants have also been shown to direct the formation of mesoporous structures (route 2), such as the AMS family,[6] but through co-structuring directing agents (CSDAs) mediated interactions ($S^-(^+X^0)I^0$). The third route, neutral templating through hydrogen-bonding interaction $S^0I^0$ (HMS and MSU families) and ($S^0H^+$)($X^-I^0$) (SBA family), is used for MSNPs preparation from neutral non-ionic surfactants.[8-11]

Despite having been employed to prepare numerous mesoporous silica materials, these chemical synthetic routes share some common drawbacks, primarily the requirement of extreme pH, temperature, and pressure, and toxic substances.[12] Biosilicification appears to be an promising alternative to chemical synthesis, not only because it proceeds under gentler conditions,[12] but also due to the large morphological and structural diversity of biomolecular templates, which may offer new silica structures with unique properties that are not readily accessible by chemical synthesis.[13] To date, biomimetic synthesis of MSNP has being reported

using natural and synthetic biomolecules, such as cellulose,[14] polycationic peptide assemblies,[15] and viruses,[13] primarily through routes relying on direct electrostatic interactions or CSDA-mediated interactions.[13-18] As one of the three major routes in chemical synthesis of MSNP, neutral templating offers advantages over electrostatic and CSDA-mediated pathways. In particular, it facilitates the synthesis of mesostructures that are not readily achievable through the other two routes.[8] However, neutral templating has not yet been used for biomimetic synthesis of mesoporous silica NPs.[16, 19]

Vault particles are the largest naturally occurring ribonucleoprotein complexes.[20] The natural vault has a barrel-shape cage that is composed of seventy-eight copies of major vault protein (MVP), with multiple copies of TEP1 protein, VPARP protein, and untranslated vault mRNA fragments lining the inner surface of MVP shell.[21, 22] Derived from natural vaults, recombinant vaults, which are assembled solely from seventy-eight copies of MVP, display similar barrel-like shape as natural vaults and have large empty core.[23] Here, we report a biomaterial-directed neutral templating route to mesosilica, as a complement to current methods. Our approach is based on hydrogen-bonding between neutral vault protein nanocages and neutral silica precursor. By combining the unique vault encapsulation and vault-templated formation of mesosilica, we developed the vault-templated mesosilica as a facile immobilization support with remarkably high immobilization efficiency and low leaching. Proteins and enzymes entrapped in vault/silica showed improved stability and high activity.

## 5.2 Results and Discussion

### 5.2.1 Synthesis of Vault-templated Silica Composites

The vault-templated synthesis of mesoporous silica was achieved by mixing recombinant vault particles with pre-hydrolyzed tetramethyl orthosilicate (TMOS) at pH 5.5. White vault/silica composites particles developed in 30 minutes and showed a hydrodynamic diameter of around 400 nm (Figure 5.1). In contrast, no precipitate formation was observed in the absence of vaults or in the presence of bovine serum albumin (BSA) at the same protein concentration for at least a few hours. In the presence of excess TMOS, vaults completely co-precipitated with silica at all protein concentrations tested, indicating favorable interaction between vault particles and hydrolyzed TMOS. Further stoichiometric analysis revealed that the amount of silica in vault/silica composite was proportional to the amount of vaults added, at a mass ratio of 1:1 (Figure 5.2A), which is similar to that of silaffin.[16]

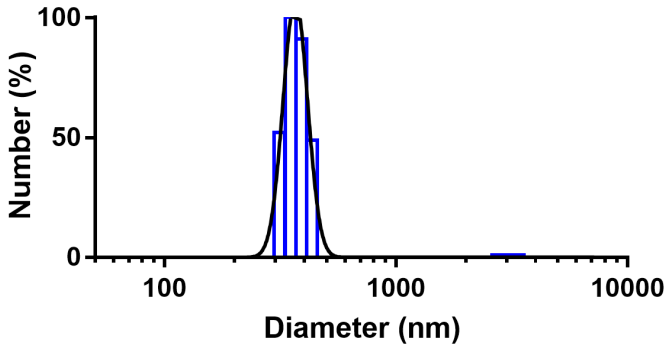


**Figure 5.1** Hydrodynamic Diameter Distribution of the As Synthesized vault/silica Nanoparticles. The average diameter was measured as 400 nm.

The vault-templated formation of vault/silica composites is believed to be through the neutral templating route, as evidenced by its unique pH dependency. Polycationic peptides directed formation of mesoporous silica, which is based on electrostatic interaction between positively charged amine groups and negatively charged silica inorganic precursors, was shown

to be predominant at neutral pH.[16, 19, 24] At acidic pH, little to no silica was formed, mainly due to the decreased negative charge of silanol groups.[24] In the charge-inversed situation, electrostatic

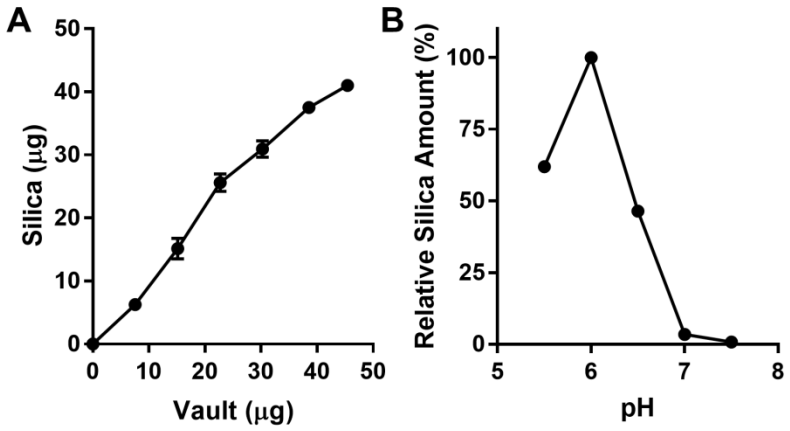


**Figure 5.2** Vault Templated Formation of Mesosilica. (A) Stoichiometric correlation between applied vaults and the amount of silica in vault/silica composites at pH 5.5. (B) Silica amounts in vault/silica composites formed at pH 5.5, 6, 6.5, 7 and 7.5 with the same amount of initially applied vaults.

interactions between hydrolyzed cellulose and silica inorganic precursors occurred in the lower pH range (acidic condition, pH < 2), in which hydrolyzed cellulose is negatively charged and silanol groups are positively charged.[14, 16] In contrast, for the vault-templated mesosilica, we found that it only occurred in the weakly acidic pH range, and peaked at pH 6 (Figure 5.2B). When pH increased to 7 or 7.5, where polycationic peptide-mediated silicification is favored, no silica precipitate was observed. MVP peptides, which assemble into vault particles, have a pI around 5.5. In the 5.5-6.5 pH range, as vaults and silanol groups both display little charge,[24] electrostatic repulsion between these two species is minimalized. Vaults, as supra-protein complexes, contain thousands of oxygen and nitrogen containing functional groups on the surface. These functional groups most likely form hydrogen-bonding interactions with $Si(OCH_3)_{4-x}(OH)_x$ that are resulted from hydrolysis of TMOS,[18] leading to further condensation of silanol groups on vaults' surface. At negative charge on both vaults and silanol groups at pH 7

or higher,[7] the resultant electrostatic repulsion between these two species prevents silica deposition on the particle surface. In addition, when using denatured MVP peptides, silica precipitation was also observed, but only in the form of amorphous silica. This result suggests that the interaction between vaults and silica precursors is independent from their bioactivity, and is mostly like through physical interactions, which further supports the proposed neutral templating route of vault-directed formation of mesosilica.

### 5.2.2 Immobilization of Fluorescent Proteins in Vault/Silica

It was also demonstrated that the vault-templated mesosilica is a promising solid support for protein immobilization applications. Vaults have been shown to encapsulate heterologous compartments, through the antigen-antibody like interactions between vault interior binding sites and a protein domain named INT.[25] By attaching with an INT domain, protein-of-interest (POI) can be directed and anchored on the inner surface of vaults, facing inward. Using vaults encapsulated with POI-INT as templates, we anticipated POI-INT would be immobilized in mesosilica through the interaction between vaults and silica precursors. To prove the concept, we first tested the immobilization of the fluorescent protein, mCherry. INT tagged mCherry (mCherry-INT) was encapsulated into vaults, and mixed with hydrolyzed TMOS at pH 5.5, resulting in formation of fluorescent mesosilica. The immobilization efficiencies and yields of fluorescence intensity in silica were both 100% over a wide concentration range of applied mCherry-INT-vaults (Figure 5.3A). Only background fluorescence intensities were detected in the supernatant collected after centrifuging reaction mixtures. The calculated protein loading of mCherry-INT in silica was 23% (w/w), which is close to the highest reported protein loading capacity in silica.[26] Further evaluation of the leaching of mCherry-INT from mCherry-

INT/vault/silica showed the protein was entirely retained in silica over 47 days without any significant leakage (Figure 5.4).

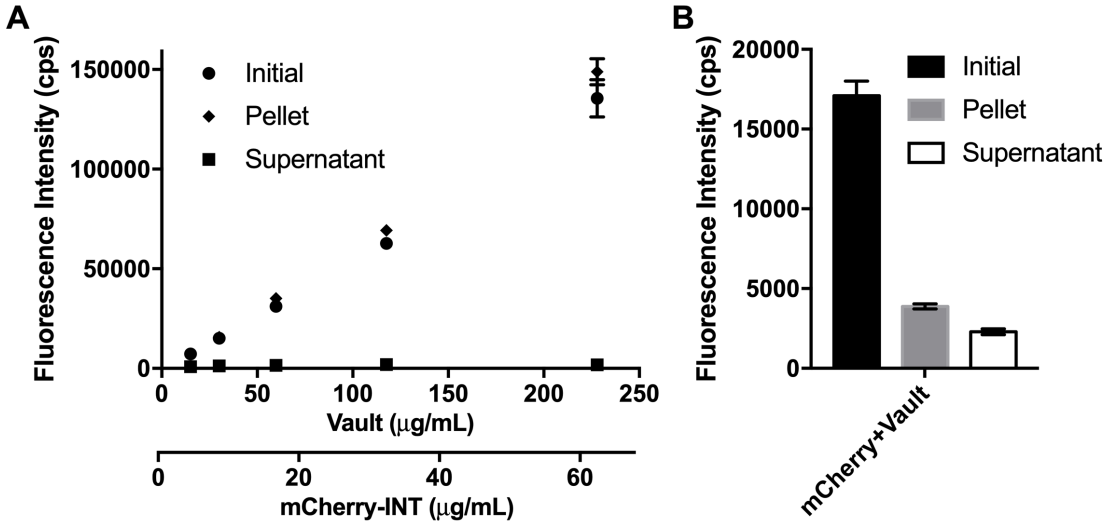


**Figure 5.3** Immobilization of mCherry Fluorescent Protein in Mesosilica. (A) Yield of fluorescence intensities in silica templated by mCherry-INT/vaults. The resultant mCherry-INT/vault/silica showed similar fluorescence intensities to initially applied mCherry-INT/vault, over a wide concentration. Fluorescence intensities in the silica free supernatant were close to background levels. (B) Immobilization of free mCherry in vault/silica using empty vaults as templates. As compared to total fluorescence intensity recovered in the vault/silica pellet and supernatant with the intensity of initially applied mCherry, significant loss was observed. The yield of fluorescence intensity in mesosilica was below 25% of the initial value.

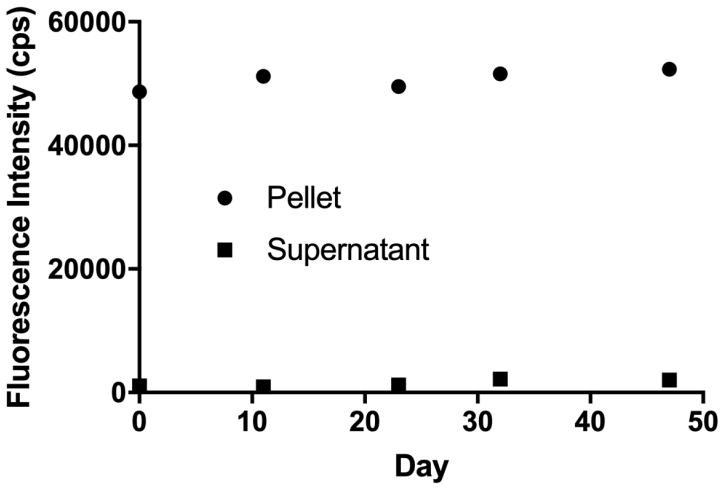


**Figure 5.4** Leaching of mCherry-INT from Mesosilica Supports. At each time point, the sample was collected and centrifuged to separate silica particles from suspension. Fluorescence intensities of pellets were from immobilized mCherry-INT, while fluorescence intensities of supernatant were from leaked mCherry-INT. Leaching was negligible after 47 days incubation at 4°C.

Using the same method, we prepared green fluorescence protein (GFP)-INT/vault/silica, which also showed 100% immobilization efficiency and fluorescence intensity yield. In addition, the silica immobilized GFP showed significantly increased stability. After three hours long incubation at pH 6.5 and at 37°C, free GFP-INT and GFP-INT/vaults exhibited ~250% and 200% more lost in fluorescent activity compared with GFP-INT/vault/silica (Figure 5.5A). In the presence of strong denaturant sodium dodecyl sulfate (SDS), while free GFP-INT was completely denatured in one minute, GFP immobilized in silica still maintained over 30% of its initial fluorescence intensity after 30 minutes (Figure 5.5B).

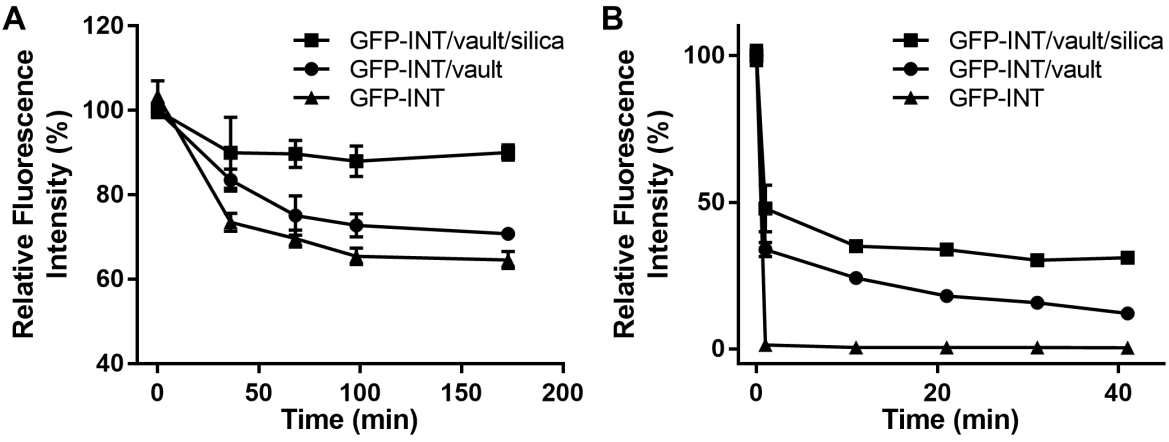


**Figure 5.5** GFP-INT/vault/silica exhibited improved stability. (A) Relative activities of GFP-INT/vault/silica, GFP-INT/vault and free GFP-INT incubated at pH 6.5 37°C. (B) Relative activities of immobilized and free GFP-INT in the presence of 0.05% SDS at pH 6.5 room temperature.

### 5.2.3 Immobilization of Enzyme in Vault/Silica

We further evaluated the applications of vault-templated mesosilica towards enzyme immobilization. Manganese peroxidase (MnP) is a member of the peroxidase family of enzymes, which catalyze substrate oxidation using $H_2O_2$ as electron donor. Using the same vault-

templating route described above, we prepared MnP-INT/vault/silica. The yield of enzymatic activity in silica was measured as 77% of initially applied MnP-INT/vault (Figure 5.6).

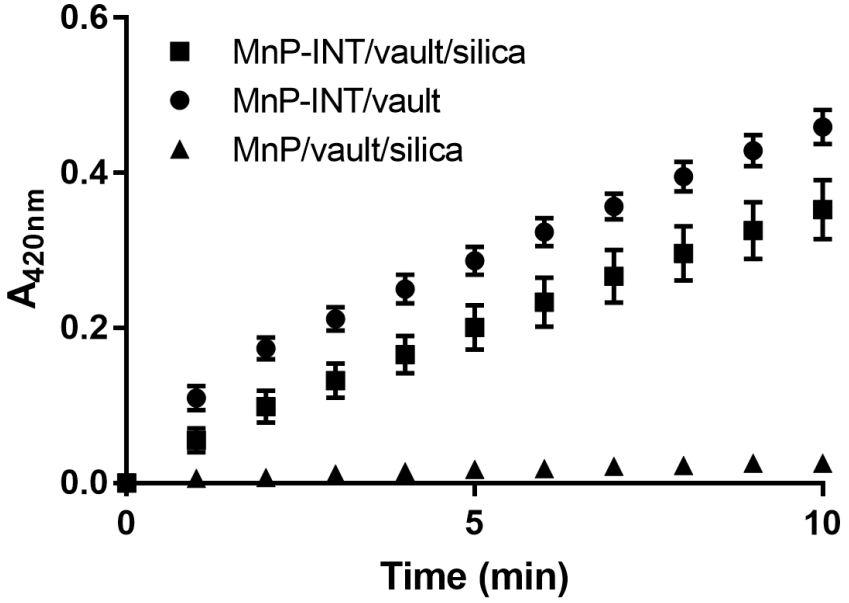


**Figure 5.6** Kinetics of ABTS Oxidation Catalyzed by MnP-INT/vault/silica, MnP-INT/vault, and free MnP immobilized in vault/silica (MnP/vault/silica).

Mesosilica immobilized MnP-INT also showed significantly improved stability against high temperature and organic solvent stress than unencapsulated MnP-INT and MnP-INT/vaults. After ten minutes of exposure to 15% methanol and isopropanol at room temperature, the silica immobilized MnP-INT maintained 80% and 92% of its initial activity, which were 150% and 40% higher than that of free MnP-INT, respectively (Figure 5.7A). At high temperature, enzyme activity loss was also significantly mitigated with silica immobilization. Thirty minutes of incubation at 45°C and 50°C completely inactivated MnP-INT and MnP-INT/vaults, however, MnP-INT/vault/silica still retained 55% and 27% of its initial activity, respectively (Figure 5.7B). When incubating enzymes in the solution containing 5%, 10%, and 15% methanol at 45°C for ten minutes, the silica immobilized enzyme still kept 27-45% of its initial activity, while other MnPs were entirely inactivated (Figure 5.7C).

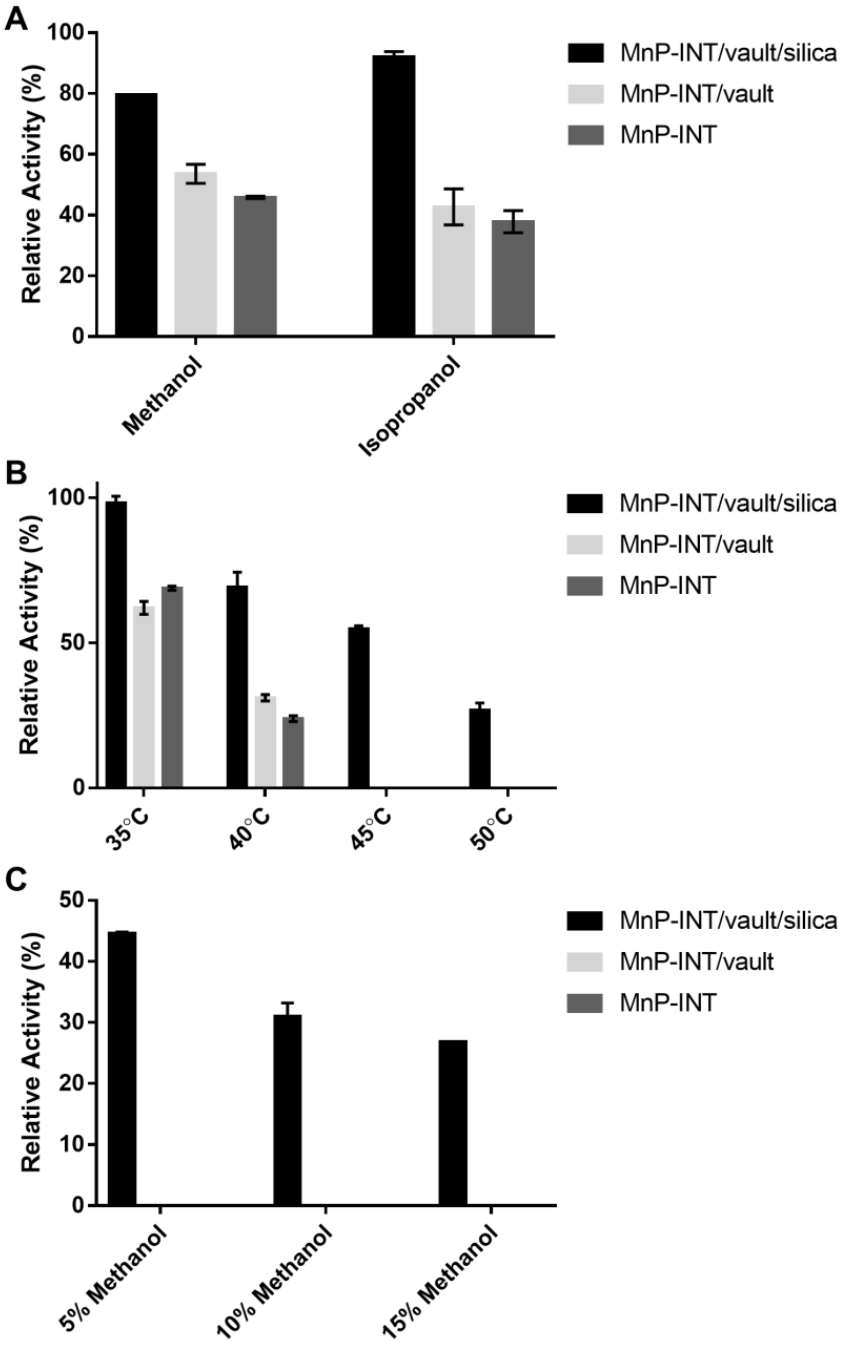


**Figure 5.7** Enhanced Stability of Silica Immobilized MnP Enzyme. (A) Relative activities of MnP-INT/vault/silica, MnP-INT/vault, and free MnP-INT after 10 minutes incubation in solutions containing 15% methanol or isopropanol at room temperature. (B) Relative activities of immobilized and free MnP enzymes incubated at 35°C, 40°C, 45°C, and 50°C for 30 minutes. (C) Relative activities of immobilized and free MnP enzymes after 10 minutes incubation in solutions containing 5%, 10%, or 15% methanol at 45°C.

Moreover, the MnP-INT/vault/silica was demonstrated to have superior reusability. Using 2,2'-azino-bis(3-ethylbenzothiazoline-6-sulphonic acid) (ABTS) as the model substrate, the MnP-INT/vault/silica maintained near 100% activity after 12 reuses and 90% activity after 25 reuses (Figure 5.8). The significant drop after 32 reuses, we believe, is not due to enzyme inactivation, but the incomplete enzyme recovery caused by silica particle cracking after repeated centrifugation.

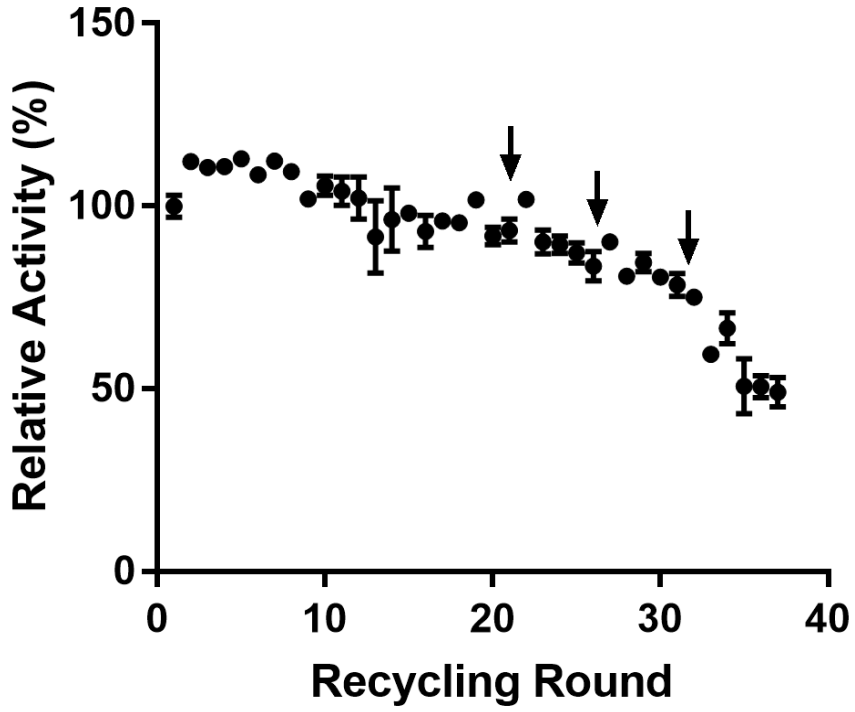


**Figure 5.8** Reusability of Silica Immobilized MnP Enzyme. Relative activities of the same MnP-INT/vault/silica in ABTS oxidation in repeated uses. Arrows indicate overnight storage at 4°C.

Bisphenolic compounds are commonly found estrogenic contaminants in water supplies, which cause adverse health effects and reproductive toxicities.[27-29] The MnP-INT/vault/silica was found to effectively remove bisphenol A (BPA) and bisphenol F (BPF). After 7 hours incubation, 74% and 63% removal were observed for BPA and BPF (Figure 5.9A), respectively.

Moreover, on reusability, the MnP-INT/vault/silica maintained robust activity after reuses, and showed no obvious decrease in BPA removal in four recycling rounds (Figure 5.9B).

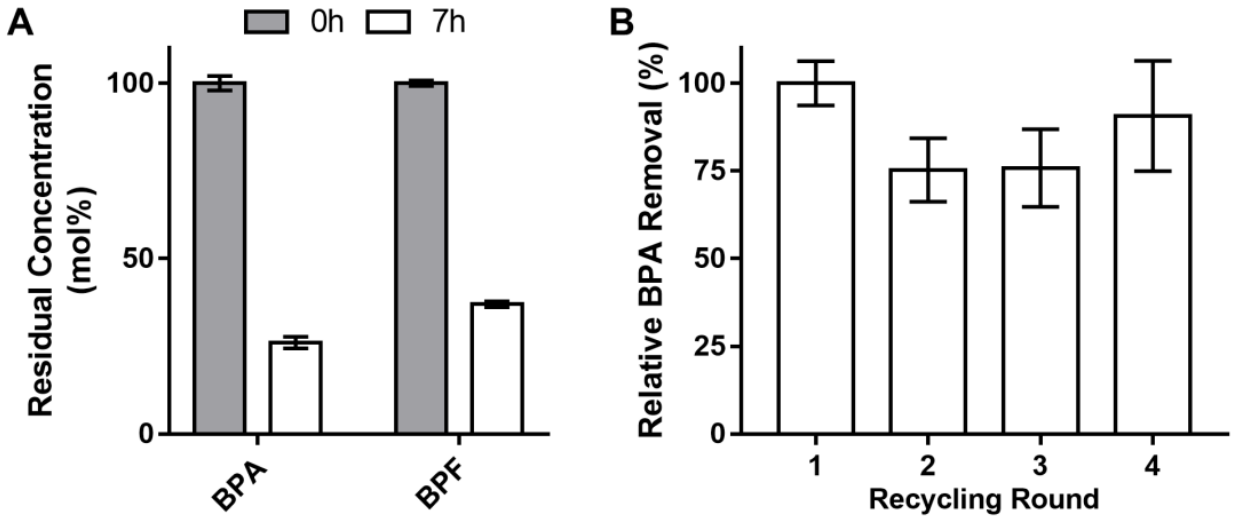


**Figure 5.9** Removal of Bisphenolic Compounds by MnP-INT/vault/silica. (A) MnP-INT/vault/silica catalyzed removal of BPA and BPF. (B) Repeated use of the same MnP-INT/vault/silica in removing BPA. Removal rates were normalized to the rate obtained in the first use.

In full-scale water treatment or point-of-use applications, the enzymes will not be used in buffered conditions, but in real water systems. Thus, we next tested MnP-INT/vault/silica stability in samples of tap water and groundwater collected from a military contaminated site. The tap water has a pH of around 7.6.[30] Total hardness and total alkalinity are around 84 mg/L (as $CaCO_3$) and 105 mg/L (as $CaCO_3$), respectively.[30] Metal ions such as aluminum, calcium, chromium, lithium, magnesium, potassium and sodium, and cations such as arsenic, bromide, chloride, fluoride, nitrate, nitrite, phosphate and sulfate, are found at trace levels in the tap water.[30] Trace amounts of organic contaminants including 1,1-dichloroethane, 1,4-dioxane, bromochloromethane, chlorodifluoromethane and trichloroethylene, are also detected, and the total organic carbon is about 1.9 mg/L.[30] The groundwater used contains trace amounts of per-

and polyfluoroalkyl substances, acetone, carbon disulfide and chlorinated solvents, and has a pH of 7-9.

As shown in Figure 5.10A, after 16 days of incubation in tap water at 15°C, silica immobilized MnP-INT maintained 50% of its initial activity, while no significant activity was detected for MnP-INT/vault or natural MnP. In groundwater, the residual activity percentage of MnP-INT/vault/silica after 16 days incubation was 110% and 1350% higher than that of MnP-INT/vault and natural MnP, respectively (Figure 5.10B).

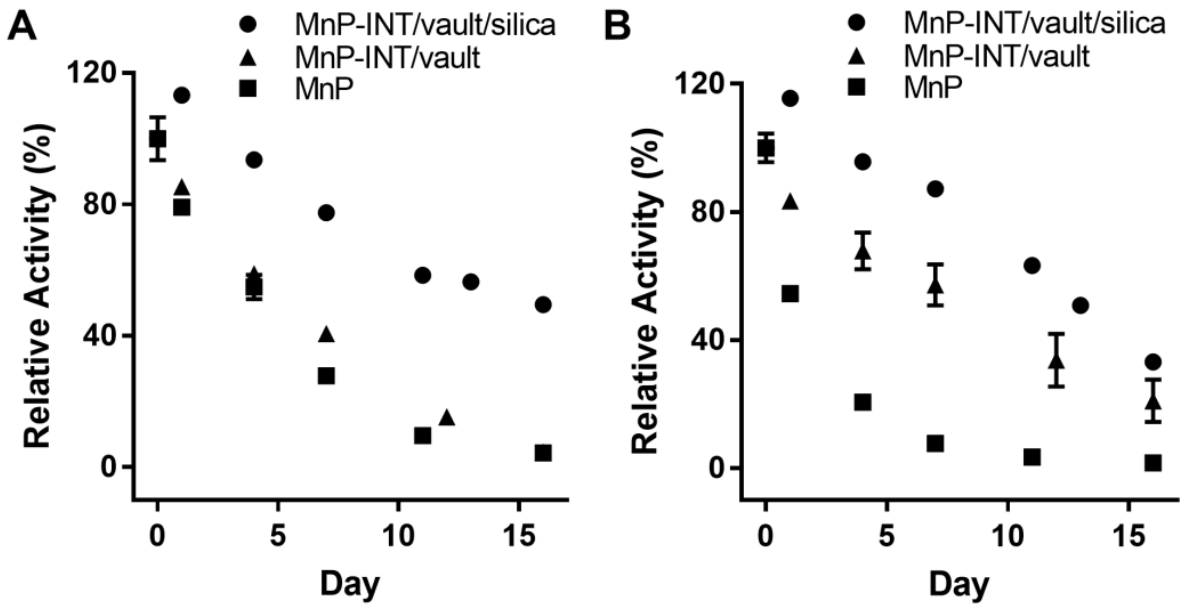


**Figure 5.10** Enhanced Stability of Silica Immobilized MnP Enzymes in Real Water Systems. (A) Relative activities of MnP-INT/vault/silica, MnP-INT/vault and natural MnP (nMnP) incubated in tap water at 15°C. (B) Relative activities of immobilized and free MnP enzymes incubated in groundwater at 15°C.

Biosilicification is a commonly used method to immobilize proteins or enzymes in silica support, however, usually requires large quantity of precipitants. In addition, previously reported procedures have relied on random entrapment event during silica formation, thus the immobilization efficiency was not ensured and changed with the precipitant and protein concentrations. For immobilization in vault-templated mesosilica, as proteins were pre-

encapsulated in vaults, which was subsequently used to induce silica polymerization, we observed 100% immobilization efficiency over a wide concentration range, even at very low vault concentrations. Theoretically, the efficiency will be maintained at 100% as long as silica inorganic precursor is in excess.

Immobilization in mesosilica, through binding on or entrapment, also leads to significant activity loss, mainly resulting from the denaturation during mesosilica formation. Similar results were also observed when we tested immobilization of unencapsulated proteins in vault-templated mesosilica. When using empty vaults as templates with free mCherry, overall fluorescence intensity decreased by 64%, and the yield in silica was below 25% (Figure 5.3B). In the case MnP, enzyme activity recovery in silica was even lower, only at 5.5% (Figure 5.6). As compared to the serious activity loss after immobilization mentioned above, using the vault encapsulation and templating strategy, we achieved 100% and 78% activity yields in mesosilica for fluorescent proteins and MnP enzyme, respectively, which are comparable to the yields reported in the well-known nanobiocatalysts including single-enzyme nanoparticles, nanogels and nanoflowers.[31-33] Two effects from the unique vault-encapsulation step probably contribute to their high activity yields in mesosilica. First, direct interactions between silica precursors and proteins are largely avoided, as proteins are covered by vault shells, while silica precursors interact and deposit on vaults' outer surfaces. Second, the large vault lumen allows free enzyme conformational change that is required for a proper catalytic cycle, and it also makes the resultant mesosilica more porous, leading to reduced substrate mass-transfer resistances.

Protein leakage and the resultant activity loss after reuses are often observed after immobilization. Laccase nanoflowers lost nearly 20% activity in the detection of epinephrine after 5 reuses. Lipase immobilized on modified mesosilica nanoparticles lost 7-74% activity after

5 reuses.[34] Amine-based silica entrapped carbon anhydrase experienced 10% leakage in 24 hours, and lost 13% activity after 5 reuses.[35] In contrast, mCherry immobilized in vault/silica showed negligible leakage in 47 days, and the vault/silica immobilized MnP enzyme was used for 25 times with only 10% activity loss. The significantly reduced leakage and improved reusability are attributed to the double encapsulation of proteins in vaults' shell and silica layers. Therefore, the immobilization in vault-templated mesosilica appears to be an approach with remarkably lower leakage and improved reusability than other techniques.

## 5.4 Conclusions

The ability of vault particles to direct the formation of mesosilica was demonstrated. To the best of our knowledge, this is the first biomaterial based neutral-templating route to synthesize mesosilica, which opens up new opportunities to use biomaterials like protein nanocages to synthesize mesosilica structures, or mesoporous metal structures that are not readily accessible by electrostatic or CSDA-mediated templating routes. In addition, the immobilization of protein in vault/silica, through the vault-templating and encapsulation, has remarkably high immobilization efficiency and low leakage, and generates enzymes with high activity as well as enhanced stability. Such highly active and robust enzyme/mesosilica composites are suitable for applications in a wide variety of fields such as industrial biofuel synthesis, food and beverage processes, pharmaceutical manufacturing, biosensors, and environmental remediation.

## 5.5 Experimental Materials and Methods

### 5.5.1 Materials

Tetramethyl orthosilicate (TMOS) and other commercial reagents were purchased from Fisher Scientific or Sigma-Aldrich. Vault particles were purified from *Spodoptera frugiperda* Sf9 insect cells expressing human MVP, which do not contain endogenous MVP homologue or vaults, as previously described.[23] mCherry, mCherry-INT, GFP, GFP-INT, and MnP-INT were expressed in *E. coli* or insect Sf9 cells. Natural MnP was extracted and purified from white-rot fungus *Phanerochaete chrysosporium* as described previously.[36] Preparation of vault encapsulated mCherry-INT, GFP-INT, MnP-INT was performed following the standard vault protocol.[23, 25, 36] Protein concentrations were determined using the bicinchoninic acid (BCA) assay (Thermo Fisher Scientific).

### 5.5.2 Preparation of vault/silica with or without encapsulated protein

Pre-hydrolyzed TMOS was prepared using a mixture containing 807 μL TMOS, 181.6 μL deionized water, and 7.6 μL 0.04 N HCl.[37] The mixture was stirred in an ice bath for 10 minutes, followed by 20 minutes of sonication at 0°C. The resultant TMOS sol was kept on ice before use. In a typical vault/silica preparation, a mixture containing 500 μL pH 5.5 50 mM malonate-Na buffer, 17 μL vault solution (3-4 mg/mL) and 17 μL pre-hydrolyzed TMOS was stirred at 4°C for 1 hour. The resultant vault/silica composites were collected by 10 minutes centrifugation at 6000 x g, and then washed three times with deionized water. The particle size distribution was measured using NanoBrook ZetaPALS Potential Analyzer. To test the relationship between applied vaults and precipitated silica, different amounts of vaults were added in the beginning. For the evaluation of pH effects on vault/silica formation, the malonate

buffer was replaced with 50 mM citrate-phosphate buffer at pH 5.5, 6, 6.5, 7, and 7.5. mCherry-INT/vault/silica, GFP-INT/vault/silica and MnP-INT/vault/silica were prepared by the same procedure described, but using mCherry-INT/vault, GFP-INT/vault and MnP-INT/vault as templating agents, respectively. After washing with deionized water, mCherry-INT/vault/silica and GFP-INT/vault/silica were stored in Buffer A (50 mM Tris pH 7.4, 75 mM NaCl, 0.5 mM $MgCl_2$), and MnP-INT/vault/silica was stored in pH 5.0 50 mM malonate-Na buffer at 4°C. To test the immobilization of unencapsulated proteins in vault/silica, free mCherry or MnP was added to the mixture containing 500 μL pH 5.5 50 mM malonate-Na buffer, 17 μL vault solution (3-4 mg/mL) and 17 μL pre-hydrolyzed TMOS, followed by 1 hour stir at 4°C, centrifugation and washing. The yield was calculated by dividing the bioactivity or enzymatic activity of mesosilica by initially applied activity.

### 5.5.3 Silica Quantification

Washed vault/silica composites were resuspended in 50 μL 1 N NaOH, and heated at 95°C for 30 minutes to dissolve silica.[12] Then, concentrations of dissolved silica were determined colorimetrically by the silicomolybdate method using EMD Millipore silicate test kit with a modified protocol. In brief, 860 μL diluted silica sample in 0.5 N NaOH was mixed with 30 μL Reagent Si-1, followed by adding 140 μL 4 N $H_2SO_4$. The reaction was then kept at room temperature for 10 minutes. Silica concentration was determined by measuring the resultant yellow silicomolybdayte absorbance at 354 nm.

### 5.5.4 Fluorescence Intensity Measurements

Activity of free and immobilized mCherry and GFP were measured in 96-well plates with black wall and black bottom. Fluorescence intensities were measured using Perkin Elmer VICTOR$^3$ 1420 Multilabel Counter with emission filter above the sample. The excitation/emission wavelengths for mCherry and GFP were 560 nm/615 nm and 485 nm/520 nm, respectively.

### 5.5.5 Estimation of mCherry-INT/vault/silica Leakage

The mCherry-INT/vault/silica was maintained at 4°C for 47 days. On day 0, 15 μL fluorescent mesosilica sample was diluted to 200 μL with 185 μL Buffer A, and measured as the initial total fluorescence intensity. After centrifuging the mixture at 13,000 x g for 10 minutes, fluorescence intensity of the supernatant was also measured to determine initial protein leaching. At each time point, 15 μL fluorescent mesosilica sample was combined with 185 μL Buffer A, and centrifuged at 6000-13000 x g for 10 minutes. Fluorescence intensities of the supernatant and resuspended pellet (200 μL in Buffer A) were recorded to examine protein leakage.

### 5.5.6 GFP-INT Stability Test

Free GL-INT, GL-INT/vault and GL-INT/vault/silica were diluted to the same initial fluorescence before each test. To determine thermal stability, samples were incubated at 37°C in 96-well plates at a given period. At each time point, fluorescence intensities were recorded and normalized to the measurements before incubation. To determine the stability against SDS denaturation, the samples were incubated at room temperature in the solution containing 0.05%

SDS, and measured about every ten minutes. The fluorescence intensity readings before adding SDS were set as 100%.

### 5.5.7 MnP Enzyme Activity Assay

MnP activity was measured as the activity in catalyzing oxidation of 2,2'-azino-bis(3-ethylbenzothiazoline-6-sulphonic acid) (ABTS). The assay was performed in pH 4.0 50 mM malonate-Na buffer containing 60 μM ABTS, 1.5 mM $MnCl_2$ and 30 μM $H_2O_2$ for 15 minutes at room temperature, and the enzyme activity was determined by measuring the product absorbance at 420 nm. Experiments evaluating enzyme stability and reusability were all performed using this assay.

### 5.5.8 Enzyme Stability Assay

Enzyme stability was evaluated under the following five conditions: (i) 10 minutes incubation in solution containing 15% Methanol or isopropanol at room temperature; (ii) 30 minutes incubation at 35°C, 40°C, 45°C or 50°C; (iii) 10 minutes incubation at 45°C in solution containing 5%, 10% or 15% methanol; (iv) 16 days incubation in tap water at 15°C (v) 16 days incubation in groundwater at 15°C. For each sample collected, enzyme activity was measured following the assay described above, and normalized to its corresponding initial activity.

### 5.5.9 Enzyme Reusability Studies

ABTS was used as the model substrate to determine the reusability of vault/silica immobilized MnP enzyme. Following the procedures described above, absorbance at 420 nm of the assay solution was immediately measured after 15 minutes reaction. Then, the solution was

centrifuged at 6000 x g for 5 minutes, followed supernatant removal. This step was repeated once to remove liquid as much as possible. The final pellet was recycled and subjected to the next use. Absorbance determined after each use was normalized to the first measurement. The supernatant after the first use was also kept for an extra 35 minutes to examine if there was any absorbance increase caused by enzyme leaching.

### 5.5.10 Removal of Bisphenolic Compounds

BPA and BPF removal tests were performed in pH 4.0 50 mM malonate buffer containing 1.5 mM $MnCl_2$, 60 μM BPA or BPF, 30 μM $H_2O_2$, 2 g/L polyethylene glycol (PEG, M.W. 8000) and MnP-INT/vault/silica, at 25°C and 250 rpm. At each time point, triplicate samples were centrifuged at 6000 x g for 5 minutes. The supernatant was collected and mixed with equal volumes of methanol to quench the reactions. To test the reusability of MnP-INT/vault/silica in removing BPA, reactions were maintained for 35 minutes at 25°C and 250 rpm. The MnP-INT/vault/silica was recycled by centrifuging at 6000 x g for 5 minutes, followed by washing with 100 μL pH 4.0 50 mM malonate buffer with 2 g/L PEG. Residual BPA and BPF concentrations were determined using a Hewlett Packard high-performance liquid chromatograph (HP 1050 HPLC system) equipped with an Agilent Eclipse Plus C18 column (4.6 x 150 mm, 5 μm particle size) and a UV detector at 277 nm. The mobile phase used was a mixture of methanol-water (70:30, v/v), and was run at 0.5 mL/min.

## 5.6 References


1. Goltner, C. G.; Antonietti, M. Mesoporous materials by templating of liquid crystalline phases. *Advanced Materials* **1997,** *9* (5), 431-&.
2. Li, W.; Liu, J.; Zhao, D. Y. Mesoporous materials for energy conversion and storage devices. *Nature Reviews Materials* **2016,** *1* (6).
3. Tarn, D.; Ashley, C. E.; Xue, M.; Carnes, E. C.; Zink, J. I.; Brinker, C. J. Mesoporous Silica Nanoparticle Nanocarriers: Biofunctionality and Biocompatibility. *Accounts of Chemical Research* **2013,** *46* (3), 792-801.
4. Kresge, C. T.; Leonowicz, M. E.; Roth, W. J.; Vartuli, J. C.; Beck, J. S. Ordered Mesoporous Molecular-Sieves Synthesized by a Liquid-Crystal Template Mechanism. *Nature* **1992,** *359* (6397), 710-712.
5. Huo, Q. S.; Margolese, D. I.; Ciesla, U.; Feng, P. Y.; Gier, T. E.; Sieger, P.; Leon, R.; Petroff, P. M.; Schuth, F.; Stucky, G. D. Generalized Synthesis of Periodic Surfactant Inorganic Composite-Materials. *Nature* **1994,** *368* (6469), 317-321.
6. Che, S.; Garcia-Bennett, A. E.; Yokoi, T.; Sakamoto, K.; Kunieda, H.; Terasaki, O.; Tatsumi, T. A novel anionic surfactant templating route for synthesizing mesoporous silica with unique structure. *Nature Materials* **2003,** *2* (12), 801-805.
7. Beck, J. S.; Vartuli, J. C.; Roth, W. J.; Leonowicz, M. E.; Kresge, C. T.; Schmitt, K. D.; Chu, C. T. W.; Olson, D. H.; Sheppard, E. W.; Mccullen, S. B.; Higgins, J. B.; Schlenker, J. L. A New Family of Mesoporous Molecular-Sieves Prepared with Liquid-Crystal Templates. *Journal of the American Chemical Society* **1992,** *114* (27), 10834-10843.
8. Bagshaw, S. A.; Prouzet, E.; Pinnavaia, T. J. Templating of Mesoporous Molecular-Sieves by Nonionic Polyethylene Oxide Surfactants. *Science* **1995,** *269* (5228), 1242-1244.

9. Tanev, P. T.; Pinnavaia, T. J. A Neutral Templating Route to Mesoporous Molecular-Sieves. *Science* **1995,** *267* (5199), 865-867.

10. Zhao, D. Y.; Feng, J. L.; Huo, Q. S.; Melosh, N.; Fredrickson, G. H.; Chmelka, B. F.; Stucky, G. D. Triblock copolymer syntheses of mesoporous silica with periodic 50 to 300 angstrom pores. *Science* **1998,** *279* (5350), 548-552.

11. Yu, C. Z.; Tian, B. Z.; Fan, J.; Stucky, G. D.; Zhao, D. Y. Nonionic block copolymer synthesis of large-pore cubic mesoporous single crystals by use of inorganic salts. *Journal of the American Chemical Society* **2002,** *124* (17), 4556-4557.

12. Kroger, N.; Deutzmann, R.; Sumper, M. Polycationic peptides from diatom biosilica that direct silica nanosphere formation. *Science* **1999,** *286* (5442), 1129-1132.

13. Fowler, C. E.; Shenton, W.; Stubbs, G.; Mann, S. Tobacco mosaic virus liquid crystals as templates for the interior design of silica mesophases and nanoparticles. *Advanced Materials* **2001,** *13* (16), 1266-1269.

14. Shopsowitz, K. E.; Qi, H.; Hamad, W. Y.; MacLachlan, M. J. Free-standing mesoporous silica films with tunable chiral nematic structures. *Nature* **2010,** *468* (7322), 422-U246.

15. Xu, H.; Wang, Y. M.; Ge, X.; Han, S. Y.; Wang, S. J.; Zhou, P.; Shan, H. H.; Zhao, X. B.; Lu, J. A. R. Twisted Nanotubes Formed from Ultrashort Amphiphilic Peptide I3K and Their Templating for the Fabrication of Silica Nanotubes. *Chemistry of Materials* **2010,** *22* (18), 5165-5173.

16. Liu, B.; Cao, Y. Y.; Huang, Z. H.; Duan, Y. Y.; Che, S. N. Silica Biomineralization via the Self-Assembly of Helical Biomolecules. *Advanced Materials* **2015,** *27* (3), 479-497.

17. Wang, F. K.; Li, D.; Mao, C. B. Genetically Modifiable Flagella as Templates for Silica Fibers: From Hybrid Nanotubes to 1D Periodic Nanohole Arrays. *Advanced Functional Materials* **2008,** *18* (24), 4007-4013.

18. Mao, C. B.; Wang, F. K.; Cao, B. R. Controlling Nanostructures of Mesoporous Silica Fibers by Supramolecular Assembly of Genetically Modifiable Bacteriophages. *Angewandte Chemie International Edition* **2012,** *51* (26), 6411-6415.

19. Aimé, C.; Coradin, T.; Fernandes, F. M. Biomimetic Sol–Gel Materials. In *The Sol-Gel Handbook*, David Levy; Zayat, rcos, Eds.; Wiley-VCH Verlag GmbH & Co. KGaA: 2015; pp 605-650.

20. Rome, L. H.; Kickhoefer, V. A. Development of the vault particle as a platform technology. *ACS Nano* **2013,** *7* (2), 889-902.

21. Kickhoefer, V. A.; Liu, Y.; Kong, L. B.; Snow, B. E.; Stewart, P. L.; Harrington, L.; Rome, L. H. The telomerase/vault-associated protein TEP1 is required for vault RNA stability and its association with the vault particle. *Journal of Cell Biology* **2001,** *152* (1), 157-164.

22. Kickhoefer, V. A.; Siva, A. C.; Kedersha, N. L.; Inman, E. M.; Ruland, C.; Streuli, M.; Rome, L. H. The 193-kD vault protein, VPARP, is a novel poly(ADP-ribose) polymerase. *Journal of Cell Biology* **1999,** *146* (5), 917-928.

23. Stephen, A. G.; Raval-Fernandes, S.; Huynh, T.; Torres, M.; Kickhoefer, V. A.; Rome, L. H. Assembly of vault-like particles in insect cells expressing only the major vault protein. *Journal of Biological Chemistry* **2001,** *276* (26), 23217-23220.

24. Wang, S. J.; Ge, X.; Xue, J. Y.; Fan, H. M.; Mu, L. J.; Li, Y. P.; Xu, H.; Lu, J. R. Mechanistic Processes Underlying Biomimetic Synthesis of Silica Nanotubes from Self-Assembled Ultrashort Peptide Templates. *Chemistry of Materials* **2011,** *23* (9), 2466-2474.

25. Kickhoefer, V. A.; Garcia, Y.; Mikyas, Y.; Johansson, E.; Zhou, J. C.; Raval-Fernandes, S.; Minoofar, P.; Zink, J. I.; Dunn, B.; Stewart, P. L.; Rome, L. H. Engineering of vault nanocapsules with enzymatic and fluorescent properties. *Proceedings of the National Academy of Sciences of the United States of America* **2005,** *102*, 4348-4352.

26. Luckarift, H. R.; Spain, J. C.; Naik, R. R.; Stone, M. O. Enzyme immobilization in a biomimetic silica support. *Nature Biotechnology* **2004,** *22* (2), 211-213.

27. Audebert, M.; Dolo, L.; Perdu, E.; Cravedi, J. P.; Zalko, D. Use of the γH2AX assay for assessing the genotoxicity of bisphenol A and bisphenol F in human cell lines. *Archives of Toxicology* **2011,** *85* (11), 1463-1473.

28. Chen, Y. C.; Shu, L.; Qiu, Z. Q.; Lee, D. Y.; Settle, S. J.; Hee, S. Q.; Telesca, D.; Yang, X.; Allard, P. Exposure to the BPA-substitute bisphenol S causes unique alterations of germline function. *Plos Genetics* **2016,** *12* (7), e1006223.

29. Yamazaki, E.; Yamashita, N.; Taniyasu, S.; Lam, J.; Lam, P. K. S.; Moon, H. B.; Jeong, Y.; Kannan, P.; Achyuthan, H.; Munuswamy, N.; Kannan, K. Bisphenol A and other bisphenol analogues including BPS and BPF in surface water samples from Japan, China, Korea and India. *Ecotoxicology and Environmental Safety* **2015,** *122*, 565-572.

30. Drinking Water Quality Report. *Los Angeles Department of Water & Power, Los Angeles, CA* **2017**.

31. Ge, J.; Lei, J. D.; Zare, R. N. Protein-inorganic hybrid nanoflowers. *Nature Nanotechnology* **2012,** *7* (7), 428-432.

32. Yan, M.; Ge, J.; Liu, Z.; Ouyang, P. K. Encapsulation of single enzyme in nanogel with enhanced biocatalytic activity and stability. *Journal of the American Chemical Society* **2006,** *128* (34), 11008-11009.

33. Kim, J.; Grate, J. W. Single-Enzyme Nanoparticles Armored by a Nanometer-Scale Organic/Inorganic Network. *Nano Letters* **2003,** *3* (9), 1219-1222.

34. Kalantari, M.; Yu, M. H.; Yang, Y. N.; Strounina, E.; Gu, Z. Y.; Huang, X. D.; Zhang, J.; Song, H.; Yu, C. Z. Tailoring mesoporous-silica nanoparticles for robust immobilization of lipase and biocatalysis. *Nano Research* **2017,** *10* (2), 605-617.

35. Forsyth, C.; Yip, T. W. S.; Patwardhan, S. V. CO2 sequestration by enzyme immobilized onto bioinspired silica. *Chemical Communications* **2013,** *49* (31), 3191-3193.

36. Wang, M.; Abad, D.; Kickhoefer, V. A.; Rome, L. H.; Mahendra, S. Vault nanoparticles packaged with enzymes as an efficient pollutant biodegradation technology. *ACS Nano* **2015,** *9* (11), 10931-10940.

37. Luo, T. J. M.; Soong, R.; Lan, E.; Dunn, B.; Montemagno, C. Photo-induced proton gradients and ATP biosynthesis produced by vesicles encapsulated in a silica matrix. *Nature Materials* **2005,** *4* (3), 220-224.

## Chapter 6 Conclusions and Perspectives

Enzymes, bearing excellent catalytic properties, are shown to have great potential in environmental applications. In comparison to microbial remediation that uses living microorganisms, enzymatic bioremediation uses formulated enzymes as remediation agents, and removes environmental contaminants faster, has better applicability and causes less public concern than. However, due to the sensitive nature of protein molecules, enzymes are easily inactivated and destructed by harsh conditions, metal ions, natural ligands, proteases, microorganisms, and even the products from their own activities. Immobilization on solid supports has been shown to be an effective approach to stabilize enzymes and increases their reusability. Although numerous immobilization supports and methods have been developed, several issues still have not been resolved, especially towards the environmental applications. For examples, enzyme leaching is commonly observed for immobilized enzymes, which limits enzyme life and reusability under read environmental conditions. Enzyme activity loss after immobilization, resulted from strong interaction between solid supports or mass transfer resistance caused by surrounding solid matrices, is another common issue. Perhaps the most environmentally-relevant issue with current immobilization technologies, however, is that toxic substances are usually used in synthesizing solid supports, which leads to extra hazardous waste emission to the environment. The application of such materials water treatment or soil remediation also possesses environmental and health risk. The development of a suitable enzyme immobilization method for environmental application is still challenging.

In recent years, protein nanocages are emerging as promising delivery vessels in medical applications. Being made of amino acids, these materials are synthesized by cell cultures at gentle conditions and are completely biodegradable, which make them attractive candidates as

enzyme immobilization supports, particularly, for environmental applications. Vaults are the largest natural ribonucleoprotein particles, and have been isolated from many eukaryotic species including human. Natural vaults compromise a protein shell assembled from major vault proteins (MVP) with other molecules lining inside. Derived from natural vaults, recombinant vaults are solely assembled from 78 copies of MVP in insect cells, and exhibit similar morphology as natural vaults. With a large empty core, the recombinant vault can hold up to hundreds of protein molecules, which make it a promising candidate for enzyme immobilization. The INT domain, which was derived from a protein interacting with natural vaults, strongly interacts with the binding sites on MVP that are located inside of vault particles. By attaching to INT domain, heterologous compartments can be directed and anchored in vaults, facing towards the core.

Manganese peroxidase (MnP), a peroxidase enzyme produced by white-rot fungus, catalyzes substrates oxidation using $H_2O_2$ as the oxidant, and has been applied to remove various contaminants. In this dissertation, MnP was employed as the model enzyme to test the effectiveness and applicability of using vault particles as enzymes carriers for environmental applications. Using the readily developed INT strategy, MnP was encapsulated into vaults, which was confirmed by Western blot, dynamic light scattering, and TEM images. As the MVP peptide shell of vaults is highly porous and permeable, and the sequestration of MnP in vault particles is through specific non-covalent interaction between the INT domain and binding sites on MVP, the encapsulated MnP showed 5-12% activity loss. For all substrates tested, $K_m$ values increased by -20-38%, and $k_{cat}$ numbers decreased by 5-24% after vault encapsulation. The vault-encapsulated MnP also exhibited improved resistance to thermal inactivation, as compared to free enzymes. Further inactivation kinetics studies revealed that the vault shell mainly prevented enzyme three-dimensional conformation change that happens during the second enzyme

inactivation step, whereas the first step in enzyme inactivation involving tertiary bonds broken was not mitigated. Using phenol as a model contaminant, we found significant higher removal with vault-encapsulated MnP.

We further evaluated the performance of encapsulated MnP in decontaminating and detoxifying bisphenolic compounds, including BPA, BPF, and BPAP. Bisphenolic compounds are commonly used in plastic manufacturing and have been detected in various water bodies. Being shown to have estrogenic activity and reproductive toxicity, bisphenolic compounds possess environmental and health risk to aquatic organisms and human. Compared to free MnP enzymes, vault-encapsulated MnP removed bisphenolic compounds at higher rates and survived longer in reactions. Products yielded from different MnPs were extracted and analyzed for composition. Vault-encapsulated MnP catalysis resulted in less product species with significant amount of bisphenolic polymers, while catalysis by free MnP led to formation of more species, mainly on small molecular mass side. Previous studies have shown that active MnP enzyme catalyze coupling between bisphenolic molecules, resulting formation of bisphenol polymers that are relative inert. However, in real conditions with less enzyme dosage, free MnP was inactivated quickly, leaving abundant active intermediates, which were further chemically converted to those species with small molecular masses found in the product profile. Vault-encapsulated MnP, on the contrary, was more stable and survived longer in reactions, thus converting bisphenolic compounds to dimer, trimer or polymers. Such significant product difference led to a thought that products from different MnP treatments might exhibit different toxicity. Products with small molecular mass may possess similar structure as parental bisphenol compounds and may still have estrogenic activity and reproductive toxicity, whereas polymeric products should be more insert and less toxic. Thus, toxicity studies targeting on reproductive

effects were performed in *C. elegans*. As expected, free MnP treatment resulted products significantly increased germline apoptosis or reduced fertile rates depending on the parental compounds, while treatment by vault-encapsulated MnP completely brought the effect in germline apoptosis and fertility assays to background levels.

Baculovirus-insect cell expression is the only system that has been developed to produce recombinant vault particles. However, the large quantity of vaults that will be required for real environmental application, is not economically achievable through the baculovirus-insect cell system. Thus, we developed a more cost-effective vault-production system using yeast *Pichia pastoris* as the expression host. By solely expressing codon optimized human MVP coding sequence in *P. pastoris*, recombinant vault particles were successfully formed. The yeast vaults displayed similar size and morphology as natural vaults purified from various species and recombinant vaults from insect cells, and was indistinguishable from insect vaults under TEM. The yield of yeast vaults at laboratory scale was about 8 mg/L culture, which is close to that of insect vaults, but at a ten times lower cost. It has also been demonstrated that yeast vaults maintained the ability to anchor INT domain fused. Similar to insect cells produced vaults, yeast vaults were able to encapsulate INT tagged MnP enzymes, and the resultant yeast vault-encapsulated MnP maintained high activity and showed improved stability and BPA removal efficiency as compared to free MnP enzymes.

One drawback of using vaults as enzyme carriers is that they can hardly be recovered and reused. To overcome this issue, we developed a vault-based silica immobilization strategy, which enables indirect enzyme immobilization in mesosilica structures through vault bridging. This strategy is based on vault encapsulation and vault-templated formation mesosilica materials. In the first step, proteins or enzymes are encapsulated in vaults using the INT strategy as

described above. The second step involves *in situ* deposition and polymerization of silica on vault surface at pH 5.5-6.5. The resultant protein/vault/silica composites are fully recoverable and reusable by low-speed centrifugation. As proteins are immobilized in silica through vault bridging, their bioactivities are largely preserved. For three proteins tested, two fluorescent proteins maintained full activity, and MnP enzyme experienced 20% activity lost. The immobilization efficiency of this approach was 100% over a wide protein concentration range. MnP enzyme immobilized in vault/silica composites showed improved stability at high temperature or in the presence of organic solvents, in comparison to vault encapsulated MnP and free MnP enzyme. Superior reusability was also observed for mesosilica entrapped MnP. It maintained near 100% activity after 12 reuses and 90% activity after 30 reuses in activity assays. With respect to environmental remediation, the MnP-INT/vault/silica was demonstrated to effectively remove bisphenolic compounds and maintain robust activity in removal of BPA. No obvious decrease in BPA removal rate was observed in four repeated uses. This technique allows more cost-effective use of vault-encapsulated enzymes, for example, in fixed-bed columns with continuous flow of contaminated water, and also enables their application in bioremediation under more complicated environment such as soil and groundwater.

In conclusion, my research establishes a vault-based enzyme immobilization technology for environmental application. The feasibility of using vault-encapsulated enzymes in contaminant removal was demonstrated in this work, and the development of cost-effective vault product system and vault/silica immobilization technique enables the use of vaults in large scale bioremediation under various environmental conditions.

As a platform technique, vault particles can be packaged with enzymes degrading targeted contaminant groups, thus can be customized to treat specific environmental issues. In

addition, migration, fate and transport of vault particles and vault/silica composites in real environmental conditions, such as different soil layers and groundwater flow, should be studied to evaluate and optimize the performance of vault-encapsulated enzymes in fields. Furthermore, this work also promises the exploration of more protein nanocages such as virus-like particles, ferritin and lumazine synthase, as enzymes carriers for environmental applications.